UNIWERSYTET JAGIELLOŃSKI
W KRAKOWIE

Faculty of Biology

Institute of Environmental Sciences

ER bodies and their impact in shaping root microbiota

Arpan Kumar Basak

PhD thesis supervised by

prof. dr hab. Kazimierz Strzałka

Malopolska Centre of Biotechnology,

and

Department of Plant Physiology and Biochemistry

Faculty of Biochemistry, Biophysics and Biotechnology

Kraków 2022


The scholarship of the author was provided by the project entitled “WIN. Wsparcie Interdyscyplinarności kierunku PhD Programme in Biology” of the Jagiellonian University, co-financed by the European Union under the European Social Fund - Operational Programme Knowledge Education Development Axis III Higher Education for Economy and Development, Action 3.2 PhD Programme (from 2017 to 2021).

This work was supported by funds from Polish National Science Center OPUS (2011/01/N/NZ4/00124) granted to Kenji Yamada and PRELLUDIUM20 (UMO-2021/41/N/NZ3/04537) granted to Arpan Kumar Basak.

Author: Arpan Kumar Basak,
Jagiellonian University

Supervisor: Prof. dr. hab Kazimierz Strzałka,
Jagiellonian University

Co-supervisor: Dr. Kenji Yamada,
Jagiellonian University

Advising supervisor: Dr. Ryohei Thomas Nakano,
Max-Planck Institute of Plant Breeding and Research

Reviewers:

Prof. dr hab. Zofia Szweykowska-Kulińska,
Instytut Biologii Molekularnej i Biotechnologii,
Uniwersytet im. Adama Mickiewicza w Poznaniu

Prof. dr hab. Hazem Kalaji,
Instytut Biologii,
Szkoła Główna Gospodarstwa Wiejskiego w Warszawie

Dr hab. Tomasz Płociniczak,
profesor Uniwersytetu Śląskiego,
Instytut Biologii, Biotechnologii i Ochrony Środowiska,
Uniwersytet Śląski w Katowicach

Date of submission: 21st, June, 2022

Dedicated to everyone sharing common soil to walk, air to breathe and water to drink

“When an idea exclusively occupies the mind, it is transformed into an actual physical or mental state.” – Swami Vivekananda

SUMMARY

Plants in nature are exposed to stress from a plethora of microbes in the soil that compete for the organic carbon produced by the plants. Some microbes are beneficial to plants, and some are pathogenic. Similarly, plants are exposed to herbivores that eat plants for their diet. Some herbivores and insects show mutualistic behaviour by either assisting in pollination or defense against other herbivores. Over the years, plants have evolved their defense systems to counter their enemies. Plants of *Brassicales* order have evolved a sophisticated defense system to protect themselves from above and below ground, these plants produce a class of secondary metabolites called the glucosinolates that provide protection against their enemies upon defense activation. Glucosinolates are stored in vacuoles and activated by β-glucosidase localized in so-called myrosin cells. This activation system is popularly known as the mustard oil bomb system, and is found in cruciferous vegetables including model plant *Arabidopsis thaliana*. Among the reported β-glucosidases in *A. thaliana* is PYK10 which is stored in specialized endoplasmic reticulum (ER) network-derived compartments, namely ER bodies. Interestingly, roots of *A. thaliana* are abundant in indole glucosinolates that are downstream products of the Trp-derived metabolism. PYK10 is reported to be one of the most dominant myrosinases in roots with high specific activity toward indole glucosinolates. It is unclear whether the ER-body-localized myrosinases play a crucial role in shaping the root-microbiota assembly by hydrolyzing the Trp-derived secondary metabolites. The ER bodies encapsulate PYK10 with a potential scaffold protein NAI2, making it a protein-dense cellular compartment. The ER bodies are membrane-bound structures, containing two integral membrane proteins MEMBRANE OF ER-BODIES (MEB1) and MEB2. It is shown that MEB1 and MEB2 genes are homologous to *A.thaliana* VACUOLAR IRON TRANSPORTER (VIT1) transporter, and these proteins are responsible for iron transportation in yeast. However, the function of MEB1 and MEB2 *in planta* is not known. At first, I investigate the role of MEB1 and MEB2 in *A. thaliana*. As MEB1 and MEB2 are reported to be transporters, I hypothesized that MEB1 and MEB2 are involved in cation homeostasis. Secondly, I addressed the role of ER bodies and their substrates in root microbiota community assembly. To date, several studies have suggested that indole glucosinolates and their degradation products play a role in shaping root microbiota but the precise role of PYK10-mediated degradation of the indole glucosinolates is not known.

In this thesis, firstly, I have demonstrated the potential role of MEB1 and MEB2 in ER body morphology, ER body movement, and nutrient homeostasis. By advanced confocal microscopic analysis of the texture features I have shown that MEB1 and MEB2 are responsible for ER body

morphology and movement. By plant ionomics and by measuring the physiological parameters of the plants in controlled nutrient condition I suggested that ER bodies have a role in cation homeostasis. Overall, I have shown the potential role of MEB1 and MEB2 in ER bodies *in planta*.

Secondly, I have demonstrated the role of PYK10 and Trp-derived secondary metabolites in the composition of the root exudates by performing untargeted metabolomics. Further, I investigated the role of ER bodies in shaping the root-microbiota assembly. Considering the results from greenhouse experiments and root exudates, together with the fact that PYK10 and Trp-derivatives are abundant in roots, it is likely that compounds downstream of PYK10 and Trp-pathway in the root exudates are responsible for shaping the root-microbiota assembly. By conducting treatment experiments using natural soil and reconstituted microbiota with root exudates collected from a set of ER body and Trp-pathway compromised plants, I investigate the role of ER body-localized PYK10 myrosinase and Trp-pathway in modulating the composition of root microbiota. Particularly, I found that PYK10 and Trp-derived secondary metabolites produce root-exuding compounds that trigger the community shift in soil and synthetic bacterial community. Further, I examined the role of ER bodies in plant-fungi interactions in a mono-association setup using fungal strains, mutant plants, and wild type plant. I found that both the PYK10 and Trp-pathway have an overlapping behaviour toward a set of fungal strains.

Overall, in my thesis, I investigated the role of ER body membrane proteins MEB1 and MEB2 *in planta* and the role of ER body-localized PYK10 in shaping root microbiota.

Keywords: *Arabidopsis thaliana, ER bodies, glucosinolate, plant defense, membrane, organelle morphology, organelle movement, cation homeostasis, plant physiology, root-microbiota, root-secretions, secondary metabolites*

TABLE OF CONTENTS

1. INTRODUCTION: ER bodies as a single cell defence system

1.1. The ER body is a unique compartment of the plant cell associated with protein packing

The gateway to the secretory pathway in all eukaryotic cells is the endoplasmic reticulum (ER) (Robinson et al., 2015). Many ER-derived vesicles have been identified in plant cells, such as coat protein complex (COP) II vesicles and precursor accumulation (PAC) vesicles. The ER compartments in monocots such as maize and rice accumulate specific proteins called protein bodies (PBs) that contain prolamin and zein (Herman & Larkins, 1999), those in mungbean contain KDEL-tailed protease-accumulating vesicles (KVs) (Toyooka et al., 2000), and the ricinosomes in castor bean accumulate papain-type proteases (M. Schmid et al., 2001). These microstructures are considered the storehouse of proteins and are deployed when necessary (Figure 1.1).

In my research, I focused on one of the ER-derived compartments called the ER body, which is also known as a fusiform body. This microstructure is an ER domain with a different shape from the ER and is taxonomically distributed in unique plants. The ER body was first discovered in root epidermal and cortical cells of radish in 1965 by Bonnett and Newcomb (Bonnett & Newcomb, 1965). Using microscopy, this microstructure was described as dilated cisternae with luminal continuity to the ER. Since this discovery, over the following two decades, researchers characterised these microstructures to understand their functions (Behnke & Eschlbeck, 1978; Cresti et al., 1974; Endress & Sjolund, 1976; Gailhofer et al., 1979; Hoefert, 1975; T. H. Iversen, 1970; T.-H. Iversen, 1970; T.-H. Iversen & Flood, 1969; Jørgensen, 1981; Jørgensen et al., 1977). Three independent studies revealed that the dilated cisternae-like microstructures were primarily restricted to species of the order Brassicales. It was thought that, upon glucoside hydrolysis, these dilated cisternae store enzymes like glucosidases that produce metabolites similar to glucosinolates which are distributed in Brassicaceae plants (Behnke & Eschlbeck, 1978; T. H. Iversen, 1970; Jørgensen, 1981).

A glucosidase that uses glucosinolates as substrates is specifically called myrosinase. Activity-labelled transmission electron microscopy (TEM) revealed that the dilated cisternae potentially contained myrosinase and showed specific activity towards sinigrin (T.-H. Iversen, 1970). Therefore, it is possible that the contents of ER bodies metabolise glucosinolates (Behnke & Eschlbeck, 1978). However, ER bodies were not detected in Resedaceae plants containing glucosinolates. Consequently, the specificity of ER bodies towards glucosinolates compared with other glucosides has remained elusive.

After two decades of advances in genetic engineering and recombinant DNA technology in the field of molecular and cell biology, these rod-shaped structures in the model plant *Arabidopsis thaliana* were labelled with ER-localised green fluorescent protein (GFP) and were suggested to be equivalent

to dilated cisternae (Gunning, 1998). In the early 2000s, Hayashi et al., (2001) showed that these rod-shaped microstructures resembled the dilated cisternae described previous literature and coined the term ER bodies. The cotyledons of the transgenic line expressing ER-localised GFP (GFP-h) revealed bright rod-shaped microstructures of ER bodies in addition to the ER network (Hawes et al., 2001; Hayashi et al., 2001; Ridge et al., 1999). Electron microscopy revealed that the ER body is membrane-bound and surrounded by ribosomes, which is a typical characteristic of the ER. On electron micrographs, the ER body was observed as a structure that interconnects the ER tubules and cisternae (Gunning, 1998; Hayashi et al., 2001); those studies showed that the ER bodies are continuous throughout the ER network and are suggested to be a subdomain of the ER with specific functions.

The research of Matsushima et al., (2004) identified the transcription factor responsible for the formation of ER bodies and termed it NAI1 also known as AtbHLH20. Mutants without NAI1 transcription factor showed no ER bodies. Until now, research has focused on genetic and biochemical studies that provide information on the functions, importance, structure, and biogenesis of this unique organelle. However, the morphology and function of the ER bodies are still elusive. In my thesis, I primarily focus on the morphology of the ER bodies and their function.

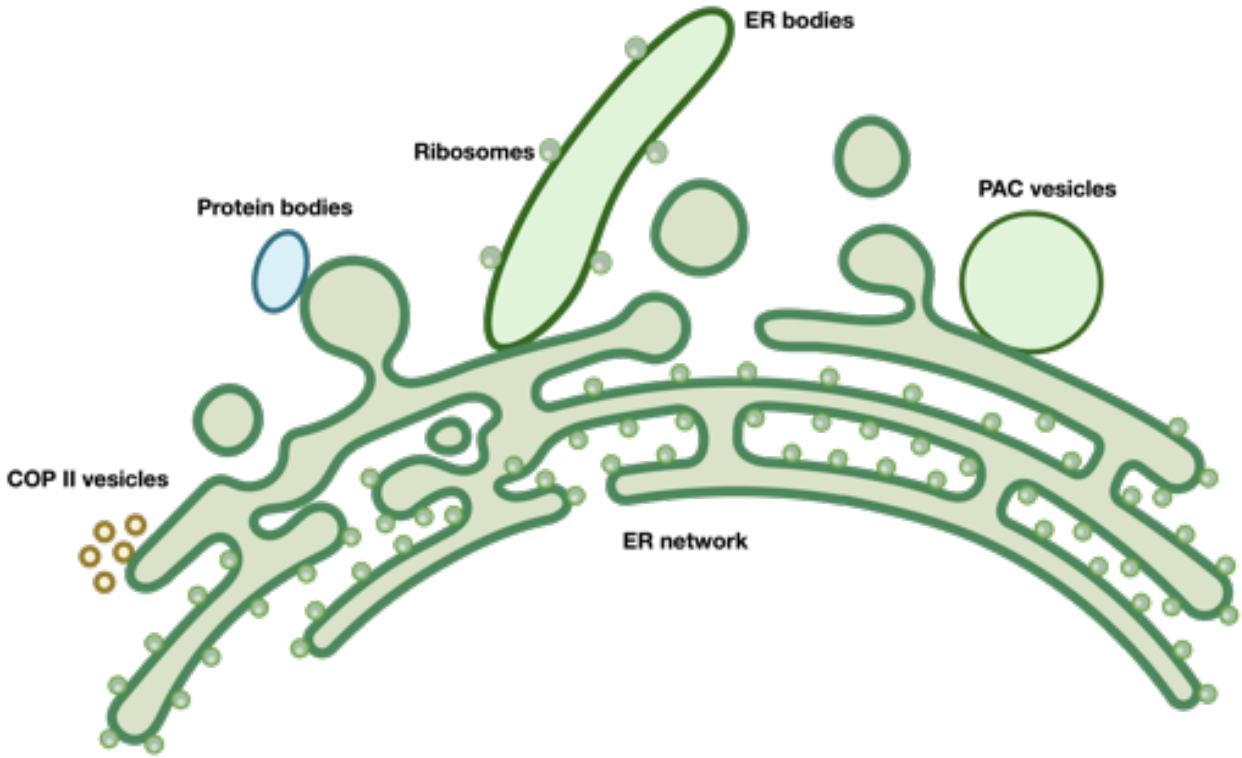

Figure 1.1: ER-derived compartments like COP II vesicles, protein bodies, PAC vesicles and ER bodies.

1.2. Different types of ER bodies

ER bodies are conserved in the order Brassicales and are distributed among members of the Brassicaceae, Capparaceae, and Cleomaceae. Additionally, it is known that Brassicales plants have unique defence strategies to cope with biotic stresses that may lead to the relevance of ER bodies in the plant defence system (Nakano et al., 2014; Yamada et al., 2020). In general, ER-derived compartments form spherical structures, but ER bodies have a rod or spindle shape.

Based on the expression difference of ER bodies, they can be separated into two types: (a) constitutive ER bodies and (b) inducible ER bodies (Hara-Nishimura & Matsushima, 2003; Ogasawara et al., 2009). In *A. thaliana* seedlings constitutive ER bodies are mainly formed throughout the epidermis and are highly abundant in the roots of adult plants, but are sparsely distributed in siliques, sepals, and mature leaves (Figure 1.2), whereas inducible ER bodies are formed *de novo* in rosette leaves when subjected to wounding or jasmonic acid treatment and are only formed when plants are subjected to stress. Moreover, the main constituents of inducible ER bodies are not identical to those of constitutive ER bodies (Stefanik et al., 2020); this shows that there is tissue specificity with regard to inducibility of ER bodies and their role in stress response.

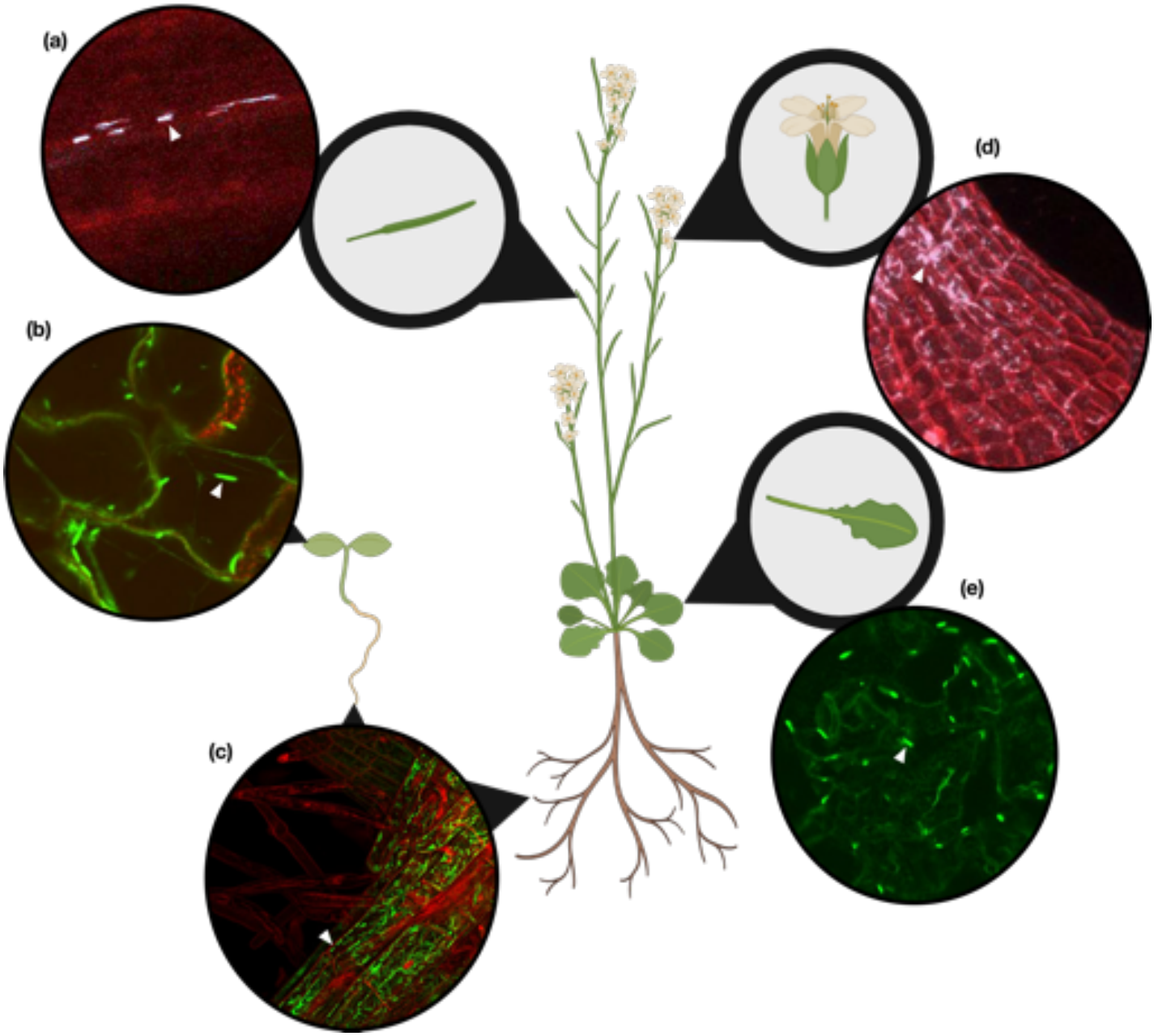

Figure 1.2: Distribution of constitutive ER bodies (arrowheads) across different organs in *Arabidopsis thaliana*. The ER bodies are in siliques (a), cotyledons (b), roots (c), sepals (d) and in sparsely rosette leaves (e). The red channel indicates the propidium iodide (PI) fluorescence of the cell wall. The green or cherry colour represents the GFP signal from ER bodies.

1.3. Constituents of ER bodies that make up this spindle-shaped endomembrane structure

Constitutive ER body formation is regulated by the NAI1 transcription factor in *A. thaliana*. NAI2 is a component responsible for the shape of constitutive ER bodies, and it acts as a scaffold protein for PYK10 accumulation in ER bodies (Yamada et al., 2008). PYK10 (also known as BGLU23) is a main component of constitutive ER bodies and has β -glucosidase activity (Nakano et al., 2017). ER bodies have two integral membrane proteins, MEMBRANE OF ER BODY (MEB) 1 and MEB2, that are regulated by the NAI1 transcription factor (Yamada et al., 2013). In addition to ER body components, the NAI1 transcription factor regulates other genes products of which are localised in both the ER

bodies and in the cytosol. In this section, I elaborated on the role of each component of the constitutive ER bodies.

1.3.1. NAI1 transcription factor is the master regulator of ER body constituents

Matsushima et al., (2004) isolated a *A. thaliana nai1* mutant that lacked ER body formation. They found that a basic helix–loop–helix (bHLH) type transcription factor, NAI1 (AtbHLH20), regulates the formation of ER bodies in seedlings and roots. Microarray data analysis of the *nai1* mutant revealed that NAI1 regulates the genes encoding ER body proteins. The set of proteins affected includes PYK10 (BGLU23), NAI2, MEB1, and MEB2 (see section 1.3.4), indicating that NAI1 is the master regulator of ER body formation.

1.3.2. PYK10 is the major component of constitutive ER bodies and is abundant proteins in roots.

The main protein component of the ER body in *A. thaliana* seedlings and roots was identified as a β-glucosidase called PYK10 (Matsushima, Kondo, et al., 2003). PYK10 is one of the most abundant proteins in *A. thaliana* roots (Matsushima, Kondo, et al., 2003) and, in contrast to generic luminal ER proteins, PYK10 is actively recruited from ER bodies to accumulate in ER bodies (Matsushima, Hayashi, et al., 2003). The lumen of the ER body showed relatively high electron density in electron microscopy, suggesting that the ER body accumulates large amounts of proteins (Gunning, 1998; Hayashi et al., 2001). Similarly, centrifugation-based fractionation analysis revealed that ER bodies are enriched in a relatively heavier fraction than those fractions from other subcellular compartments (Hayashi et al., 2001; Matsushima, Kondo, et al., 2003). These studies on *A. thaliana* suggested that PYK10 and its closest homologous genes, *BGLU21* and *BGLU22*, are stored in the ER body compartment.

It was shown that, upon cellular disruption, PYK10 forms a protein complex (Nagano et al., 2005, 2008). Additionally, Nakano et al., (2017) found that in *A. thaliana* roots of PYK10 knock-out mutant, the total myrosinase activity towards indole glucosinolates (IGs) was reduced in comparison with that of wild type. This indicates that PYK10 is a dominant myrosinase in *A. thaliana* roots, thus the dense proteins accommodated in the ER bodies of root epidermal cells have high specific activity towards glucosides.

1.3.3. NAI2 is associated with ER body formation

It was shown that, in *A. thaliana*, the *nai2* mutant lacked ER bodies in seedlings and roots (Yamada et al., 2008). NAI2 specifically accumulates in the ER bodies but not in the ER network, indicating that NAI2 is a major component of the ER body and is responsible for the biogenesis of the ER body in *A.*

thaliana. In the absence of NAI2, PYK10 is distributed throughout the ER network, with reduced protein levels compared with wild-type *A. thaliana*.

1.3.4. The integral membrane proteins MEB1 and MEB2 are putative cation transporters

There are two integral membrane proteins, designated as MEB1 and MEB2, that specifically accumulate in the ER body membranes in *A. thaliana* (Yamada et al., 2013). *MEB1* and *MEB2* were discovered by coexpression analysis (ATTED-II; http://atted.jp) and transcriptomic analysis of the *nai1* mutant. MEB1 and MEB2 are homologous to each other and have weak similarity to the iron/manganese transporters Ccc1p in *Saccharomyces cerevisiae* and AtVIT1 in *A. thaliana* (Kim et al., 2006; Li et al., 2001). MEB1 and MEB2 are believed to have metal transporter activity, and it is possible that MEB1 and MEB2 play a role in the transportation of metal ions or translocation of nutrients; however, their physiological role in plants remains unknown (Yamada et al., 2013).

With regard to the formation of the ER body, MEB1 and MEB2 may form a protein complex with the scaffold protein NAI2. However, this was not observed in the *nai2* mutant, in which MEB1 and MEB2 were distributed throughout the ER network; this suggests that NAI2 coordinates the distribution of MEB1 and MEB2 in the ER body membrane. The possibility of an ER body interacting with adjacent ER bodies was not considered. Therefore, MEB1 and MEB2 might be important for ER body movement and the separation of ER bodies from other ER bodies.

Previous studies indicated that the ER body membrane has a specific protein composition that differs from that of the ER network and suggested that NAI2 is responsible for the organization of these ER body membrane proteins (Nakano et al., 2014; Yamada et al., 2013). Because MEB1 and MEB2 form a protein complex with NAI2 but are distributed throughout the ER network in the *nai2* mutant, it is possible that there is NAI2-dependent allocation of MEB1 and MEB2 in the ER body membrane. Moreover, MEB1 and MEB2 could play a crucial role in the biogenesis and maturation of ER bodies because they interact with NAI2, which regulates constitutive ER body formation and potentially distributes MEB1 and MEB2 in the ER body membrane. However, the role of MEB1 and MEB2 in the morphology and maturation of the ER body has not been investigated. In my thesis, I reveal the role of MEB1 and MEB2 in ER body morphology and movement.

1.3.5. NAI1 also regulates gene expression of proteins localised outside of ER bodies

In addition to the crucial activity of the NAI1 transcription factor in regulating the major components of ER bodies such as PYK10 and NAI2 and the membrane proteins MEB1 and MEB2, NAI1 also regulates the expression of *JACALIN-RELATED LECTIN* genes (*JAL22*, *JAL23*, *JAL31*, and *PYK10-BINDING PROTEIN 1* [*PBP1*]/*JAL30*), *GDSL LIPASE-LIKE PROTEIN* genes (*GLL23* and *GLL25*), and *MD2-RELATED LIPID RECOGNITION PROTEIN 3* (*ML3*) (Hakenjos et al., 2013; Nagano et al.,

2005, 2008). JAL proteins are thought to localise in the cytosol and lack signal peptides (Nagano et al., 2005), whereas GLL25 and ML3 have signal peptides and are found in vacuoles (Hakenjos et al., 2013; Nakano et al., 2012). Both JAL and GLL proteins form a large protein complex with PYK10 after cellular disruption (Ahn et al., 2010; Nagano et al., 2005, 2008), suggesting their functional link to ER bodies. It is possible that proteins localised inside and outside of ER bodies may interact with MEB1 and MEB2 to condense materials for ER bodies or separate the ER bodies from each other and other cytosolic proteins. The specific role of MEB1 and MEB2 proteins *in planta* remains elusive, and my research objectives are to assess phenotypic differences due to the lack of MEB1 and MEB2 in transgenic lines of *A. thaliana* seedlings and investigate the function of MEB1 and MEB2 *in planta*.

1.4. Recent findings revealed that ER bodies are involved in the mustard oil bomb system

In vitro assays revealed that PYK10 has glucosidase activity towards substrates such as IGs (Nakano et al., 2014), 4-methylumbelliferyl (4MU)-glucoside (or 4MUG), 4MU-fucoside (Matsushima et al., 2004), scopolin, and esculin (Ahn et al., 2010). Glucosinolates are thioglucosides that are specific to Brassicales (Halkier & Gershenzon, 2006) and are involved in plant defence against insects and microorganisms. Ahn et al., (2010) used the recombinant PYK10 protein expressed in insect cells and the enzyme-hydrolysed scopolin with high efficiency. Scopolin is a secondary metabolite that belongs to the coumarin class, which widely occurs in the plant kingdom, including the model plant *A. thaliana* (Bayoumi et al., 2008; Bednarek et al., 2005; Kai et al., 2006; Shimizu et al., 2005). Scopolin is a β-O-glucoside of scopoletin and both are considered phytoalexins because they inhibit germ tube growth during plant–fungi interactions, such as with *Sclerotinia sclerotiorum*, *Fusarium oxysporum*, *F. solani*, *Rhizopus stolonifer*, and *Lasiodiplodia theobromae* (Peterson et al., 2003; Prats et al., 2006). However, there is no experimental evidence that scopolin hydrolysis by PYK10 is important for plant defence against fungal infection.

1.4.1. Glucosinolates are activated by myrosinase enzymes

The β-glucosidases (BGLUs) of Brassicales include a unique class of enzymes named myrosinases/β-thioglucoside glucohydrolases (TGGs); they are responsible for hydrolysing glucosinolates, which are precursors of active defence molecules. Myrosinases are involved in defence against insects, fungi, and bacteria (Hopkins et al., 2009) because they convert glucosinolate to active molecules by cleaving a glucoside from glucosinolates. Canonical myrosinases (e.g. *Sinapis alba* myrosinase MB1) contain a unique amino acid signature that enables *in silico* prediction of their identity based on nucleotide sequence data (Burmeister et al., 1997). These myrosinases are localised in special cells called the myrosin cells within plant tissues. One of the unique features of this signature is a conserved basic residue (lysine or arginine) in the substrate pocket which can form

electrostatic interactions with the negatively charged sulfate group of glucosinolates. The glutamate residue that serves as a proton donor in O-glucosidases was found to be substituted by glutamine in these myrosinases, resulting in the strict reduction of O-glucosidase activity (Burmeister et al., 1997).

In *A. thaliana*, six genes (*TGG1–6*), including two pseudogenes, *TGG3* (J. Zhang et al., 2002) and *TGG6* (Andersson et al., 2009), encode these canonical myrosinases and contribute to the mustard oil bomb system. *TGG1* and *TGG2* are primarily expressed in leaves (Xue et al., 1995), whereas *TGG4* and *TGG5* are primarily expressed in roots (Andersson et al., 2009; Barth & Jander, 2006; Zhou et al., 2012). These four myrosinases have conserved lysine/arginine and glutamine residues in the substrate pocket and have hydrolytic activity towards glucosinolates. The activation of glucosinolates are triggered upon cellular damage, as the substrate and the enzymes stored in the vacuoles of S-cells and myrosin cells respectively.

Alternatively, the other β-glucosidases without these specific amino acids were thought to be inactive towards glucosinolates (Rask et al., 2000). However, PEN2 (also known as BGLU26) was shown to have myrosinase activity to hydrolyse indol-3-ylmethyl glucosinolate (I3G) and 4-methoxy-I3G (4M-I3G) (Bednarek et al., 2009). PEN2 plays an important role in *A. thaliana* immunity through its myrosinase activity (Bednarek, 2012) against various microbes, including fungal pathogens such as *Blumeria graminis*, *Plectosphaerella cucumerina* (Sanchez-Vallet et al., 2010), *Magnaporthe oryzae* (Maeda et al., 2009), *Leptosphaeria maculans* (Elliott et al., 2008), *Colletotrichum* species (Hiruma et al., 2010), and the growth-promoting endophytic fungus *Piriformospora indica* (Jacobs et al., 2011). Similarly, in plant interactions with another class of arbuscular eukaryotes named Oomycetes, it was reported that PEN2 plays a significant role in immunity against *Phytophthora brassicae* (Schlaeppi et al., 2010) and *Pythium irregularum* (Adie et al., 2007). However, PEN2 myrosinases and glucosinolates act against both pathogens and beneficial microbes.

To avoid constitutive hydrolysis of glucosinolates, which are likely to accumulate in vacuoles, myrosinases may be separated from their substrates into distinct cellular or subcellular compartments. However, in a mustard oil bomb system using canonical myrosinases, enzymes and substrates accumulate in different cells called myrosin cells and S cells respectively, which initiate the enzymatic reaction upon damage (Andersson et al., 2009; Ferber et al., 2020; Ratzka et al., 2002). This intercellular partitioning does not require specific subcellular compartments for storage, and myrosinases accumulate in the vacuoles of myrosin cells, possibly because vacuoles are the largest organelles.

1.4.2. PYK10 has myrosinase activity

A wider range of β-glucosidases are distributed in the *A. thaliana* genome and they are classified into 10 subfamilies (Z. Xu et al., 2004); however, only one subfamily, which includes BGLU18–26, has an

ER retention signal. Besides PYK10/BGLU23, BGLU21 seems to accumulate in the constitutive ER bodies. Alternatively, BGLU34–39 are canonical myrosinases, and they have glutamine and glutamate (Q and E) in the active site and a lysine or arginine at aglycone-binding site (Nakano et al., 2017).

Although the recombinant PYK10 is unable to hydrolyse a glucosinolate, sinigrin (Ahn et al., 2010), it does hydrolyse another glucosinolate, I3G. Sinigrin consists of a core thioglucoside structure with a short aliphatic side chain, and belongs to aliphatic glucosinolates (AGs), which are largely different from the indolyl group present in IGs, such as I3G and 4M-I3G. Therefore, it is suggested that PYK10 may show glucosinolate substrate specificity that depends on the difference of the side chain. Brown et al., (2003) reported that IGs are abundant in *A. thaliana* roots, and ER bodies and PYK10 are also highly abundant in roots. Based on a coexpression analysis from a public microarray database (ATTED-II; http://atted.jp), there was a strong correlation between PYK10 and set of genes corresponding to glucosinolate metabolism, suggesting a functional link between PYK10 and IGs (Pfalz et al., 2011). Finally, research conducted by Nakano et al., (2017) showed that PYK10 has specific activity towards I3G and 4MUG, and reduction in total myrosinase activity in root extracts from *pyk10 bglu21* knockout mutants. Taken together, these lines of evidence demonstrate that PYK10 is a myrosinase.

1.4.3. PYK10-associated proteins modulate enzyme activity of PYK10

JAL proteins, GLL proteins, and proteins containing the MATH domain form a large protein complex with PYK10 after cell disruption or damage (Ahn et al., 2010; Nagano et al., 2005; Yamada et al., 2008). These proteins constitutively accumulate in separate cellular organelles: PYK10 in the ER body, GLLs in the vacuole, JALs in the cytosol, and MATHs in the plasma membrane (Marti et al., 2010; Nagano et al., 2005; Nakano et al., 2012; Oelmüller et al., 2005). The β-glucosidase activity of PYK10 is higher after complex formation; this also suggests plausible roles of JALs and GLLs as activators of PYK10 (Nagano et al., 2005, 2008).

Stimulation of β-glucosidase activity of PYK10 can also be carried out solely by PBP1 (Ahn et al., 2010). PBP1 recruits PYK10 and its two homologues, BGLU21 and BGLU22, that may form oligomers to hydrolyse their substrates. ER body-mediated defence against herbivory has been shown in a dual choice feeding experiment using woodlouse (*Armadillidium vulgare*). Woodlouse preferred to eat seedlings of an ER body BGLU-deficient mutant (*pyk10 bglu21*) and a glucosinolate-deficient mutant (*myb28 myb29 cyp79b2 cyp79b3*) compared with wild-type seedlings, suggesting that both glucosinolate and ER bodies are crucial for plant defence against herbivory. Therefore, ER bodies are likely involved in glucosinolate bioactivation (Yamada et al., 2020). Collectively, these findings combined with wound inducibility indicate that ER body BGLUs assemble with JALs and

GLLs to efficiently produce toxic substances when cells are damaged by insect feeding or pathogen infection.

1.4.4. ER body myrosinase activation differs from classical myrosinases

The differential subcellular localisation of β-glucosidases in epidermal cells and myrosin cells indicates that β-glucosidase activities are required for specific cellular functions, including those of endomembrane systems. Evolutionary events related to the loss of signal peptides appear to occur independently, suggesting that each event could reflect the acquisition of specificity in enzyme function. For example, PEN2 is known to be localised in the periphery of peroxisomal membranes, which may enable their accumulation at the penetration sites in response to the challenge of *Blumeria graminis f. sp. hordei* (Bgh) (Lipka et al., 2005).

PEN2 acts as a component of plant resistance against pre-invasion of fungi. Additionally, PEN2 is required for pathogen-triggered callose deposition, which indicates that the PEN2-dependent callose accumulation works as physical barrier for resistance to microbial pathogens (Clay et al., 2009). PEN2 also activates a glucosinolate, 4MI3G, upon pathogen challenge, and pathogen entry increases in the absence of PEN2 (Bednarek et al., 2009). PEN2 and PYK10 have similar myrosinase activity, and their mechanism of resistance against soil-borne fungi could be similar. However, the mechanism of glucosinolate activation by PEN2 is different from that of canonical myrosinases because PEN2 activates glucosinolate without inflicting cell damage or cell disruption during Bgh challenge on the leaf epidermis, whereas canonical myrosinases activate glucosinolate only after damage to tissues, including myrosin cells and glucosinolate accumulating cells, which are located close to leaf veins. Therefore, the canonical myrosinase system may not interfere with the PEN2 myrosinase system at the epidermis.

Brassicales plants may have evolved ER bodies as a defence strategy different from these myrosinase systems. Because glucosinolates accumulate in vacuoles, PYK10 accumulation in the ER bodies facilitates separation of the enzyme from the substrates at the subcellular level in a single cell. A recent study of the cell type-specific metabolome revealed the detailed cellular distribution of glucosinolates in *A. thaliana* roots (Moussaieff et al., 2013). The data showed that IGs accumulate in the columella, cortex, epidermis, endodermis, and stele. These findings and that of Nakano et al., (2017) indicated that PYK10 and IGs co-exist in the same cells in *A. thaliana*.

The canonical myrosinase system might be energetically expensive as the glucosinolates, and enzymes are allocated in the same compartment of cells but in different cells. In this scenario, activation of glucosinolates would require physical damage to the plant tissues. However, ER body-mediated defence allocates the substrate and enzyme into different subcellular compartments; activation of the substrate in this manner may not require substantial tissue damage. This could be

facilitated by either vesicle transport of the ER body enzyme to the vacuolar substrate, co-secretion of the enzyme and the substrate on the epidermal surface, or collapse of membrane structures within a single cell due to wounding. It is possible that, depending upon the nature of the stress, either of the scenarios could impact the ER body-mediated bioactivation system of glucosinolates. Therefore, subcellular compartmentalization of enzymes by ER bodies could be highly effective against fungal and bacterial pathogens that usually start the infection process by invading single plant cells (Figure 1.3).

Signal transduction, as a cue of either enzyme or substrate translocation, is necessary to activate the IGs. In such cases, biotic stress can trigger the translocation of enzymes and/or substrates in living cells and activate the ER body-mediated defence system, similar to PEN2 (Bednarek et al., 2009; Lipka et al., 2005). Alternatively, it is also possible that chemical factors, such as pH or protein factors (including chaperones), regulate the activity of ER body-accumulating β-glucosidases. It is plausible that, similar to PEN2, PYK10-mediated activation of IGs has a potential role in biosynthesis of active compounds that are important for plant–microbe interactions. However, the precise role of PYK10 in plant–microbe interactions remains unknown.

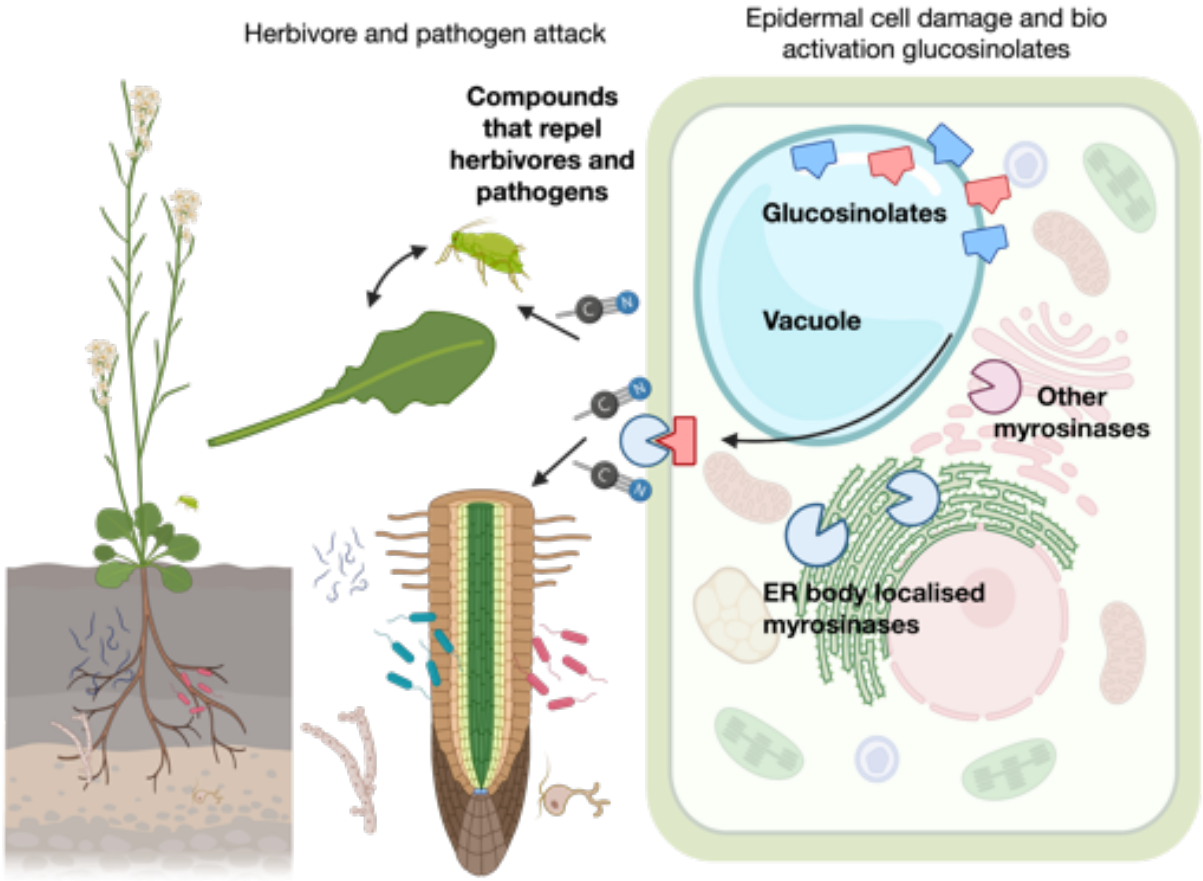

Figure 1.3: The single-cell mustard oil bomb system releases compounds that repel herbivores and pathogens. The indolic and aliphatic glucosinolates are localised in vacuoles are shown in red and blue colours respectively, other myrosinases and PYK10 myrosinases localised in ER bodies are shown in red and blue colours respectively. PYK10-mediated hydrolysis of indole glucosinolates produce compounds that repel herbivores and pathogens.

1.5. Research objective

In first chapter of my thesis, I address the question *"What is the role of MEB1 and MEB2 proteins in the morphology of the ER body?"* It is known that MEB1 and MEB2 are membrane proteins that show putative transporter activity of metal ions in a yeast assay system. It is likely that MEB1 and MEB2 play a role in the morphology of the ER body and the accumulation of cations within plant cells. Therefore, I hypothesised that, compared with wild-type plants, *meb1meb2* mutants show (a) different ER body phenotypes and (b) altered ion accumulation.

In the second chapter, I answer the question *"What is the role of ER bodies and their substrate in shaping the root microbiota?"* PYK10 is known to have myrosinase activity towards IGs and provides resistance against microbes (Nakano et al., 2017; Sherameti et al., 2008). Both PYK10 and IGs are abundant in roots, and it is likely that PYK10 and IGs play a role in the structure of the root microbiota assembly. Therefore, I hypothesised that (a) mutants with genetically impaired PYK10/BGLU21 genes have altered root microbiota assembly, (b) the structure of the root microbiota of mutants is altered because of the lack of compounds produced that are coordinated by PYK10-mediated hydrolysis of IGs, and (c) the performance of mutant plants is reduced after germinating with fungi because of the role of PYK10 and IGs in fungal invasion.

2. CHAPTER I: ER body membrane proteins MEB1 and MEB2 are involved in ER body morphology and metal ion allocation

2.1. Summary

In this chapter, I assess the role of the MEB1 and MEB2 proteins in the ER body phenotype and their impact on the plant ionome. First, I established a method to quantitatively capture morphological characteristics and movement of ER bodies from micrograph images. Micrographs are made up of pixels that have information on position and intensity. From the pixel information, I calculated three types of features (spatial, intensity, and Haralick) of the ER bodies in *A. thaliana* cotyledons. Together, these parameters were subjected to multivariate analysis to estimate the morphological diversity of the ER bodies in the *meb1* and *meb2* knockout mutants. Next, I calculated the movement of the ER bodies using positional information in a series of time-lapse images. I captured similar morphological diversity and movement within ER body phenotypes in several microscopy experiments performed in different settings and scanned with different objectives. In addition, I found differences in the morphology and movement of the ER bodies between wild-type *A. thaliana* and mutants deficient in ER body-related genes. The results indicated that multiple genetic factors are involved in determining the shape and size of the ER bodies in *A. thaliana*. Additionally, the method established in this study enables robust estimation of plant phenotypes by recognizing small differences in complex cell organelle shapes and their movement, which is useful for comprehensive analysis of the molecular mechanism for cell organelle formation that is independent of technical variations.

To understand the physiological function of MEB1 and MEB2, I examined the impact of MEB1 and MEB2 on the plant ionome. Previous studies in yeast cells suggested that MEB1 and MEB2 have cation transport activity. Here, I show that MEB1 and MEB2 have an impact on the overall ion distribution *in planta*. Consistently, I found that the ionome of ER body-deficient mutants differed from that of wild-type plants. These results suggest that ER bodies are essential components for ion homeostasis, and MEB1 and MEB2 are associated with ion distribution within the plant cell. Furthermore, I found that seedling growth differed in mutants lacking ER bodies when subjected to higher concentrations of iron (II) or zinc. The plant ionome and seedling growth results demonstrate that the ER body may play a role in cation homeostasis.

2.2. Introduction and hypothesis

MEB1 and MEB2 are integral membrane proteins that accumulate specifically on the ER body in *A. thaliana* (Yamada et al., 2013). MEB1 and MEB2 are co-expressed with NAI1, and the NAI1 transcription factor regulates the expression of MEB1 and MEB2 (Yamada et al., 2013). MEB1 and MEB2 are homologous to each other and share phylogenetic similarity with the iron/manganese transporters Ccc1p in *S. cerevisiae,* and AtVIT1 in *A. thaliana* (Kim et al., 2006; Li & Ward, 2018). It was shown that MEB1 and MEB2 possess metal transporter activity in the yeast heterogeneous expression system, although their specific role in plant physiology remains unknown (Yamada et al., 2013).

MEB1 and MEB2 may allocate cations that are necessary for ER body function, but the influx or efflux of metal ions in ER bodies is not known. MEB1 and MEB2 form a protein complex with the NAI2 scaffold protein, and these MEB proteins diffuse throughout the ER network in the *nai2* mutant; this indicates a role of NAI2 in recruiting MEB1 and MEB2 into ER body membranes (Yamada et al., 2013). Additionally, the ER body membrane has a specific composition of proteins that differs from that of the ER network because the ER body membrane contains MEB1 and MEB2, which suggests that NAI2 is responsible for the organization of the ER body membrane proteins. MEB1 and MEB2 may interact with cytosolic proteins because they have a potential cytosolic domain. MEB1 and MEB2 on ER bodies may prevent the fusion of ER bodies to the vacuole; this prevents the release of PYK10 and mix with its substrate glucosinolates in vacuoles, preventing unwanted hydrolysis. There might be MEB1- and MEB2-interacting proteins that facilitate ER body movement for ER body compartmentalisation in the cell.

2.2.1. MEB1 and MEB2 are putative metal ion transporters

Previous studies have shown that MEB1 and MEB2 proteins are homologous to the proteins of the VACUOLAR IRON TRANSPORTER 1 (VIT1) family, which are involved in metal transport in plants (Kato et al., 2019; Yamada et al., 2013). Both MEB1 and MEB2 appear to have iron and manganese ion transport activity because overexpression of *MEB1* or *MEB2* yields growth of Ccc1p knock-out mutant yeast (*Saccharomyces cerevisiae*) in excess metal condition indicating the gain of metal transportation function in mutant phenotype (Yamada et al., 2013). However, its precise role in plants is still unknown.

2.2.2. MEB1 and MEB2 potentially regulate ER body morphology

Organelle morphology plays a crucial role in cellular functions in plants and animals. Some organelles have definite shapes that have specific functions in cells. In plants, vacuoles do not have a definite shape, yet they are the largest compartments that store biomolecules and compounds that are utilised

or released later. In contrast, mitochondria have a definite shape that plays a specific role in the electron transport system that is facilitated by membrane proteins. However, even a slight morphological change may alter the physiological function of organelles in the cell.

ER bodies are reported to have a spindle-shaped structure unlike other secretory and storage vesicles in plants (as shown in Figure 1.1). There are two mutants of ER body morphology in *A. thaliana*: *nai1-1* and *long ER body-1* (*leb-1*) (Nagano et al., 2009). The *leb-1* genotype has a mutation in *PYK10* and this mutation changes the PYK10 protein from cysteine to tyrosine at amino acid position 29 (C29Y). This PYK10 mutation causes morphological changes by forming longer ER bodies (Nagano et al., 2009); this showed that the packaging of PYK10 is affected by this point mutation, which suggests that the disulfide link at C29 plays a crucial role in ER body morphology.

MEB1 and MEB2 are located in the membrane of the ER bodies. It is possible that they interact with the cytosolic and ER body-luminal proteins because they have a large potential cytosolic domain. However, there is no direct evidence supporting protein–protein interaction of MEB proteins, and it is not clear whether the spindle-shaped ER body morphology is modulated by MEB1 and MEB2 proteins.

2.2.3. MEB1 and MEB2 are associated with NAI2 to form a protein complex

It was hypothesized that, during the formation of ER bodies, NAI2 interacts with PYK10 to form the inner compartment of the ER bodies and independently interacts with MEB1 and MEB2 to localise on the surface of the ER body (Nakano et al., 2014; Yamada et al., 2013). Previous studies showed that MEB1 and MEB2 deficiency does not affect the accumulation of NAI2 proteins, and there is no evidence that the structure of NAI2 differs in the absence of MEB1 and MEB2 (Yamada et al., 2013). Moreover, it remains unclear whether MEB1 and MEB2 interact with the major ER body constituent PYK10. A previous report stated that the protein expression of NAI2 and PYK10 remains unaltered in the absence of MEB1 and MEB2 (Yamada et al., 2013). MEB1 and MEB2 of the ER body may influence the ER body morphology by interacting with proteins localised in the ER body and proteins in the cytosol and ER network. It was shown by Ueda et al., (2010) that, in triple knock-out mutants of MYOSIN XI-K, MYA1/XI-1 and MYA2/XI-2 functional genes, both ER and ER body morphology were disorganised. A link between myosin proteins and MEB proteins has not been discovered, but it might be possible that the disorganised ER body morphology in the mutants was due to the lack of interaction between the cytosolic proteins that are involved in maintaining ER morphology and the MEB proteins. The aggregation of ER and ER bodies in the mutant phenotypes raises the possibility that MEB1 and MEB2 are involved in ER body maturation rather than ER body formation by interaction with cytosolic proteins like myosin XI and F-actin (Ueda et al., 2010). As NAI2 primarily regulates ER

body formation (Ueda et al., 2010), the role of NAI2 on membrane structure by gathering specific proteins may point to the biogenesis of ER bodies and maturation by MEB1 and MEB2.

2.2.4. MEB1 and MEB2 are among a plethora of transporters in plant cellular compartments

Among the plethora of transport-related proteins in plant cells, *A. thaliana* has transporters that are specifically localised in the vacuolar membrane, the ER, and the plasma membrane. A typical membrane metal-transporter protein contains a transmembrane domain and a metal-binding domain. Transport-related proteins coordinate the influx or efflux of the ions within the cell to maintain overall ion homeostasis. Among cation transport-related proteins, the cation diffusion facilitator (CDF) family member METAL TOLERANCE PROTEIN (MTP1) transports heavy metals to vacuoles of leaf epidermal cells (Dräger et al., 2004), IRON-REGULATED TRANSPORTER (IRT1) is localised in the plasma membrane and is responsible for the transportation of iron in seedlings under iron-limiting conditions (Connolly et al., 2002; Dubeaux et al., 2018; Eide et al., 1996), MAGNESIUM TRANSPORTER (MGT3) is responsible for magnesium transport to mitochondria (Conn et al., 2011; Maguire, 2006), ZINC TRANSPORTER (ZIP) and ZINC TRANSPORTER PRECURSOR (ZTP) are responsible for zinc transportation (Grotz et al., 1998; M. Wang et al., 2010), and COPPER TRANSPORTER (COPT5) is responsible for copper transport and modulates interorgan metal translocation (A. Carrió-Seguí et al., 2015; À. Carrió-Seguí et al., 2019). These proteins were determined to transport the corresponding metal cations within plants, which suggests that cation transportation is relevant in physiological processes such as photosynthesis. The genes encoding cation transport-related proteins are up-regulated when plants are grown in cation-deficient conditions in plants. These transporters are located on the membrane of the cellular compartments and play an important role in maintaining overall cation homeostasis through cation influx (Cointry & Vert, 2019; Dräger et al., 2004; Iuchi et al., 2007; S. A. Kim et al., 2006; Sinclair & Krämer, 2012). However, it is unclear how these cations are accumulated or allocated within the cell compartments.

Metal ions act as cofactors for specific enzymes of metabolic pathways associated with the cell cycle, mitosis, defence, growth, and development. Importantly, *Sinapis alba* myrosinases have zinc-binding sites to form a homodimeric structure (Burmeister et al., 1997). Because of the unavailability of the PYK10 crystal structure, it is not clear whether the ER body BGLUs form a similar dimeric structure of canonical myrosinases. Zn or similar divalent cations may be required for the structure of PYK10 myrosinase. Because MEB1 and MEB2 may have Fe influx activity, it is possible that Fe can be used by PYK10 for catalytic activity.

In *A. thaliana* seedlings, VIT1 expression increases under excess iron (Gollhofer et al., 2011, 2014), indicating that VIT1 is involved in the transport of excess iron from the cytosol to the vacuole to reduce cytotoxicity. Even though MEB1 and MEB2 are predicted to be homologous to VIT1, it is

not clear whether MEB1 and MEB2 are functionally similar to VIT1. It is possible that MEB1 and MEB2 play a role in the allocation of cations between the ER bodies and the cytosol to maintain cation homeostasis within the ER bodies and in plant cells. *In silico* analysis and a previously reported gain-of-function experiment in yeast revealed that MEB1 and MEB2 show affinity towards cations such as iron and manganese (Yamada et al., 2013). Therefore, MEB1 and MEB2 are potentially associated with the accumulation of cations within ER bodies.

2.2.5. Research question and hypothesis

In this chapter, I addressed whether MEB proteins are associated with the morphology, movement, and nutrient allocation of ER bodies in plants.

1. *Do MEB1 and MEB2 decorate the surface of ER bodies to modulate the spindle-shaped morphology of ER bodies?*

To address this question, I hypothesised that the morphology and movement of the ER bodies in the *meb1* and *meb2* mutant plants would differ from that of wild-type plants. To test this hypothesis, I conducted confocal microscopy and performed advanced image analysis on mutant and wild-type seedlings of A. thaliana expressing ER-localised GFP (GFPh).

First, I used confocal microscopy to observe ER bodies of the mutant and wild-type plants, and quantified the morphological diversity across the genotypes using image analysis.

Second, I performed a time series experiment using confocal microscopy to observe the mutant plants and estimated the difference in the overall ER body movement over a 10 second time frame.

2. *Do MEB1 and MEB2 have an impact on the ionome of the plants?*

To address this question, I hypothesised that the ionome (the total ion composition) of the plant is altered in mutant plants (*nai1-1*, *meb1-1*, *meb2-2*, and *meb1-1 meb2-1*) compared with wild-type plants. I conducted a plant ionomics experiment by exposing mutant and wild-type plants to conditions with and without methyl jasmonate treatment. I showed that ER bodies both impact the plant ionome and play a role in plant growth under cation-deficient and -excess conditions.

2.3. Materials and methodology

2.3.1. Plant growth conditions

2.3.1.1. Seedling growth conditions

I used wild-type transgenic *Arabidopsis thaliana* cotyledons (Columbia accession) of the following lines: as wild-type (GFP-h), *nai1-1*, *leb-1 bglu21-1* (heterozygous mutant), *meb1-1*, *meb2-1*, *meb1-1 meb2-1* expressing ER-targeted GFP (Table 2.1). The *A. thaliana* seeds were sterilised and cultured in solid media (1/2× Murashige-Skoog [MS] salt [Sigma Aldrich], 250 mM 4-Morpholineethanesulfonic acid (MES)-KOH pH 5.5, 1% sucrose (w / v), and 0.4% gellan gum [Fujifilm]) for 5 or 7 days.

2.3.1.2. Nutrient manipulation experiments

2.3.1.2.1. Cation stress experiment preparation

A stock solution of 100 mM of iron (II) sulfate and zinc sulfate was prepared separately. Fresh half-strength MS medium was prepared with 100 μM of either iron or zinc sulfate from the prepared stock without sucrose. As a mock treatment, the same MS media were used without cation manipulation. In the depleted condition, the stock solution of the chemicals was prepared in half-strength MS (Harbort et al., 2020). Iron was replaced with di-sodium ethylene-dinitrilo-tetra-acetic acid (EDTA) Na_2-EDTA for Fe-depleted conditions and $ZnSO_4$ was replaced with Milli-Q water for Zn-depleted conditions. The pH was adjusted to 5.5 using MES–KOH, and no sucrose was added to the media.

2.3.1.2.2. Seedling growth and treatment

The *A. thaliana* seeds were cultured in a similar way as described in section 2.3.1.1. After 5 days, the seedlings were transferred to new plates containing 100 μM of cation sulfate solution or in the absence of cations and mock treatment.

Table 2.1: Transgenic lines of *Arabidopsis thaliana* used in this study.

Genotype and alias	ER body phenotype in cotyledons	Description
wild-type (GFP-h)	Normal	Considered as wild-type as it is the background of all other mutant lines
nai1-1 (*nai1*)	No ER bodies	Mutation in a transcription factor
leb-1 bglu21-1 (*leb1bglu21*)	Long and few	Mutation in ER body components
meb1-1 (*meb1*)	Similar to wild-type but smaller	Mutation in an ER body membrane protein
meb2-1 (*meb2*)	Round, aggregate, and less movement	Mutation in an ER body membrane protein
meb1-1 meb2-1 (*meb1meb2*)	Round, aggregate, and less movement	Mutation in ER body membrane proteins

2.3.2. Transmission electron microscopy

Seven-day-old cotyledon tissue samples were fixed with 2.5% glutaraldehyde and 2% paraformaldehyde in 0.1 M cacodylic buffer for 18 h at 4°C. The samples were then postfixed for 1 h in 1% osmium tetraoxide and dehydrated by a graded series of ethanol (50%, 70%, 90%, and 100%) and propylene oxide. The samples were embedded at 60°C using the PolyBed 812 kit. Ultrathin sections were collected on 300-mesh grids made of copper from embedded samples by microtomy and later covered with formvar film. Microtomy was performed with the Leica EM UC7 microtome. The sections were then contrasted using uranyl acetate and lead citrate. Microscopic observations were made with a JEOL JEM 2100HT electron microscope (Jeol Ltd, Tokyo, Japan) using an accelerating voltage of 80 kV. The images were taken with a 4000 × 4000 camera (Tietz Video and Image Processing Systems [TVIPS]) equipped with EMMENU ver. 4.0.9.87.

2.3.3. Phenotypic analysis of seedling growth

2.3.3.1. Scanning of seedlings

After transferring the seedlings to a new plate containing the treatment media, I used the Cannon Lide 120 scanner to scan the bottom part of the plate. Plates were scanned before and after treatment to quantify growth under cation stress in the absence of functional genes related to the ER body.

2.3.3.2. Measurements of overall seedling length

Scanned images were used to track seedling length before and after treatment using the free hand tool available in Fiji software. The freehand tool was used to mark the epicotyl and the hypocotyl all together and calculate the length (mm) of the selected region of interest.

2.3.4. Phenotype analysis using confocal microscopy

2.3.4.1. Image acquisition

After cultivation, the cotyledons were dissected and the cell walls were stained with a 100 μg/mL propidium iodide (PI) solution by implementing some modifications to the protocol described by M. Li & Sack, (2014). Then, the cotyledons were subjected to confocal imaging under 20× and 25× objectives. I performed three independent experiments using two different staining methods:

(1) Cotyledons were treated in PI solution for 10 min and then immediately observed (setting 1, Figure 2.1);

(2) Cotyledons were treated in PI solution for 5 min, infiltrated with a vacuum pump for 1 min, and then washed with deionised water for 2 min (setting 2, Figure 2.1).

Subsequently, three image datasets were generated: setting 1 with a 20× objective, and setting 2 with 20× and 25× objectives.

Image acquisition was performed with a confocal laser scanning microscope (Zeiss LSM 880) under 20× and 25× objective lenses with a gain range between 450 and 500 and a digital gain of 1 to reduce the saturation of the pixel intensity. Glycerol was used on the coverslip during slide preparation for the 25× objective lens. An Argon 488 laser and a HeNe laser were used for image acquisition, and the magnitude of intensity was kept at 10 to reduce photobleaching and autofluorescence. The pinhole was set at 10 μm for optimal laser accommodation on the objective lens. The images were acquired for the two distinct settings in the 1024 × 1024 pixel range by averaging 2 pixels in such a way that each pixel explained 0.42 μm^2 of the area of the object in the 20× objective and 0.54 μm^2 in the 25× objective. Scanning was performed bi-directionally across the stage and with a colour depth of 8 bits at a scan speed of 5. Z-stack acquisition was performed at a depth of 2 μm/slice to obtain volumetric image information. Images were acquired from the surface of the epidermal cells of the cotyledons in a randomised order.

2.3.4.2. Image analysis for morphological diversity

Raw images were pre-processed and segregated by correcting dimensions and RGB channels, merged by the *MaxContrastProjection* package in R (Sauer & Fischer, 2019), and, finally, the pixels were normalised. Image pre-processing and statistics were conducted using the R packages *EBImage* (Pau et al., 2010), *vegan* (Dixon, 2003), and *r-base*, respectively. The z-stack images were merged using specific criteria for the *MaxContrastProjection* package (https://github.com/arpankbasak/ERB_DynaMo) (Basak et al., 2021). The red channel was specified for the cell walls, and the green channel was specified for the ER bodies to segregate the merged image of 3D plant tissue in 2D representation.

Segregation was performed to maintain homogeneity among images for downstream analysis (*segregate* script in the ERB_DynaMo pipeline) (Basak et al., 2021). Specific masks were generated to assign cell and ER body borders for the corresponding channels. Knitted images from the projection were taken as input for the analysis pipeline, and feature extraction was performed using adaptive thresholding and segmentation principles (parameters in ERB_DynaMo (Basak et al., 2021). Adaptive thresholding of the intensity of the pixels was used to detect the cell and ER body borders. Quartile-based selection was considered for ER body segmentation and cell segmentation. An ER signal emits 95% of the total GFP in a tissue section; therefore, in an image, an ER body showed a dense signal in a small pixel area. PI fluorescence showed a jigsaw puzzle pattern of the cell walls. Two masks for the ER bodies and cell walls were set separately with a given range of parameters. Segmentation was conducted using Voronoi tessellation with both masks. Segmented cells with a surface area of

5000 pixels per unit were also chosen for analysis of ER body characteristics. The image-, segmented cell-, and ER body-wise morphological features were computed (Figure 2.1).

2.3.4.3. Analysis of ER body movement

Time-lapse images were obtained with a confocal microscope using the same procedure as described above. The z-stack merged images were used from an independent experiment, and the blue channel was set as the initial positions of an ER body (ER body at time 0). Every time-point image stores information of the initial position of the ER bodies in the blue channel. Subsequently, these images were segmented into cell-wise images, and ER bodies were extracted at each specific time point while retaining their initial position. The initial and specific time-point images were projected to show the movement across the time period. These images were used to extract position features that showed dislocation (*segregate_dynamics* and *segmentation_dynamics* scripts; https://github.com/arpankbasak/ERB_DynaMo) (Basak et al., 2021). The processed images were converted into a movie to visualise the dynamics (*MomentProjection* script; https://github.com/arpankbasak/ERB_DynaMo) (Basak et al., 2021).

Table 2.2: List of features used to estimate the ER body morphology and movement. The Haralick features were estimated in the minimum and maximum ranges for accurate quantification.

Types of features	Feature short name	Definition	Description
Intensity			
	b.mean	Mean intensity	Fluorescence intensity features provide independent statistics of the pixel distribution of objects detected in the images.
	b.sd	Standard deviation of intensity	
	b.mad	Mean absolute decrease of intensity	
	b.q001	1% Quantile of intensity	
	b.q005	5% Quantile of intensity	
	b.q05	50% Quantile of intensity	
	b.q095	95% Quantile of intensity	
	b.q099	99% Quantile of intensity	
Haralick			
	h.asm	Angular second moment	The Haralick features in an image are computed from statical properties of the Gray-Level Co-Occurrence Matrix (GLCM). These sets of features provide an association of the detected objects with neighbouring pixels, which provides estimates of morphological differences within the detected objects
	h.con	Contrast	
	h.cor	Correlation	
	h.var	Variance	
	h.idm	Inverse difference moment	
	h.sav	Sum of averages	
	h.sva	Sum of variance	
	h.sen	Sum of entropy	
	h.ent	Entropy	
	h.dva	Difference in variance	
	h.den	Difference in entropy	
	h.f12		

	h.f13	Measurement of the correlation coefficient	
Spatial and shape			
	s.area	Surface area	Shape and spatial properties provide descriptive statistics of the structure of the detected object.
	s.perimeter	Perimeter	
	s.radius.mean	Mean radius of the object	
	s.radius.sd	Standard deviation of the mean radius	
	s.radius.max	Maximum radius	
	s.radius.min	Minimum radius	
Position (used for quantification of movement)			
	m.cx	Centre of mass on the x-axis;	The centre of mass detects the exact location of the object (x- and y-axis) in the image. This information is also used to calculate the total distance covered by the object in a time series experiment.
	m.cy	Centre of mass on the y-axis	
			All measures are in pixels.

2.3.4.4. Image data analysis

2.3.4.4.1. Analysis of the dynamics of the cellular features

I used the initial and final position of the ER body characteristics from the location parameter (m.cx and m.cy in the feature matrix, Table 2.2) to calculate the cosine distances; this represented the displacement of the cellular characteristics along the pathway. I calculated the moving average to obtain a better approximation of the organelle dynamics across time. I used a non-linear regression method, locally estimated scatterplot smoothing (LOESS), and a generalised linear model (GLM) for statistical analysis.

2.3.4.4.2. Feature extraction in segmented cells

Data analysis of the images was conducted in the R environment using customised scripts in an Argon server x86_64-conda_cos6-Linux-gnu (64-bit): CentOS Linux 7 (Core). The features were detected based on the Otsu method (Otsu, 1979) with adaptive thresholding at the 97% quantile of pixel intensity. After adaptive thresholding, a feature matrix was generated from the stack of cells and ER body-like features describing intensity, spatial, Zernike moment (W.-. Y. Kim & Kim, 2000), and Haralick features (Haralick et al., 1973). Statistical analysis was performed on the characteristic matrix of the spatial, intensity, and Haralick features within the segmented cells of the images (Table 2.2).

The obtained features were distinguished by unique feature IDs that are referred to as the feature matrix for further analysis (*segmentation* script). The z-scores of the morphological parameters in the feature matrix were grouped and aggregated for the corresponding samples, and the mean z-score was calculated. The feature matrix was aggregated to analyse the sample images, segmented cells, and features. Further stratification was performed based on experimental settings, staining method, genotype, days after germination, and objective lens. Constrained canonical analysis (CCA) was used

to show the variation of ER body characteristics explained by genotype. I used a permutation-based analysis of variance (PERMANOVA) test over 1000 iterations to compute statistical significance. The feature matrix was further merged, and selected features were used to compute the morphological variation (*featurematrix* script) (Basak et al., 2021; Haralick et al., 1973). The feature matrix was used to compute descriptive statistics and compare genotypes (*image* and *segmentedcells* scripts) (Basak et al., 2021). Segmented cells were clustered and copied into a new directory for visualisation (*pool_features* script) (Basak et al., 2021). The morphological differences in the cellular features within the clustered cells were analysed. The statistical analyses that are suggested to be performed on the feature matrix are described below, and the feature matrix can also be used for customised data analysis.

2.3.4.4.3. Multivariate analysis

Multidimensional scaling (MDS) analysis was performed with normalised feature matrices between the images of the samples. Pearson's correlation was used to compute the dissimilarity. This type of analysis was performed between segmented cells or between plants. Furthermore, clustering of k-means was performed on a normalised feature matrix of the segmented cells. To compute statistical relevance, genotype was a fixed factor, whereas the objective used and corresponding experiment were random factors. Descriptive statistics were performed on the set of 40 characteristics measured in the samples followed by multiple hypothesis correction using a false discovery rate (FDR) cut-off ≤ 0.05.

2.3.4.4.4. Flexible and mixture discriminant analysis

The proportion of features in segmented cells that showed a distinct ER body morphology was calculated by flexible (FDA) and mixed discriminant analysis (MDA). Normalised z-score characteristics were also used to model the proportion of ER bodies that were distinct for the observed genotypes. MDA and FDA were conducted based on whether the characteristics of the corresponding genotypes are linearly separable (Hastie et al., 1994; U. Schmid et al., 2009).

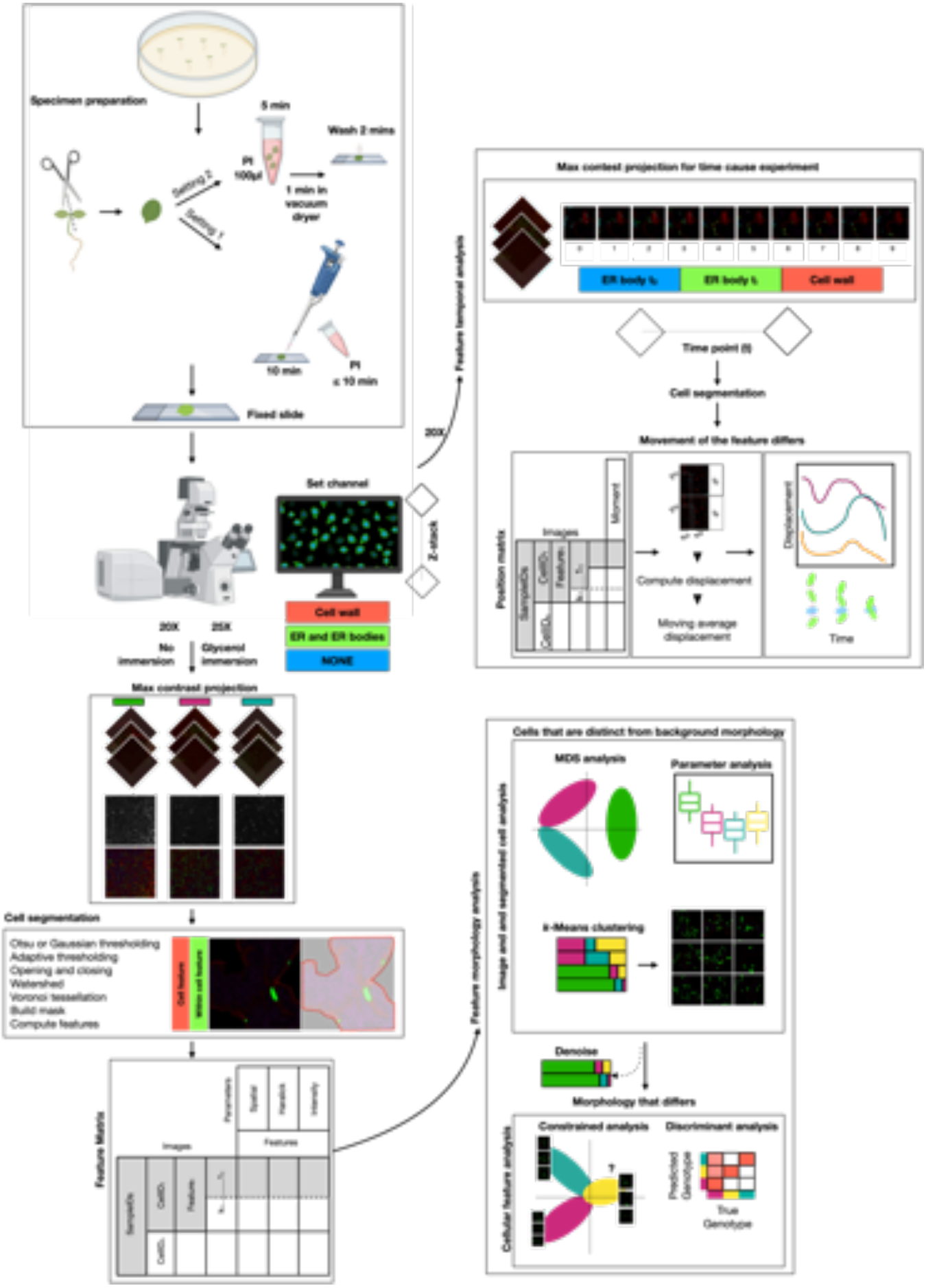

Figure 2.1: Flow chart showing image acquisition in different settings, image processing, segmentation, quantification, and data analysis of ER body morphology and dynamics.

2.3.5. Ionome analysis of seedlings

The 5-day-old seedlings of wild-type plants were sprayed with 100 mM methyl jasmonic acid (meJA treatment) acid for 48 h and harvested for ionome analysis. All seedlings were freeze-dried overnight using a lyophiliser until the dry weight was 10% of the fresh weight. The total ion content was quantified by inductively coupled plasma mass spectrometry (ICP-MS) following the method described by Almario et al., (2017). The dried plant material was homogenised to a fine powder and approximately 5 mg were digested in 15 mL Falcon tubes using 500 μL of HNO_3 (67%) overnight at room temperature. The next day, loosely closed samples were placed in a 95°C water bath until the liquid was completely clear (approximately 30 min). After being cooled to room temperature for 10–15 min, the samples were placed on ice and 4.5 mL of deionised water was carefully added to the tubes; then, the tubes were weighed. The final solutions were centrifuged at 4°C at 2000 g for 30 min and the supernatants were transferred to new tubes. The elemental concentration was determined using an inductively coupled plasma mass spectrometry Agilent 7700 ICP-MS (Agilent Technologies) following the manufacturer's instructions. The dilution factor was calculated as follows: dilution factor = (final weight – empty Falcon tube weight) / sample dry weight).

2.4. Results

2.4.1. MEB1 and MEB2 are associated with ER body morphology

2.4.1.1. Image projection and single-cell segmentation

To analyse the morphology of the ER bodies, I acquired images from confocal microscopy of 7-day-old cotyledons and performed single-cell segmentation. Morphological analysis was carried out on 240 images of wild-type and mutant plants using EBImage, with 18 z-stacks on average. These images were merged with the max contrast projection, resulting in 41 images of wild-type plants, 42 images of *nai1-1* mutants, 40 images *leb-1 bglu21-1* mutants, 40 images of *meb1-1* mutants, 38 images of *meb2-1* mutants, and 39 images *meb1-1 meb2-1* mutants (Table 2.3). Subsequently, cell segmentation based on red fluorescence of cell walls provided 12408 cell images in wild-type plants, 17205 cell images in *nai1-1* mutants, 9109 cell images in *leb-1 bglu21-1* mutants, 10664 cell images in *meb1-1* mutants, 6862 cell images in *meb2-1* mutants, and 10357 cell images in *meb1-1 meb2-1* mutants (Table 2.3). Furthermore, segregation of 66605 cells from 240 images resulted in 29629 cells with ER body-like features (Table 2.4). The objective of cell segmentation was to distinguish between the cells that showed ER body and ER phenotypes. To overcome this bias in the image-level resolution, I performed cell segmentation to quantify the morphological parameters.

Table 2.3: Summary of cell segmentation analysis.

Genotype and alias	Setting	Objective	Days after germination	Segmented cells	Images
wild-type (GFP-h) (GFPh)	1	20×	7	6181	19
	2		5	830	5
			7	1712	6
		25×	5	1401	5
			7	2284	6
nai1-1 (*nai1*)	1	20×	7	8901	20
	2		5	1215	5
			7	2712	6
		25×	5	1514	5
			7	2863	6
leb-1 bglu21-1 (*leb1bglu21*)	1	20×	7	5188	20
	2		5	630	5
			7	804	5
		25×	5	1078	5
			7	1409	5
meb1-1 (*meb1*)	1	20×	7	6723	20
	2		5	292	5
			7	1208	5
		25×	5	695	5
			7	1746	5
meb2-1 (*meb2*)	1	20×	7	2552	18
	2		5	613	5

			7	1428	5
		25×	5	829	5
			7	1440	5
meb1-1 meb2-1 *(meb1meb2)*	1	20×	7	4893	19
	2		5	1021	6
			7	1797	5
		25×	5	1117	5
			7	1529	4

Table 2.4: Summary of the ER body-like features.

Genotype	Objective	Days after germination	Cells with ER-body-like features	No. of Images
wild-type (GFPh)	20×	5	271	3
		7	5949	21
	25×	5	813	4
		7	811	6
leb-1 bglu21-1	20×	5	251	3
		7	4920	23
	25×	5	504	5
		7	732	4
meb1-1	20×	5	52	2
		7	5234	22
	25×	5	275	5
		7	767	5
meb2-1	20×	5	71	2
		7	1989	17
	25×	5	529	4
		7	494	5
meb1-1 meb2-1	20×	5	518	4
		7	4509	19
	25×	5	406	5
		7	531	3

2.4.1.2. Image-wise and segmented cell-wise analysis

The z-scores of 40 features (6 spatial, 8 intensity, and 26 Haralick features) were calculated from the merged micrograph images of the wild-type and mutant plants based on GFP fluorescence of ER and ER bodies. Based on these characteristics, I calculated the Pearson correlation coefficient (PCC) and performed MDS analysis (Figure 2.2).

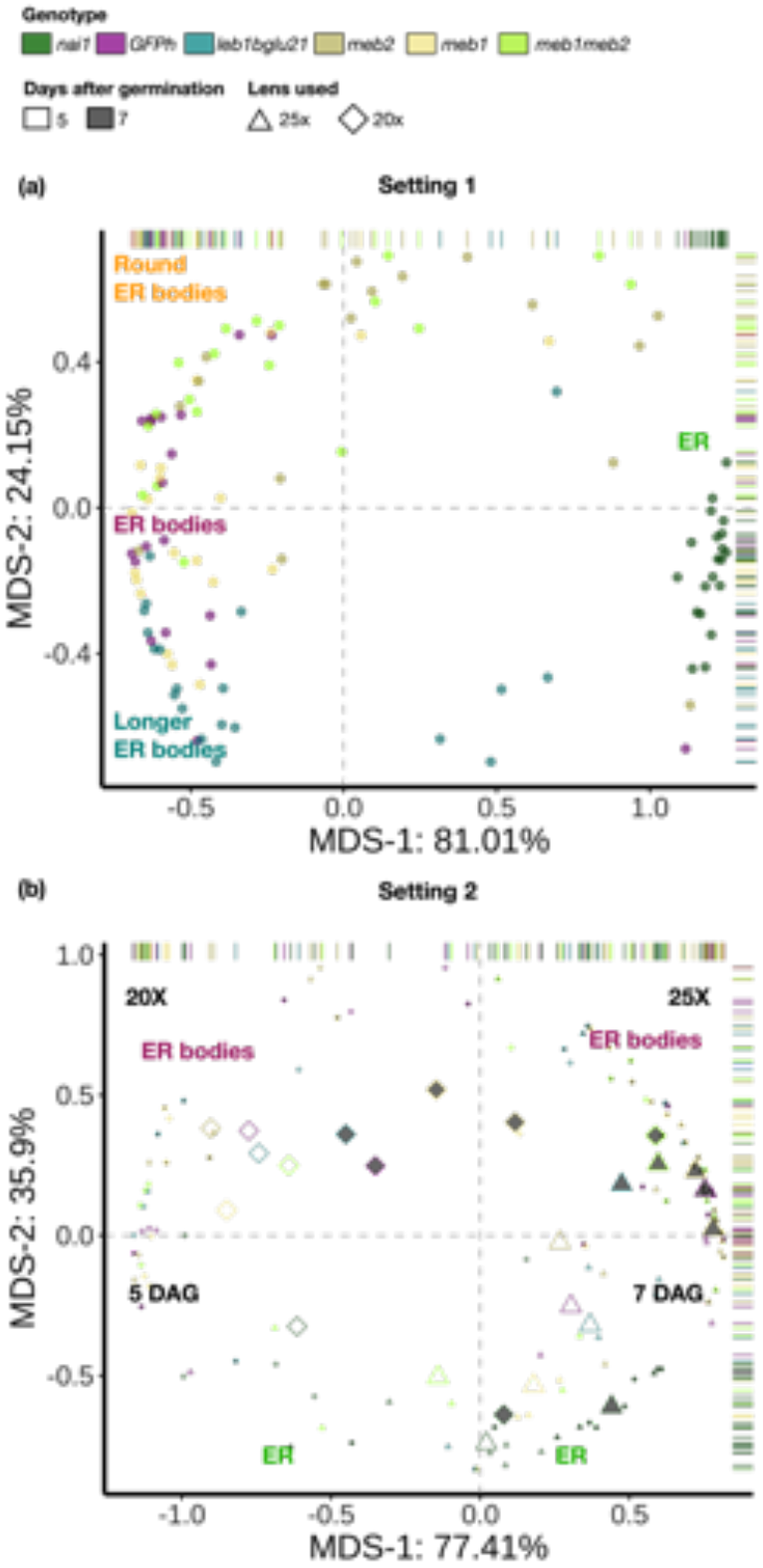

Figure 2.2: Image-wise analysis of cotyledons in setting 1 (a) and setting 2 (b) by MDS of 40 features extracted from microscope images. The x- and y-axes indicate the variation explained in MDS-1 and MDS-2 (eigen values), respectively. The colours indicate the genotype in both settings. Only in setting 2 (b), the shape indicates the lens used to acquire the images, the colour fill indicates the days after germination, and the larger size indicates the median of the group in axes 1 and 2.

The MDS analysis showed that the micrograph images can be separated on the chart according to ER body morphology. The MDS1 and MDS2 axes explained 81.01% and 24.15% in the image analysis, respectively (Figure 2.2a). Separation between the images of the wild-type and *nai1-1* mutant plants occurred along the MDS1 axis, showing that the axis indicates the presence or absence of ER bodies (Figure 2.2b). Separation between wild-type plants and *leb-1 bglu21-1* double mutants occurred along the MDS2 axis; this suggests that the MDS2 axis explains the ER body length because *leb-1 bglu21-1* double mutants had longer ER bodies compared with wild-type plants. I found that the *meb1-1* and *meb1-1 meb2-1* mutants had a higher variation along the MDS2 axis, suggesting that these mutants had shorter ER bodies (Figure 2.2b). The micrograph images were even further separated in the chart, explaining 24.15% of the MDS2 axis.

In addition, I also performed MDS analysis other image data from a different batch of experiments performed with setting 2 with a 25× objective lens and differently (5- and 7-day old seedlings) aged cotyledons (Figure 2.b). With these data, the variation in the image captured the difference in the objective lens and cotyledon age along the MDS1 axis (77.41%). Additionally, I found

image variation with the presence or absence of ER bodies along the MDS2 axis (35.9%). Moreover, it was clear that samples from *nai1* mutants were separated along the MDS2 axis, and the difference in morphological diversity, i.e., the variation explained in first two axes, was large (eigen value > 1); this may be due to an insufficient number of variables in MDS that explained morphological differences in image-wise analysis.

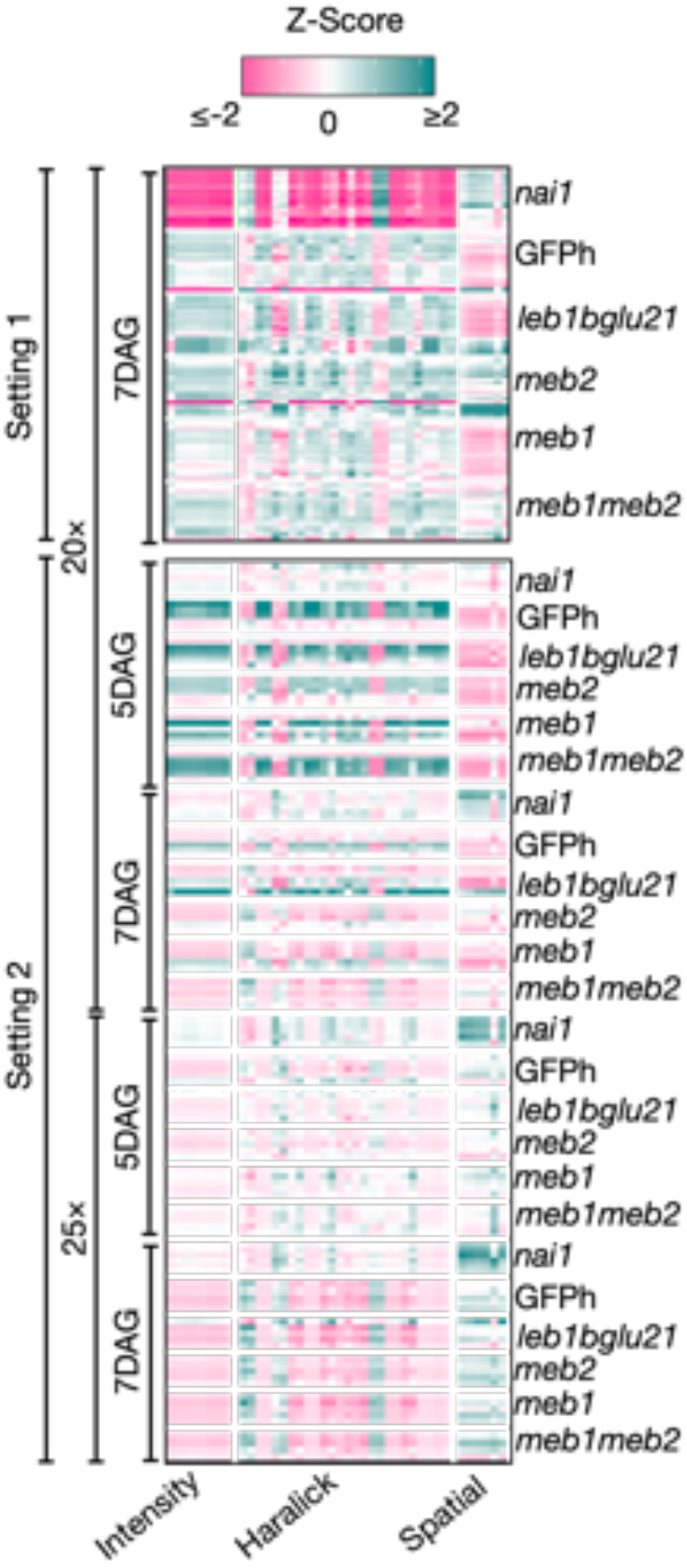

Figure 2.3: Heatmap of the 40 features (z-scores) for the mutant and wild-type seedling sample images with setting 1 and setting 2.

In the heatmap of the feature matrix (Figure 2.3) and box plots (Figure 2.4), significant differences were found in the pattern between plants with ER bodies (e.g. wild-type) and plants without ER bodies (*nai1* mutants). This dataset included 7-day-old plants, PI staining setting 1, and a 20× objective lens, which indicates that the images can be separated into two groups depending on the presence or absence of ER bodies in this dataset. The difference in the intensity, Haralick, and spatial features demonstrated that the morphology was altered in the MEB1- and MEB2-deficient mutants, which is consistent with the previously reported longer ER bodies in the *leb-1 bglu21-1* mutant. These findings suggest that MEB1 and MEB2 regulate ER body morphology. Furthermore, the distribution of the Haralick features that corresponded to genotype showed differences in z-scores between the ER and ER bodies. Among the ER body mutants, the *meb1* and *meb2* mutants showed slight texture differences compared with the wild-type GFPh (Figure 2.3 and 2.4).

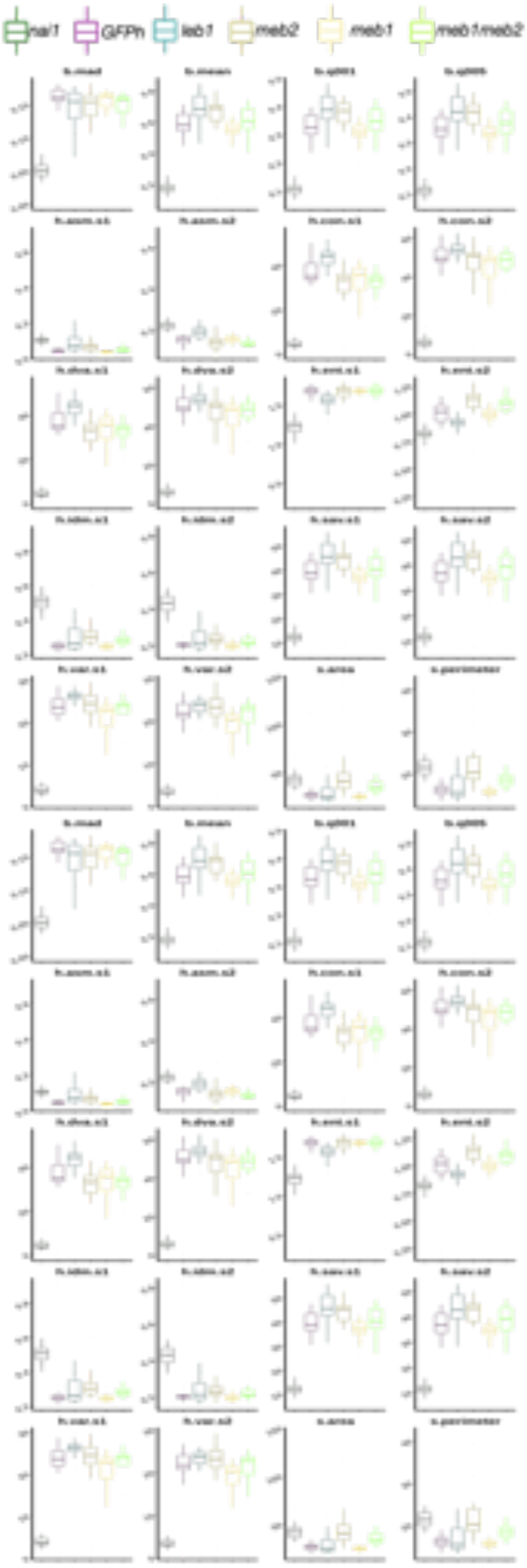

Figure 2.4: Box plots showing the pixel distribution of the 40 features (Table 2.2) quantified from the micrographs of wild-type and mutant seedlings.

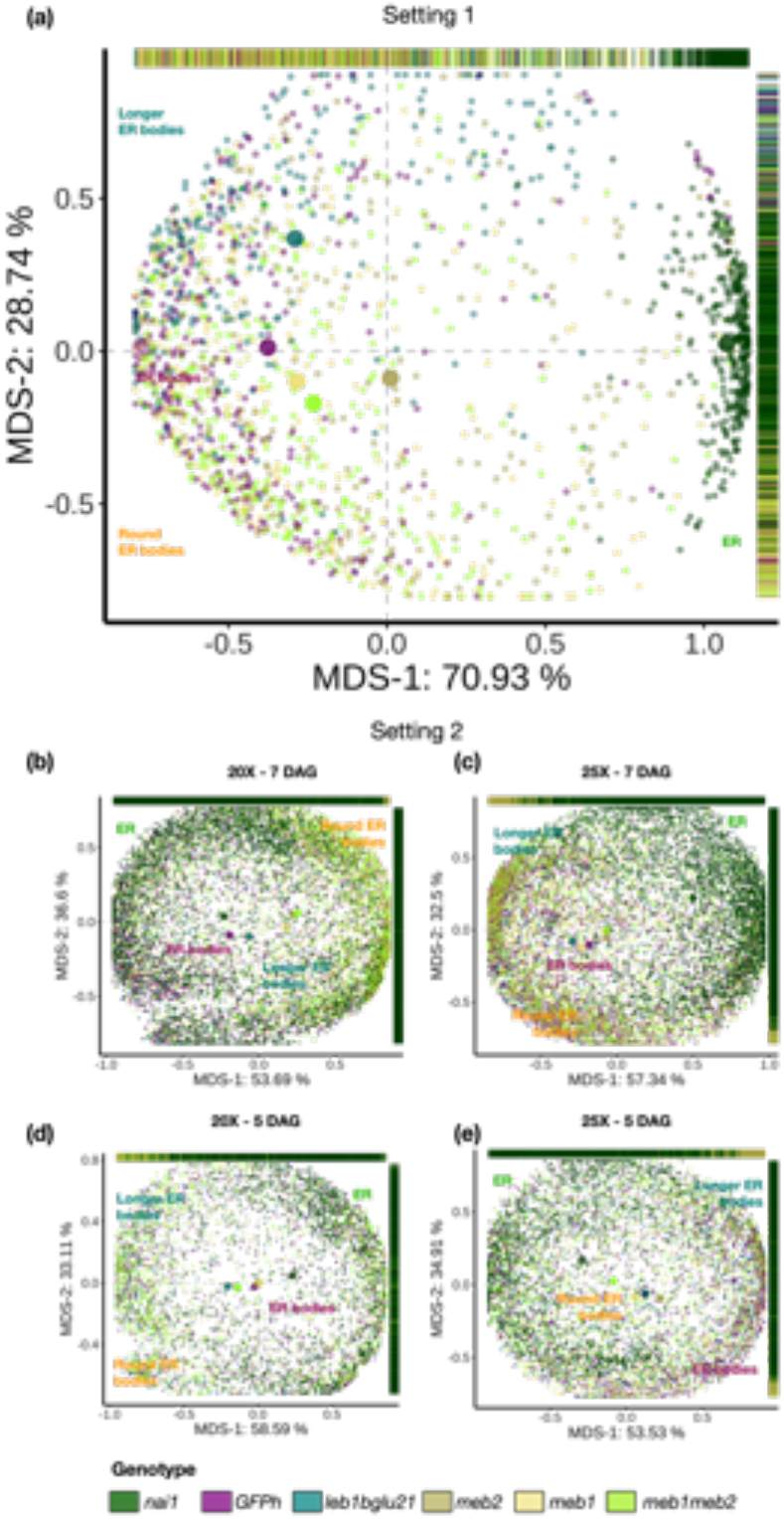

Figure 2.5: Segmented cell-wise analysis of cotyledons in setting 1 (a) and setting 2 (b,c,d and e) by MDS of 40 features extracted from microscope images. The x- and y-axes indicate the variation explained in MDS1 and MDS2 (eigen values), respectively. The colours indicate the genotype in both settings. Only in setting 2 (bottom four panels), the morphological diversity in 7-day-old seedlings using 20× objective lens (b) and 25× objective lens (c), and the morphological diversity in 5-day-old seedlings using 20× objective lens (d) and 25× objective lens (e).

The MDS analysis was carried out on segmented cell images from another dataset with 7-day-old plants, PI staining setting 1, and a 20× objective lens. Cells that had ER bodies were clustered from cells devoid of ER bodies in the MDS plots, showing the maximum variations of MDS1 is 70.93%, and MDS2 is 28.74% respectively (Figure 2.5a). This suggests that the morphological parameters for the ER bodies are specific and discrete from those of the ER network. When I performed the MDS analysis of segmented cells with other image data for groups with different objective lenses and seedling ages, the separation between cells with and without ER bodies became mild. In the images with the 20× objective, the variation explained with and without ER bodies was 53.69% and 58.59% in MDS1, and 36.6%, and 33.11% in MDS2, respectively (Figure 2.5b and d); consistently, the variation explained in the images from the 25× objective were 57.34% and 53.53% in MDS1, and 32.5% and 34.91% in MDS2, respectively (Figure 2.5c and e). Therefore, although the estimation is robust for image taking methodology, an experiment is desirable to precisely predict the variation in the ER body morphology in MDS analysis. Using multiple measures, I found morphological diversity between cells with ER and

ER bodies. The cells with ER bodies showed subtle differences in MEB1- and MEB2-deficient mutants.

2.4.1.3. Image-wise and segmented cell-wise analysis

The characteristic data of the cell-wise images were subjected to k-means clustering (k = 60) within each genotype (Figure 2.6) to determine the group of cells that have different ER body phenotypes. The x-axis of the heatmap represents the sample images and the y-axis represents the clusters. The colour intensity represents the mean z-scores obtained for the segmented cells within the images. The k-means clustering separated cells that were devoid of ER bodies similar to cells of the *nai1-1* mutant, and the remaining cells were showing ER body phenotypes with morphological differences. Clusters showing features similar to those of the ER body and not similar to ER were used for further analysis to evaluate the overall effect of the genotype that explained the ER body morphological diversity.

The features of the segmented cell clusters in different experimental settings were merged in one dataset. Furthermore, individual images were observed from the cluster representatives to verify the presence of ER bodies (Figure 2.6). The images from the majority of the clusters showed variations in ER body morphology that were consistent with the k-means clustering of groups of cells with similar phenotypic variants among the genotypes. In clusters 10, 12, 19, 31, and 54, I found that cells mostly belonged to plants without *leb-1 bglu21*. In clusters 2, 18, 28, and 44, I observed that cells mostly belonged to mutants (Figure 2.6 left heatmap). Clusters 2, 7, 50, 51, and 54 revealed morphologically distinct ER bodies (Figure 2.6 right bar plot and segmented cells). Cluster 16 was identified as an autofluorescence-like feature and was presumably noise in images.

For this approach, I excluded cell images from *nai1-1* mutants and stomata cells without ER bodies or autofluorescence. Consequently, 29629 cells from 66605 cell-wise images were classified as having ER bodies after k-means clustering analysis. At the resolution of segmented cells, I found difference in the ER and ER body morphology between the mutant and wild-type plants. Furthermore, anomalies in texture features within ER bodies were detected in clustered cells.

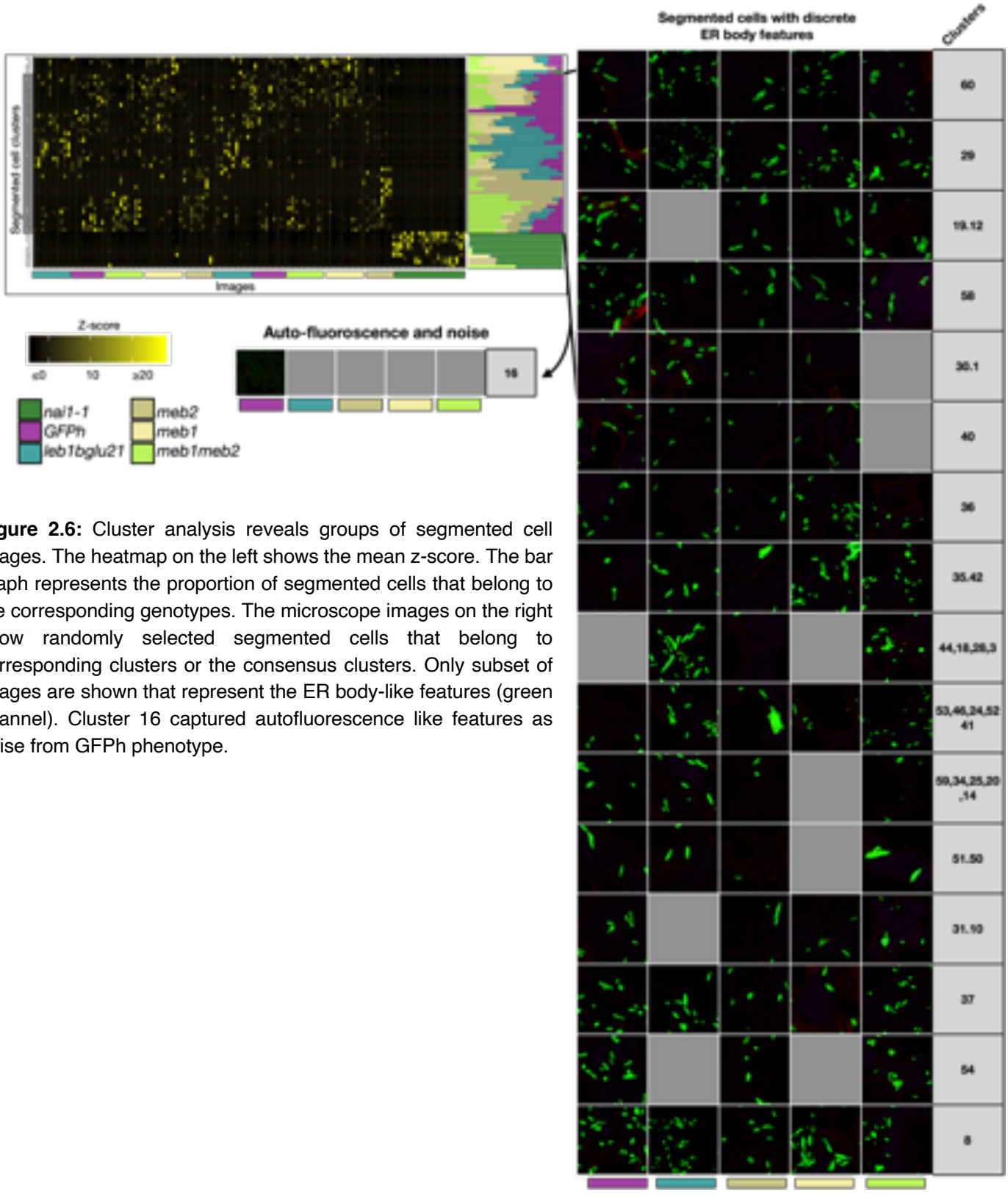

Figure 2.6: Cluster analysis reveals groups of segmented cell images. The heatmap on the left shows the mean z-score. The bar graph represents the proportion of segmented cells that belong to the corresponding genotypes. The microscope images on the right show randomly selected segmented cells that belong to corresponding clusters or the consensus clusters. Only subset of images are shown that represent the ER body-like features (green channel). Cluster 16 captured autofluorescence like features as noise from GFPh phenotype.

2.4.1.4. Feature analysis of cells with ER bodies

I re-examined the morphological variations of ER bodies by grouping the cell-wise images that showed ER bodies. However, I found differences in the features between 20× and 25× objective lenses when integrating the z-score values of intensity, Haralick, and spatial features (Figure 2.7).

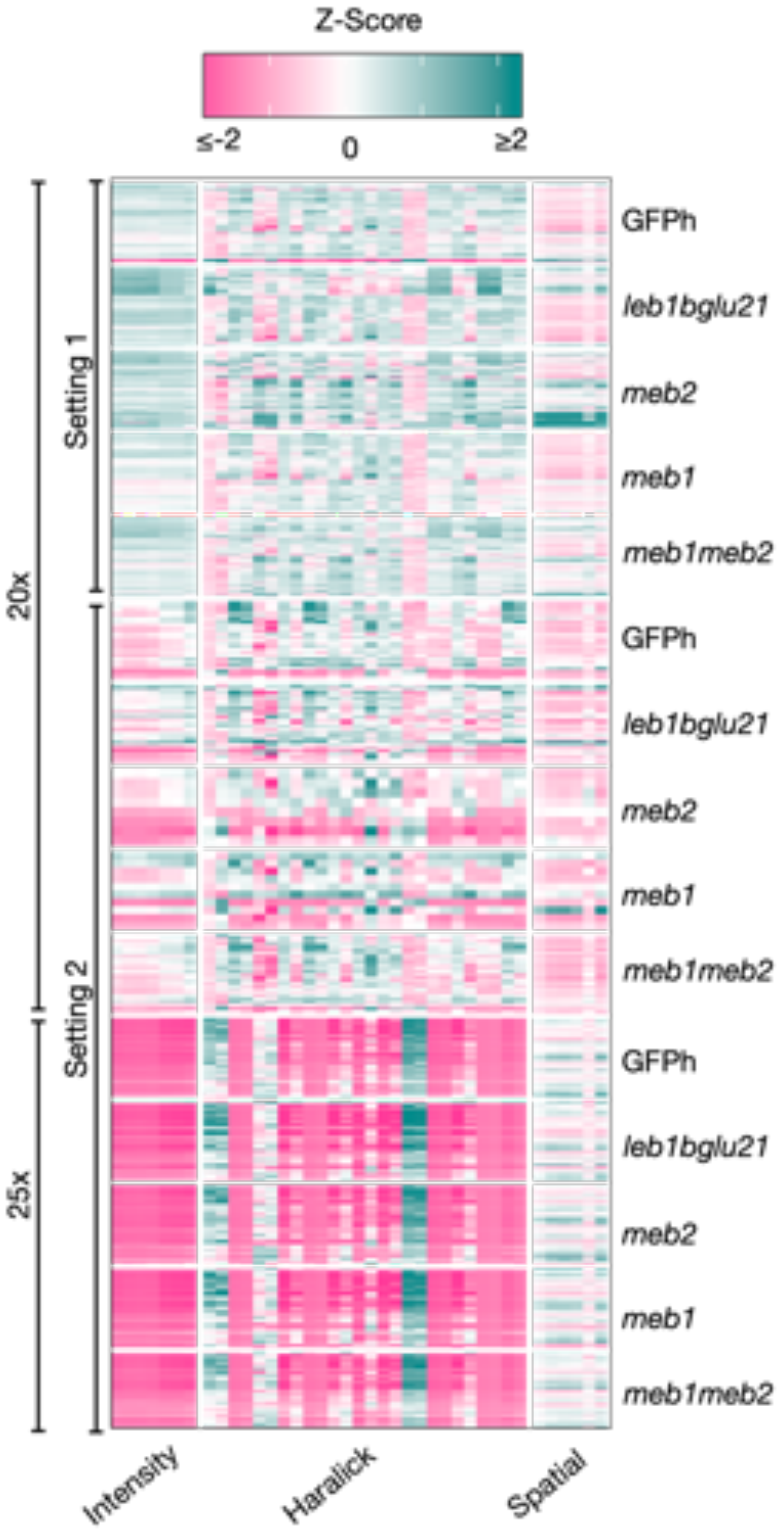

Figure 2.7: Heatmap representing the z-scores of the 40 morphological parameters (x-axis) and the segmented cells clustered to show the ER body phenotype. These clustered cells were obtained from independent experiments conducted in two different settings (setting 1 and setting 2) and under two objectives (20× and 25×).

Therefore, I performed constrained canonical analysis (CCA) on the ER body phenotype within these cells using Pearson's correlation coefficient (PCC) distances to identify variation among the characteristics (Figure 2.8). I set genotype as a fixed factor and the other features (objective lens, plant age, staining method) as random factors in the analysis. The variation explained in CCA1 and CCA2 was 67.49% and 30.7%, respectively. After conditioning the random factors, I observed a significant difference in the feature diversity that depended on genotype. The significance was determined by performing PERMANOVA and CCA using Pearson's correlations between each ER body-like features from each cell (pseudo *p*-value < 0.05, 1000 iterations) (Table 2.5).

Despite the low morphological variation, the constrained ordination revealed that the genotype difference could explain 1.37% of the variance (Figure 2.8a). The segmented images could be grouped image-wise by tracing back to the image source, and different

ER body morphologies, such as long, rounded, and aggregated structures, were found (Figure 2.8b). Therefore, I grouped the segmented images according to k-means clustering (Figure 2.6) within the genotypes and performed constrained ordination of the mean features image-wise.

In this new feature dataset, I found that mutants showed a tendency to separate from each other. This may be due to difference in ER body morphology (Figure 2.8b). Genotype explained 7.56% of the variation (pseudo *p*-value < 0.01), and the variation shown in CCA1 and CCA2 was 60.14% and 31.77%, respectively (Figure 2.8b). The difference between the wild-type and mutant plants were subtle, with marginal deviation of the mutants. Figure 2.8 shows that the wild-type and *meb1-1* mutant plants were placed in the centre, whereas *leb-1 bglu21-1* with long ER bodies shifted to the upper left, and *meb2-1* and *meb1-1 meb2-1* mutants with rounded and aggregated ER bodies shifted to the upper right. Despite such marginal differences, I observed morphological changes in the mutants. This indicates that the effect was consistent in certain populations of segmented cells.

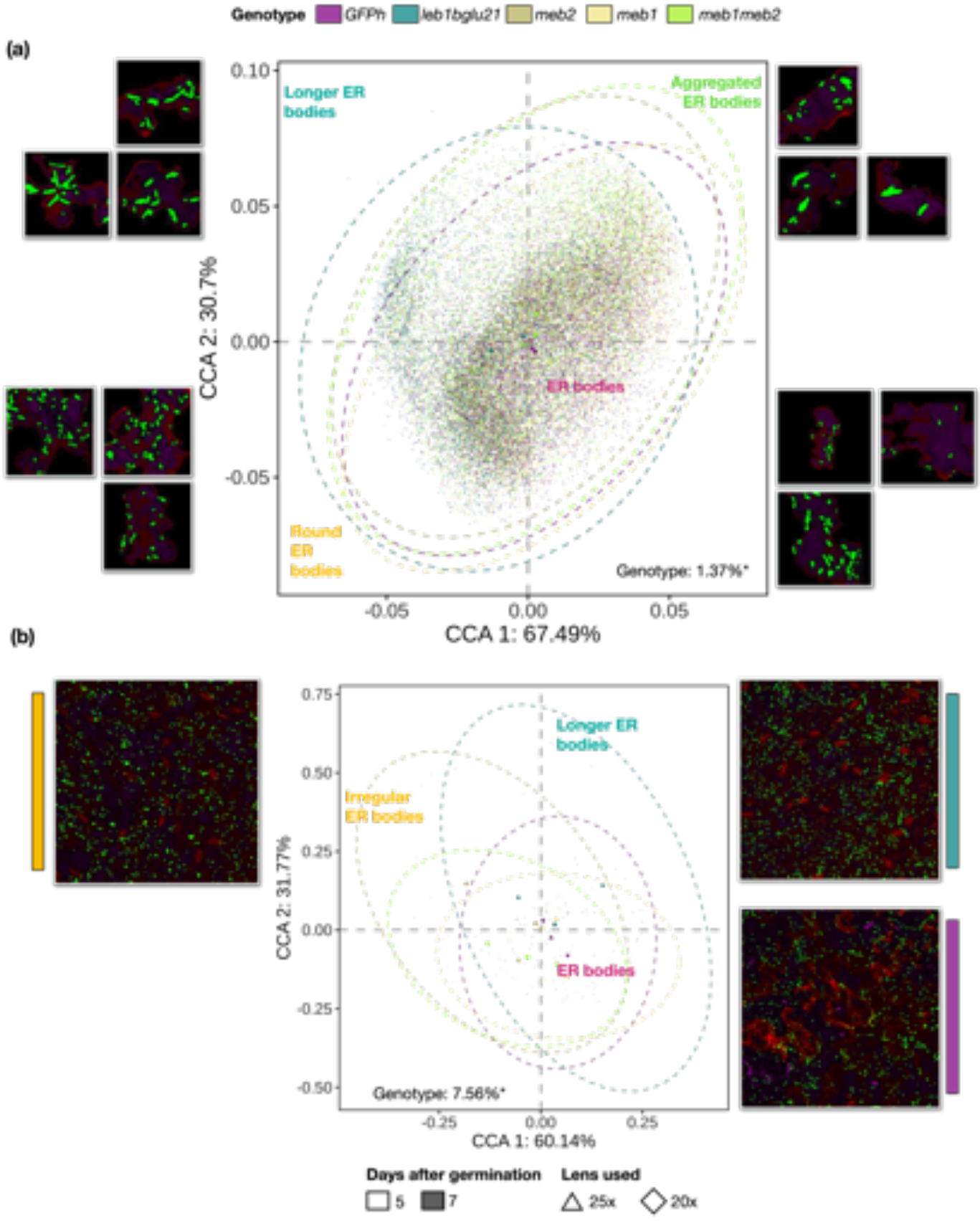

Figure 2.8: CCA performed on the z-scores of the morphological parameters of the clustered cells for each ER body detected from the independent experiments using genotype as a fixed factor. Differences in the colour of the dotted circle represent genotypic differences. The variance explained by genotype was 1.37% (a). CCA was performed on the aggregated morphological parameters of the clustered cells. The variance explained by genotype was greater than 7%. Note that the subtle dispersion of *leb-1 bglu21-1* (blue-dotted circle), *meb2-1* (dark brown-dotted circle), and *meb1-1 meb2-1* (light green-dotted circle) is distinct from the wild-type ER bodies (purple-dotted circle) in the scatterplot (b). The ER bodies are visualised in green channel and the cell wall in the red channel.

Table 2.5: PERMANOVA summary.

		Inertia	Proportion
Image-wise analysis	**Total**	77.678	1
	Constrained	5.8763	0.07565*
	Unconstrained	26.0686	0.33559
Segmented cell-wise analysis	**Total**	14512.0392	1
	Constrained	199.4591	0.01374*
	Unconstrained	11253.6069	0.77546

2.4.1.5. TEM images show altered ER body morphology in the absence of MEB1 and MEB2

Transmission electron microscopy (TEM) image analysis was performed to check whether the morphology was different in ER bodies without MEB1 and MEB2 (Figure 2.9). Subcellular micrographs showed that wild-type ER bodies were generally spindle-shaped, whereas meb1 mutants had smaller, rounded ER bodies (Figure 2.9). Similarly, *meb2* mutants showed aggregated ER bodies with a lower electron density within the ER bodies compared with the wild-type plants. The double mutant deficient in both MEB1 and MEB2 showed ER body morphology similar to that observed in MEB1- and MEB2-deficient single mutants. It should be noted that MEB1 and MEB2 are responsible for ER body morphology and may interact with the proteins inside the ER bodies. Therefore, the TEM images tended to show deformed ER bodies in the MEB1 and MEB2 mutants.

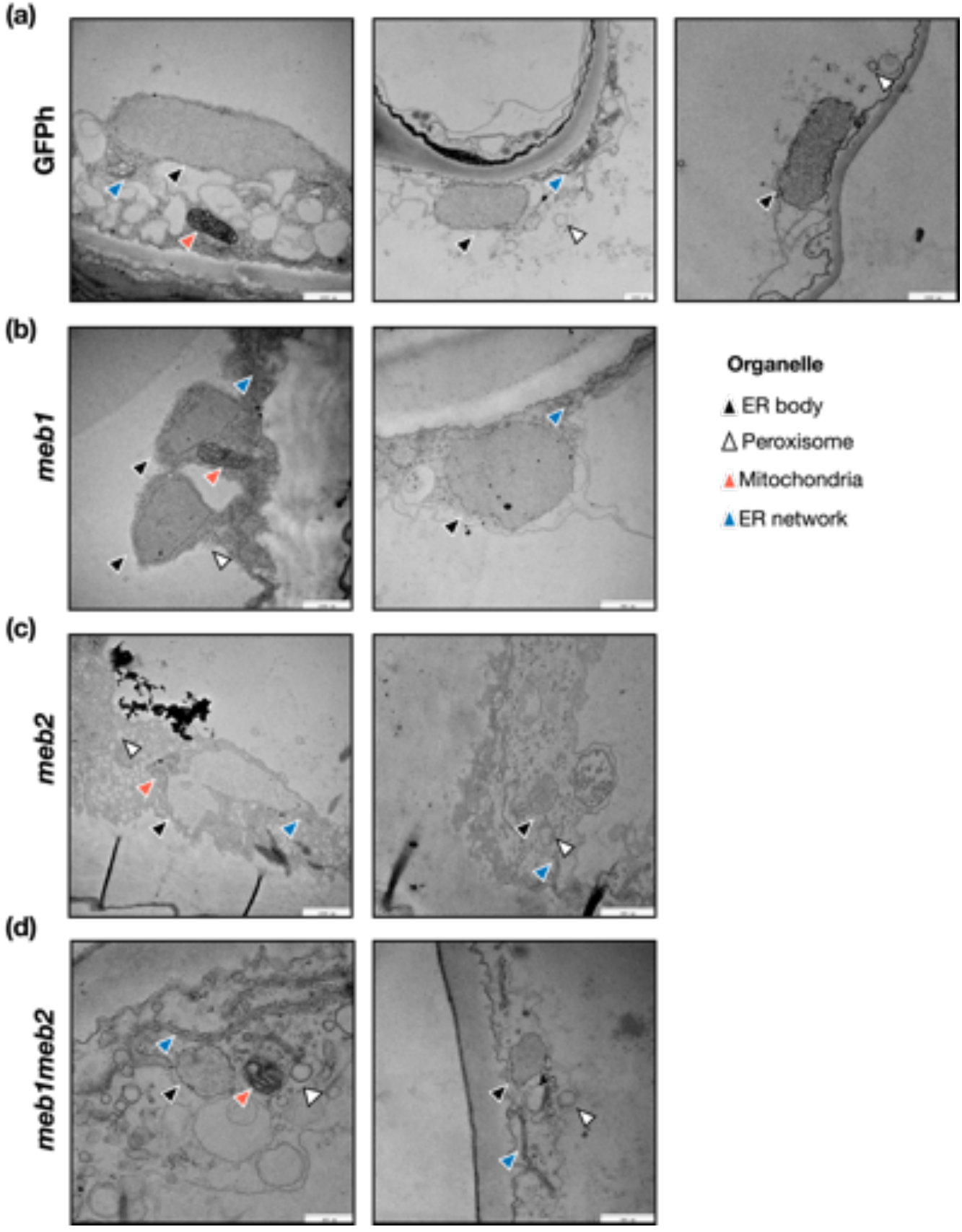

Figure 2.9: TEM images showing that ER body morphology is altered in the absence of MEB1 and MEB2. (a) GFPh, (b) *meb1* is similar to *meb1meb2* (last), and (c) *meb2* is similar to *meb1meb2*. The arrowheads indicate the ER bodies and organelles such as the mitochondria, peroxisome, and ER.

2.4.2. MEB2 proteins are associated with ER body movement

Time-lapse image analysis was performed to examine the difference in ER body movement between wild-type and mutant plants. The blue channel corresponds to the ER body at t_0 and the green channel corresponds to the movement at specific time (t_n). In *meb2-1* mutants, the ER bodies did not separate from the blue channel, indicating that the movement was reduced over time. The merged image showed this in the colour cyan. This was observed in *meb1-1 meb2-1* double mutant but no other genotype. ER body movement occurred over time in wild-type (separation in blue and green channels) and mutant plants; however, I noticed that there was reduced ER body movement in the *meb2-1* and *meb1-1 meb2-1* mutants (mostly cyan, green, and blue merged) (Figure 2.10).

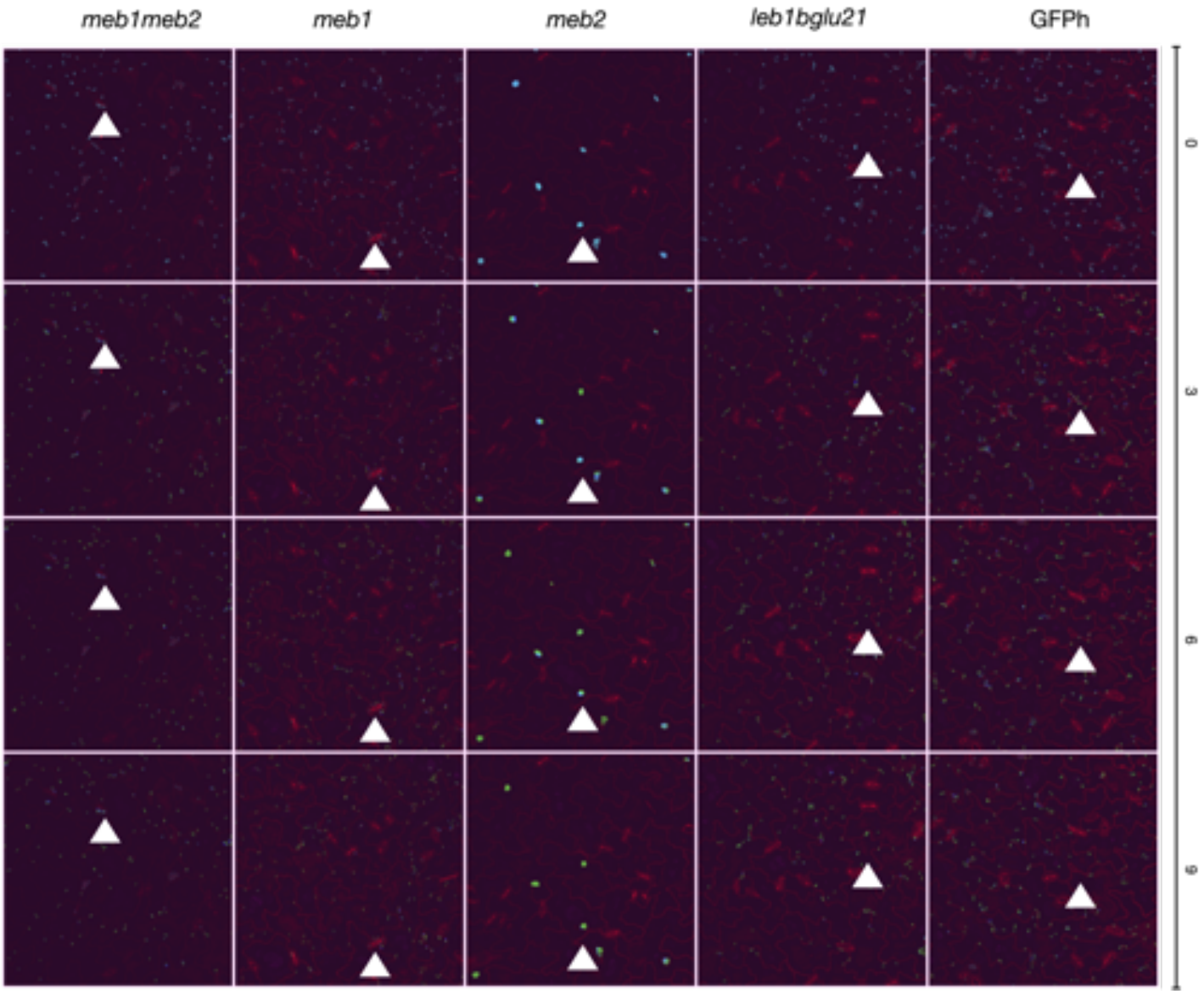

Figure 2.10: Sequential images of 10-s time-lapse. The red channel represents the cell wall, the green channel represents the ER body at the respective time (t_n), and the blue channel represents the ER body at time 0 (t_0). Separation of the blue channel (t_0) and the green channel (t_n) explains the displacement of the ER body in each image. The white pointer indicates the position of the ER bodies at different time interval.

I calculated the average displacement of each ER body from its initial position by estimating the squared cosine distance between the ER bodies. I found that overall movement of the ER body was highest in the wild-type plants over time (Figure 2.11a). Similarly, I observed that the *leb-1 bglu21-1* and *meb1-1* mutants exhibited ER body movement, but not the *meb2-1* mutants, and the *meb1-1 meb2-1* mutants exhibited movement to some extent. Statistical analysis revealed that movement was reduced in the *meb2-1* and *meb1-1 meb2-1* mutant plants compared with the wild-type, and *leb-1 bglu21-1* and *meb1-1* mutant plants (FDR ≤ 0.01) (Figure 2.11b). The findings suggest that the MEB2 protein is involved in ER body movement.

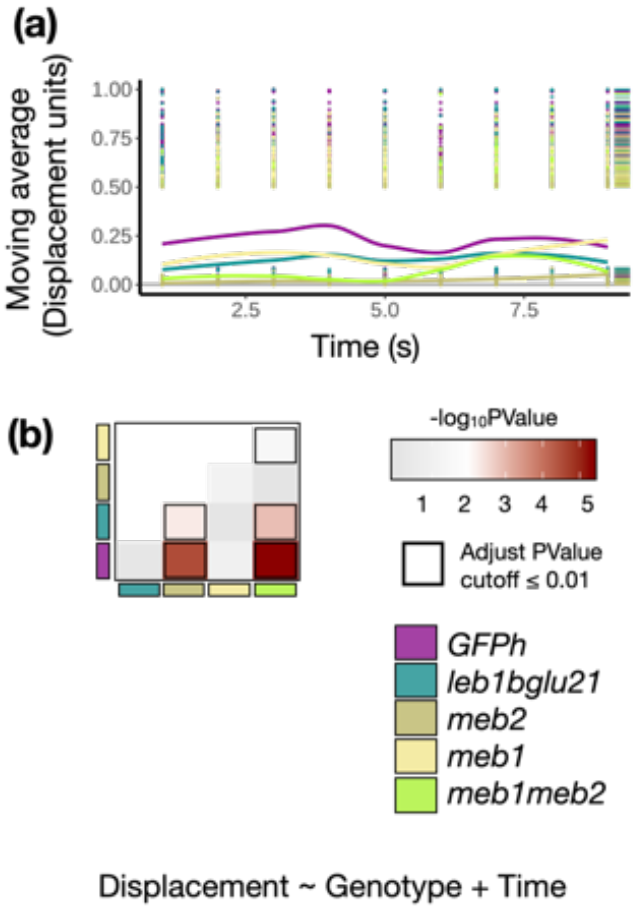

Figure 2.11: Trend of moving average displacement of ER body features detected in mutants over time. (a) Mutant genotypes are marked in different colours. The overall distribution is marked on the strip next to the plot. The lines indicate the median of the distribution among the two populations. (b) Generalised linear model (GLM) analysis. I used genotype as a fixed factor and time as a covariate. The colour intensity indicates the statistical significance denoted by the $-\log_{10}$ *p*-value adjusted by the Benjamini–Hochberg procedure, which was obtained from pairwise comparison between the genotypes with the Tukey HSD method. The box indicates FDR ≤ 0.01.

2.4.3. MEB1 and MEB2 are involved in indirect nutrient allocation

2.4.3.1. Plant ionomics reveals potential ions that are allocated by the presence of ER bodies

Previous studies suggested that MEB1 and MEB2 have a role as a cation transporter (Yamada et al., 2013). Therefore, I investigated whether cation accumulation is altered by MEB1 and MEB2. I hypothesised that the MEB1- and MEB2-deficient mutants trigger plant ionome shifts. To address this, I conducted a plant ionomics experiment using ICP-MS technology to detect differences in ion abundance of mutant compared with wild-type ER bodies (Figure 2.12a). Interestingly, I found that the ion composition differed in wild-type compared with mutant ER bodies (Figure 2.12b). I showed that iron accumulation was significantly altered in the absence of ER bodies. Specifically, I found that iron was depleted in mutant genotypes lacking MEB1 or MEB2 or that had defective PYK10.

Based on constrained ordination analysis and PERMANOVA, I found that the variance explained by genotype and methyl jasmonic acid (meJA) treatment was 33.33% (pseudo p-value = 0.001, PERMANOVA). Using a similar approach, I found that the ionome of genotypes differed when subjected to meJA treatment (variation explained = 35.13%, pseudo p-value = 0.003; PERMANOVA). This was also consistent within the genotype independent of JA treatment (variation explained by genotype = 37.56%, pseudo p-value < 0.001, PERMANOVA). Interestingly, I observed that the ionome of MEB1-deficient mutants with JA treatment was similar to that of wild-type plants (Figure 2.16c). Additionally, the ionome of the double mutant *meb1meb2* differed from that of single mutant and wild-type plants, indicating that cation accumulation depends on the presence of both MEB proteins. Consequently, MEB2 could be associated with JA or stress-induced ER bodies and therefore be involved in plant ER body-mediated defence.

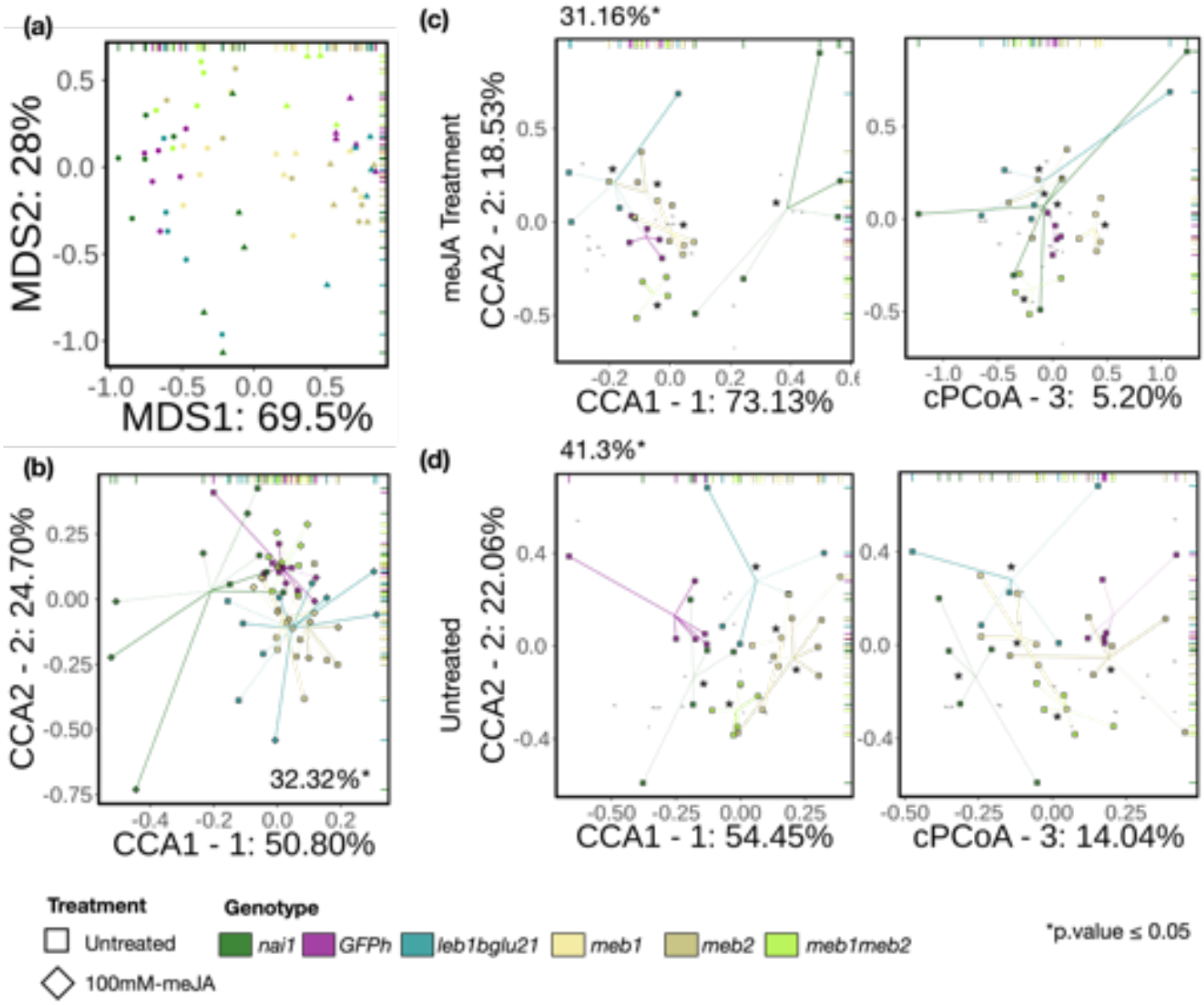

Figure 2.12: The impact of ER bodies in the structure of the seedling ionome. (a) Difference in ionome composition due to the lack of ER bodies. Overall change in ionome by MDS analysis. (b) Change in ionome when 7-day-old seedlings were subjected to 100 mM meJA treatment based on a 1000-iteration CCA PERMANOVA-like test. (c–d) CCA showing the ionome diversity in mutant and wild-type plants under meJA treatment and untreated conditions. The solid and dotted lines indicate further separation in the positive and negative axes, respectively of the third component.

The accumulation of elements such as Fe, P, Mg, and Na significantly differed in mutant compared with wild-type plants. This indicates that these divalent cations are distributed differently in the absence of ER bodies and MEB proteins (Figure 2.13). Therefore, the allocation of these cations depends on MEB proteins. Specifically, Ca was enriched in MEB2-lacking mutants compared with wild-type plants. Similarly, MEB1 and MEB2-lacking mutants showed depletion in As and Sr, and enrichment of Mg; this was consistent in the double mutant *meb1meb2*. This finding indicates that the allocation of these ions may be linked to the presence of ER bodies because they were depleted in the *nai1* and *leb1* mutants (Table 2.6). Furthermore, Ca is crucial for ER and cytosolic proteins that are important for growth, and is associated with gravitropism (Braun et al., 2004; Reuzeau et al.,

1997; Suwińska et al., 2017). In *meb2* mutants, the accumulation of Ca was higher, which indicates a potential role in the function of ER streaming proteins.

Table 2.6: Summary statistics calculated for each ion detected within mutant compared wild-type seedlings under meJA treatment and untreated conditions. Two-group comparison was conducted between Col-0 and mutants by random sampling over 100 iterations, and p-value was calculated for each iteration. The impact was estimated by calculating the proportion of p-value ≤ 0.05, and the impact of each ion was considered significant if the impact was greater than 10%.

Ion	Condition	Genotype	Mean p-value (100 iteration)	Impact (No. of p-values ≤ 0.05)	Mean difference	F-statistics	Impact > 10%
Al	meJA Treated	*leb1*	0.4324	0.06	0.0066	0.3527	FALSE
Al	meJA Treated	*meb1*	0.4718	0.07	0.0065	0.6245	FALSE
Al	meJA Treated	*meb1meb2*	0.4650	0.10	0.0060	0.3617	FALSE
Al	meJA Treated	*meb2*	0.2457	0.31	0.0223	2.4249	TRUE
Al	meJA Treated	*nai1*	0.2057	0.24	0.0479	2.6704	TRUE
Al	Untreated	*leb1*	0.4427	0.01	0.0030	0.1445	FALSE
Al	Untreated	*meb1*	0.4430	0.11	0.0013	0.8771	TRUE
Al	Untreated	*meb1meb2*	0.4778	0.12	-0.0036	0.5564	TRUE
Al	Untreated	*meb2*	0.4436	0.08	-0.0068	-0.8795	FALSE
Al	Untreated	*nai1*	0.5130	0.10	-0.0003	0.6351	FALSE
As	meJA Treated	*leb1*	0.4139	0.04	0.0025	0.7175	FALSE
As	meJA Treated	*meb1*	0.4568	0.05	0.0029	0.5841	FALSE
As	meJA Treated	*meb1meb2*	0.4508	0.19	-0.0045	-0.5871	TRUE
As	meJA Treated	*meb2*	0.3387	0.14	-0.0054	-1.4539	TRUE
As	meJA Treated	*nai1*	0.4647	0.05	0.0006	0.1890	FALSE
As	Untreated	*leb1*	0.2595	0.37	-0.0220	-2.2096	TRUE
As	Untreated	*meb1*	0.0226	0.86	-0.0325	-8.3039	TRUE
As	Untreated	*meb1meb2*	0.0224	0.82	-0.0309	-6.1826	TRUE
As	Untreated	*meb2*	0.0238	0.86	-0.0322	-5.0171	TRUE
As	Untreated	*nai1*	0.0766	0.46	-0.0226	-3.3561	TRUE
Ca	meJA Treated	*leb1*	0.3259	0.57	0.0035	5.4422	TRUE
Ca	meJA Treated	*meb1*	0.2737	0.47	-0.0025	-2.8288	TRUE
Ca	meJA Treated	*meb1meb2*	0.0871	0.55	0.0025	3.1851	TRUE
Ca	meJA Treated	*meb2*	0.4081	0.14	0.0004	1.0344	TRUE
Ca	meJA Treated	*nai1*	0.0965	0.25	-0.0083	-3.4958	TRUE
Ca	Untreated	*leb1*	0.4367	0.17	-0.0013	-1.1281	TRUE
Ca	Untreated	*meb1*	0.4600	0.14	-0.0007	-1.2939	TRUE
Ca	Untreated	*meb1meb2*	0.2249	0.29	0.0019	2.1647	TRUE

Ca	Untreated	*meb2*	0.1466	0.28	0.0042	2.9864	TRUE
Ca	Untreated	*nai1*	0.4880	0.03	0.0003	-0.0822	FALSE
Cr	meJA Treated	*leb1*	0.4169	0.18	-0.0038	-1.3676	TRUE
Cr	meJA Treated	*meb1*	0.3664	0.12	0.0053	1.3257	TRUE
Cr	meJA Treated	*meb1meb2*	0.4826	0.17	0.0015	0.1112	TRUE
Cr	meJA Treated	*meb2*	0.5519	0.07	0.0008	-0.0112	FALSE
Cr	meJA Treated	*nai1*	0.1070	0.51	0.0325	4.7336	TRUE
Cr	Untreated	*leb1*	0.3308	0.23	0.0068	1.9014	TRUE
Cr	Untreated	*meb1*	0.3785	0.05	-0.0043	-1.0386	FALSE
Cr	Untreated	*meb1meb2*	0.4670	0.15	-0.0004	0.5336	TRUE
Cr	Untreated	*meb2*	0.4588	0.04	-0.0028	-0.7741	FALSE
Cr	Untreated	*nai1*	0.5142	0.10	-0.0005	0.3715	FALSE
Fe	meJA Treated	*leb1*	0.2011	0.23	-0.0040	-2.5381	TRUE
Fe	meJA Treated	*meb1*	0.4653	0.07	0.0004	-0.3750	FALSE
Fe	meJA Treated	*meb1meb2*	0.3362	0.29	0.0017	1.9338	TRUE
Fe	meJA Treated	*meb2*	0.4085	0.28	-0.0008	-2.0127	TRUE
Fe	meJA Treated	*nai1*	0.4198	0.20	0.0007	0.2080	TRUE
Fe	Untreated	*leb1*	0.0592	0.58	-0.0053	-4.5580	TRUE
Fe	Untreated	*meb1*	0.0612	0.54	-0.0059	-3.2972	TRUE
Fe	Untreated	*meb1meb2*	0.3298	0.17	-0.0014	-1.5960	TRUE
Fe	Untreated	*meb2*	0.0759	0.55	-0.0065	-4.5434	TRUE
Fe	Untreated	*nai1*	0.4176	0.08	0.0023	1.3170	FALSE
K	meJA Treated	*leb1*	0.3538	0.22	0.0017	1.2222	TRUE
K	meJA Treated	*meb1*	0.1871	0.31	0.0016	2.6146	TRUE
K	meJA Treated	*meb1meb2*	0.0207	0.89	0.0030	8.2010	TRUE
K	meJA Treated	*meb2*	0.4026	0.07	0.0010	0.8268	FALSE
K	meJA Treated	*nai1*	0.3723	0.07	-0.0045	-1.8206	FALSE
K	Untreated	*leb1*	0.2619	0.35	-0.0018	-2.4103	TRUE
K	Untreated	*meb1*	0.4007	0.10	-0.0011	-0.9054	FALSE
K	Untreated	*meb1meb2*	0.1050	0.55	0.0025	3.2302	TRUE
K	Untreated	*meb2*	0.4760	0.07	0.0004	-0.0915	FALSE
K	Untreated	*nai1*	0.3199	0.29	-0.0021	-2.1296	TRUE
Mg	meJA Treated	*leb1*	0.3354	0.20	0.0007	0.8038	TRUE
Mg	meJA Treated	*meb1*	0.3942	0.16	-0.0006	-1.5333	TRUE
Mg	meJA Treated	*meb1meb2*	0.1711	0.54	0.0011	3.8745	TRUE

Mg	meJA Treated	*meb2*	0.4963	0.08	0.0001	-0.4838	FALSE
Mg	meJA Treated	*nai1*	0.2094	0.10	-0.0060	-2.4645	FALSE
Mg	Untreated	*leb1*	0.3837	0.07	-0.0008	-1.0497	FALSE
Mg	Untreated	*meb1*	0.4511	0.14	0.0007	1.1194	TRUE
Mg	Untreated	*meb1meb2*	0.1429	0.47	0.0020	3.4244	TRUE
Mg	Untreated	*meb2*	0.3052	0.12	0.0017	1.7167	TRUE
Mg	Untreated	*nai1*	0.4826	0.07	-0.0001	-0.5375	FALSE
Mn	meJA Treated	*leb1*	0.3555	0.20	0.0007	1.1682	TRUE
Mn	meJA Treated	*meb1*	0.0252	0.87	-0.0060	-6.9499	TRUE
Mn	meJA Treated	*meb1meb2*	0.3978	0.11	0.0011	1.3607	TRUE
Mn	meJA Treated	*meb2*	0.2881	0.11	-0.0018	-1.5546	TRUE
Mn	meJA Treated	*nai1*	0.0704	0.44	-0.0088	-3.5263	TRUE
Mn	Untreated	*leb1*	0.4056	0.12	-0.0016	-1.1439	TRUE
Mn	Untreated	*meb1*	0.4523	0.08	0.0006	0.3076	FALSE
Mn	Untreated	*meb1meb2*	0.4434	0.07	0.0008	0.7139	FALSE
Mn	Untreated	*meb2*	0.4675	0.08	0.0011	0.2260	FALSE
Mn	Untreated	*nai1*	0.4110	0.06	0.0018	1.1227	FALSE
Mo	meJA Treated	*leb1*	0.2855	0.39	0.0001	1.5271	TRUE
Mo	meJA Treated	*meb1*	0.0078	1.00	-0.0063	-7.4068	TRUE
Mo	meJA Treated	*meb1meb2*	0.4207	0.05	0.0008	0.7818	FALSE
Mo	meJA Treated	*meb2*	0.4300	0.05	-0.0004	-0.4484	FALSE
Mo	meJA Treated	*nai1*	0.4341	0.13	-0.0006	0.1439	TRUE
Mo	Untreated	*leb1*	0.3751	0.08	-0.0029	-1.1652	FALSE
Mo	Untreated	*meb1*	0.3209	0.22	-0.0026	-1.8940	TRUE
Mo	Untreated	*meb1meb2*	0.4592	0.05	-0.0004	0.1329	FALSE
Mo	Untreated	*meb2*	0.2688	0.26	-0.0036	-1.9351	TRUE
Mo	Untreated	*nai1*	0.1468	0.43	0.0052	2.7129	TRUE
Na	meJA Treated	*leb1*	0.2473	0.56	0.0062	2.7926	TRUE
Na	meJA Treated	*meb1*	0.5045	0.06	0.0007	0.1974	FALSE
Na	meJA Treated	*meb1meb2*	0.4882	0.09	-0.0008	-2.8255	FALSE
Na	meJA Treated	*meb2*	0.0231	0.88	0.0045	5.8222	TRUE
Na	meJA Treated	*nai1*	0.2606	0.14	-0.0054	-1.8883	TRUE
Na	Untreated	*leb1*	0.5355	0.10	-0.0007	-0.5984	FALSE
Na	Untreated	*meb1*	0.3628	0.19	-0.0011	-1.4772	TRUE
Na	Untreated	*meb1meb2*	0.3758	0.07	0.0008	1.2312	FALSE

Na	Untreated	*meb2*	0.2757	0.26	0.0032	3.2028	TRUE
Na	Untreated	*nai1*	0.0719	0.50	-0.0024	-3.3550	TRUE
Ni	meJA Treated	*leb1*	0.4184	0.17	-0.0038	-1.2980	TRUE
Ni	meJA Treated	*meb1*	0.3519	0.13	0.0047	1.3463	TRUE
Ni	meJA Treated	*meb1meb2*	0.4486	0.04	0.0023	0.5569	FALSE
Ni	meJA Treated	*meb2*	0.5394	0.05	0.0015	0.0813	FALSE
Ni	meJA Treated	*nai1*	0.0968	0.51	0.0326	4.9684	TRUE
Ni	Untreated	*leb1*	0.3200	0.23	0.0072	2.1142	TRUE
Ni	Untreated	*meb1*	0.3766	0.08	-0.0037	-1.0896	FALSE
Ni	Untreated	*meb1meb2*	0.4792	0.07	-0.0004	0.3762	FALSE
Ni	Untreated	*meb2*	0.4399	0.03	-0.0024	-0.7073	FALSE
Ni	Untreated	*nai1*	0.4809	0.09	-0.0011	0.1143	FALSE
P	meJA Treated	*leb1*	0.0863	0.38	-0.0082	-3.4245	TRUE
P	meJA Treated	*meb1*	0.5161	0.05	-0.0000	-0.1382	FALSE
P	meJA Treated	*meb1meb2*	0.0648	0.49	0.0049	3.9198	TRUE
P	meJA Treated	*meb2*	0.2155	0.30	-0.0057	-3.0333	TRUE
P	meJA Treated	*nai1*	0.4731	0.14	0.0012	0.4473	TRUE
P	Untreated	*leb1*	0.0604	0.56	-0.0046	-4.4000	TRUE
P	Untreated	*meb1*	0.1228	0.21	-0.0042	-2.5574	TRUE
P	Untreated	*meb1meb2*	0.3204	0.31	0.0008	2.5894	TRUE
P	Untreated	*meb2*	0.2326	0.33	-0.0042	-2.7409	TRUE
P	Untreated	*nai1*	0.5004	0.05	-0.0000	0.1640	FALSE
S	meJA Treated	*leb1*	0.4314	0.07	0.0017	0.6836	FALSE
S	meJA Treated	*meb1*	0.4488	0.03	0.0007	0.6366	FALSE
S	meJA Treated	*meb1meb2*	0.3598	0.20	0.0012	1.4521	TRUE
S	meJA Treated	*meb2*	0.4497	0.03	0.0018	0.1484	FALSE
S	meJA Treated	*nai1*	0.5308	0.11	-0.0019	-0.4291	TRUE
S	Untreated	*leb1*	0.4376	0.12	-0.0010	-0.1075	TRUE
S	Untreated	*meb1*	0.4019	0.06	-0.0013	-0.8543	FALSE
S	Untreated	*meb1meb2*	0.4002	0.16	0.0009	1.3409	TRUE
S	Untreated	*meb2*	0.4123	0.06	0.0023	1.2302	FALSE
S	Untreated	*nai1*	0.4793	0.11	0.0011	0.4492	TRUE
Sr	meJA Treated	*leb1*	0.2861	0.28	0.0003	1.8437	TRUE
Sr	meJA Treated	*meb1*	0.0540	0.59	-0.0013	-3.8837	TRUE
Sr	meJA Treated	*meb1meb2*	0.0607	0.50	0.0019	3.2043	TRUE

Sr	meJA Treated	*meb2*	0.3645	0.16	-0.0008	-1.5151	TRUE
Sr	meJA Treated	*nai1*	0.1537	0.17	-0.0069	-3.0619	TRUE
Sr	Untreated	*leb1*	0.0536	0.61	-0.0036	-3.6991	TRUE
Sr	Untreated	*meb1*	0.0981	0.48	-0.0034	-3.5574	TRUE
Sr	Untreated	*meb1meb2*	0.3100	0.17	-0.0013	-1.8569	TRUE
Sr	Untreated	*meb2*	0.1649	0.35	-0.0021	-2.7713	TRUE
Sr	Untreated	*nai1*	0.3804	0.25	-0.0016	-1.7481	TRUE
Zn	meJA Treated	*leb1*	0.4474	0.10	-0.0028	-1.0069	FALSE
Zn	meJA Treated	*meb1*	0.3326	0.09	0.0026	1.8433	FALSE
Zn	meJA Treated	*meb1meb2*	0.0116	0.97	0.0091	736.8459	TRUE
Zn	meJA Treated	*meb2*	0.5150	0.09	-0.0004	-1.0639	FALSE
Zn	meJA Treated	*nai1*	0.3614	0.26	0.0063	2.4050	TRUE
Zn	Untreated	*leb1*	0.5156	0.22	-0.0012	-1.3682	TRUE
Zn	Untreated	*meb1*	0.2962	0.24	-0.0021	-2.4393	TRUE
Zn	Untreated	*meb1meb2*	0.3290	0.09	0.0026	1.6312	FALSE
Zn	Untreated	*meb2*	0.3171	0.18	-0.0030	-1.7235	TRUE
Zn	Untreated	*nai1*	0.4156	0.08	0.0014	0.6499	FALSE

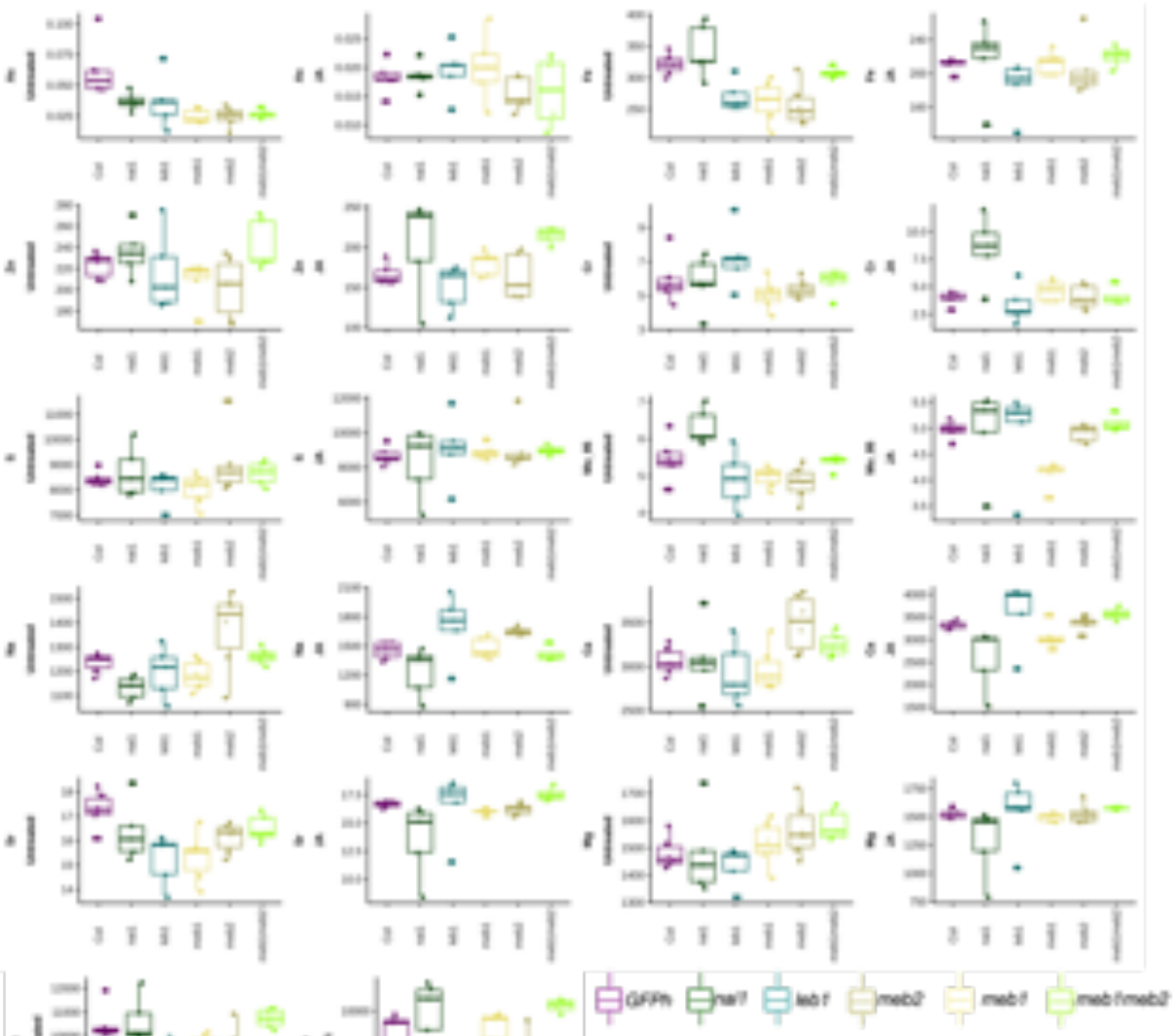

Figure 2.13: Box plots showing differences in specific ion composition in mutant plants compared with wild-type plants under untreated and meJA (indicated as JA) conditions.

Based on the ionome analysis, I found that mutation in NAI1 gene altered the overall distribution of Zn and Mg. I found that, upon meJA treatment, there was an impact on the ionome of wild-type plants because the *nai1* mutant ionome was different from the wild-type ionome. The impact of MEB1 and MEB2 is not as prominent as the impact of NAI1. Specifically, the Zn abundance of mutant seedlings was reduced in untreated condition and slightly reduced in seedlings treated with 100 mM meJA. However, Zn accumulation was slightly higher in *meb1meb2* mutant seedlings and significantly higher in *nai1* mutant seedlings. This may indicate a strategy of accumulating cations in a MEB1- and MEB2-dependent manner.

Overall, the comprehensive ionome analysis showed that MEB1 and MEB2 could be associated with the allocation of nutrients and potentially Zn. The role of MEB1 and MEB2 in other cations remains questionable. In addition, I speculate that MEB1 and MEB2 may be associated with the detoxification of arsenic and strontium because their abundance differs between mutants and wild-type plants. However, further validation is needed by determining the localisation of Zn within plant cell, and MEB1 and MEB2 gene expression in seedlings under Zn-excess and -depleted conditions.

2.4.3.2. ER body-dependent allocation of cations shows the potential function of MEBs in nutrient acquisition

To test the impact of ER bodies on nutrient allocation in plants, I performed a nutrient manipulation experiment using different concentrations of divalent Fe (II) and Zn (II) as potential ionome targets. The 7-day-old seedlings were subjected to depleted and increased concentrations of $FeSO_4$ or $ZnSO_4$ (100 μM and without sucrose) for 48 h (Figure 2.14a and b). GFPh and mutant plant growth remained altered after 48 h of treatment in the manipulated medium compared with the mock (no sucrose but in the presence of cation as in MS media). The *nai1* mutant seedlings showed reduced growth in treatment with 0.1 mM FeSO4 and 0.1 mM $ZnSO_4$ but was not as severely affected in media where Zn or Fe was depleted. However, the growth of MEB1- and MEB2-deficient mutants showed increased growth in Fe-depleted medium and in $FeSO_4$ treatment. The MEB1 and MEB2 single mutants showed reduced growth in the absence of Zn and slightly reduced growth in 0.1 mM of $ZnSO_4$ excess conditions; this was not in the case in the double mutants. Overall, in the absence of Zn and excess of Zn and Fe, I found reduced growth in *nai1* mutants. Additionally, in the absence of Zn, I found reduced growth in *meb1* mutants. Overall, the results indicate that ER bodies may be involved in tolerance to excessive Zn/Fe, but the role of MEB1 and MEB2 remains unclear.

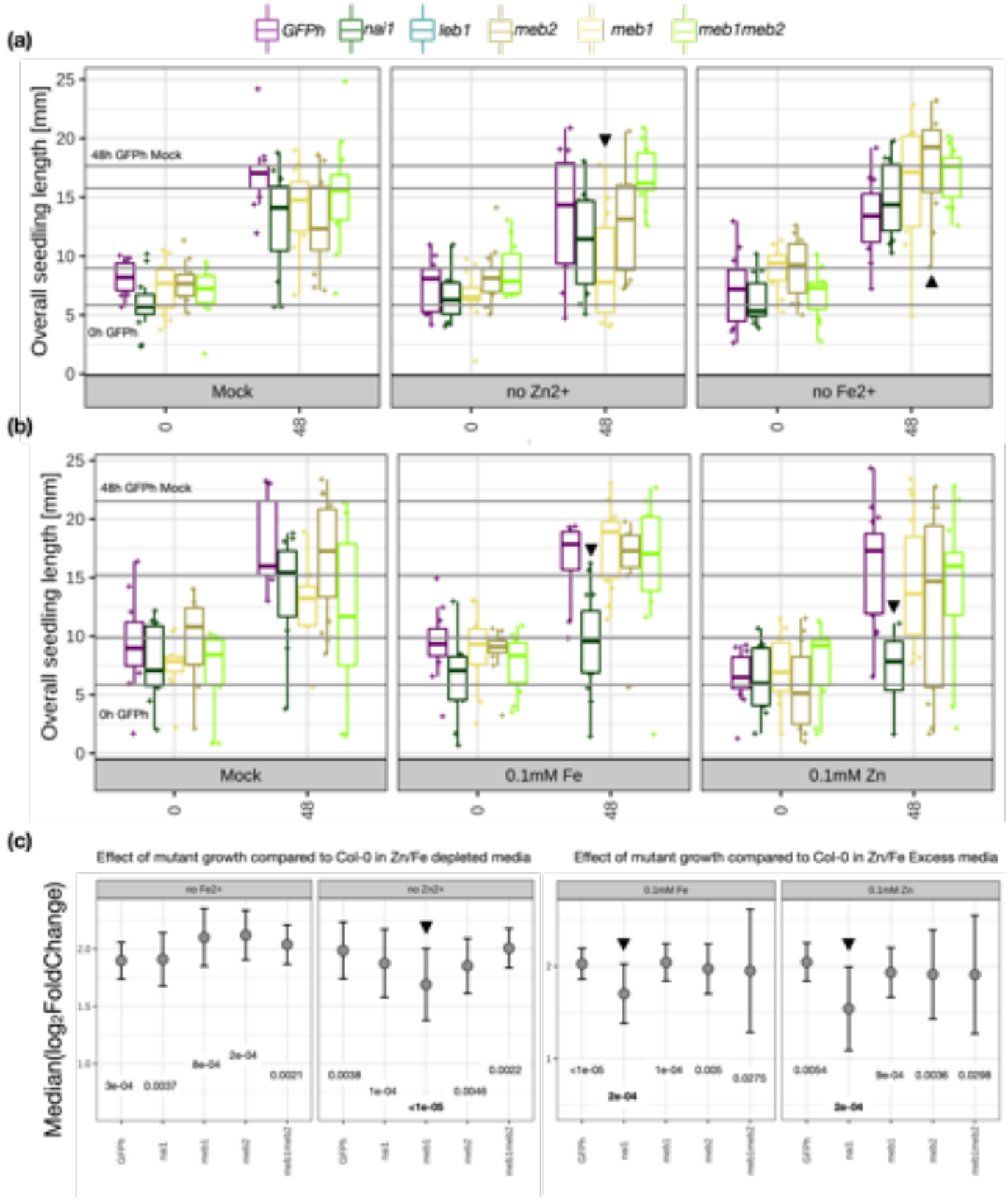

Figure 2.14: Box plots showing the difference in seedling length when subjected to cation-manipulated media: cation-depleted and mock (a), and cation stress (0.1 mM with SO_4^{2-} salts) (b). The grey lines indicate the confidence interval of the mock-treated samples at 0 h (below) and 48 h (above). The inverted triangles represent significant decrease in growth and the triangles represent significant increase in growth. The dot-plot represents the pairwise linear comparison performed between mock and treatment conditions for each genotype (x-axis) using random sampling over 100 iterations and the median of the log_2-fold change (y-axis) and the p.values are indicated in the text below the datapoints (c).

2.5. Discussion

2.5.1. ER body morphology and movement depend on MEB2 and partially depend on MEB1

The results indicate that MEB1 and MEB2 appear dispensable for ER body formation in *Arabidopsis*. However, there is another possibility: that MEB1 and MEB2 are mainly involved in ER body function rather than formation. Confocal micrograph analysis and TEM images showed a difference in ER body shape between MEB mutant and wild-type plants (Figure 2.15). This clearly indicates that MEB1 and MEB2 are associated with the ER body morphology by maintaining the dilated spindle-shaped structure. Interestingly, Takahashi et al., (2012) showed that, upon exposure to blue light, ER body changes from spindle-shaped to globular-shaped. I found that MEB2-deficient mutants showed a similar phenotype compared with GFP-h. The absence of these membrane proteins may interfere with ER body movement and possibly function. This indicates that the ER body morphology is associated with its function.

I also found that the absence of MEB2 seems to severely affect the movement of ER bodies along the ER network. ER-streaming proteins like myosin XI are associated with the dynamics of this organelle within the cell. It is possible that ER streaming or cell-to-cell mobility proteins, such as RHD4 (Thole et al., 2008), RTM1, and RTM2 (Chisholm et al., 2001), unpack ER body core proteins similar to ERD2 (Pastor-Cantizano et al., 2018). It is possible that MEB1 and MEB2 proteins interact with cytoskeletal proteins such as actin and microtubules, including FH3 (Deeks et al., 2010), which drives the movement of ER bodies. Further experiments are required to identify the proteins in cytoplasm and ER that are interaction with MEB1 and MEB2.

It was shown that the disorganised ER network under the impairment of myosin- and F-actin-related genes showed obscured structures of the ER bodies (Ueda et al., 2010). This indicates that the morphology and movement of the ER bodies are associated with ER streaming proteins like myosin XI, and our data showed change in ER body morphology and reduced movement in MEB1- and MEB2-deficient mutants. Therefore, it is likely that MEB1 and/or MEB2 proteins have a role in ER body morphology and movement. Aggregated ER bodies were found in mutants impaired in myosin XI and F-actin; therefore, these proteins may be associated with the MEB1 and MEB2 establishing potential interaction between ER body and actin.

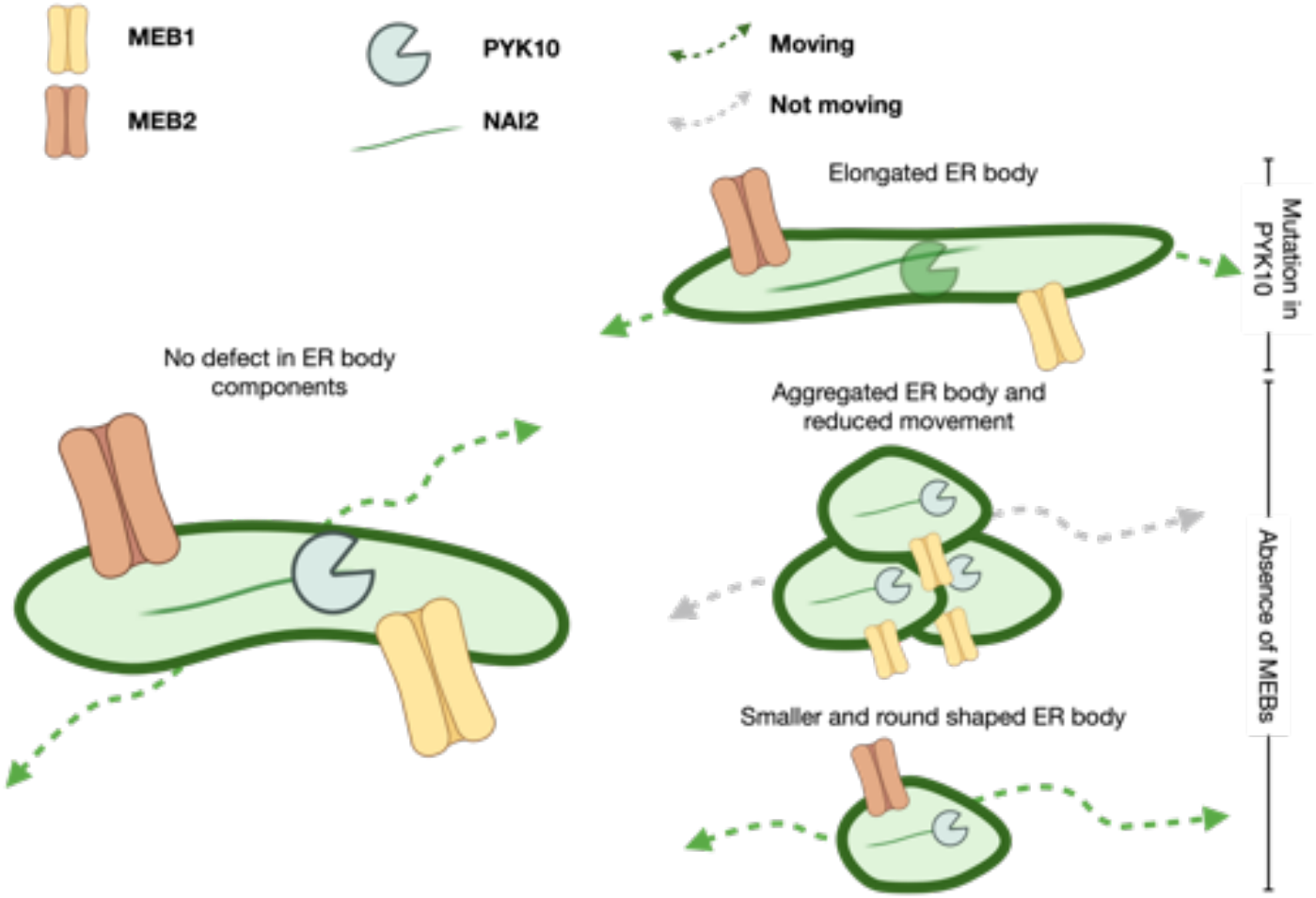

Figure 2.15: Proposed function of MEB1 and MEB2 in ER body movement and ER body morphology. MEB1 and MEB2 are associated with the ER body movement and morphology. The movement is indicated by the dashed green coloured lines with birectional arrowheads. The absence of MEBs shows reduced movement in ER bodies indicated in grey coloured lines.

2.5.2. The MEB1 and MEB2 proteins may be associated with nutrient allocation in plants

The C-terminal region of MEB1 and MEB2 contains a DUF125 sequence. Proteins containing a DUF125 sequence are assigned to the VIT family, and include Ccc1p in yeast, AtVIT1 in *Arabidopsis*, and OsVIT1 and OsVIT2 in rice. Ccc1p is a vacuolar iron/manganese transporter that is responsible for the regulation of cytosolic iron homeostasis (J. Li et al., 2001; Sorribes-Dauden et al., 2021). The *Arabidopsis* protein AtVIT1, a close homolog of Ccc1p, transports both iron and manganese, but only iron homeostasis is altered in *vit1* mutant seeds (S. A. Kim et al., 2006; Roschzttardtz et al., 2009). OsVIT1 and OsVIT2 transport iron and zinc and are responsible for the accumulation of these metals (Y. Zhang et al., 2012). Yamada et al., (2013) reported that overexpression of MEB1 and MEB2 partially reduced iron sensitivity in the yeast *ccc1* mutant and improved manganese resistance in wild-type yeast. These results suggest that the DUF125 sequence of these proteins underlies their ability to transport metal ions.

In this study, the ionomics analysis revealed that ER body mutation has an impact on the overall distribution of cations. Among the differentially abundant cations, Fe and Zn abundance differed between ER body mutants and GFPh. Because MEB1 and MEB2 are homologous to the VIT1 transporter, it is likely that the Fe accumulation within plant cellular compartments differs in knock-out mutants. I found that the growth of the ER body mutant seedlings was negatively affected to some extent in the conditions with depleted or excess Fe and Zn. This indicates that ER bodies have a role in the accumulation of Zn and Fe. It is noteworthy that PYK10, the major constituent of the constitutive ER body, and BGLU18, the major constituent of the inducible ER bodies, may require Zn, Fe, or other cations because they have myrosinase activity, and *Sinapis alba* myrosinase requires Zn for its myrosinase activity (Burmeister et al., 1997). This could be facilitated by cations maintaining the structure of the enzyme or acting as a cofactor for catalytic activation; if this is the case, then MEB1 and MEB2 could coordinate the divalent cations required for the function of PYK10 and BGLU18. Further experiments are needed to investigate the purpose of Fe and/or Zn in PYK10 enzymatic activity, and sub-cellular localisation of Fe and/or Zn in the ER bodies of MEB1- and MEB2-deficient mutants.

The ER body is constitutively observed in roots (Hara-Nishimura & Matsushima, 2003; Matsushima et al., 2002; Matsushima, Hayashi, et al., 2003). Root tissues may be exposed to high concentrations of metal ions in conjunction with other nutrients from the soil. Therefore, it is reasonable to expect that roots have detoxifying mechanisms for metals, which in part may be mediated by ER bodies. Takahashi et al., (2012) showed that, upon cellular damage, the ER body component BoWSCP (a chlorophyll-binding protein) is released and then immediately scavenges chlorophyll located in damaged thylakoid membranes to suppress the production of reactive oxygen species derived from chlorophylls. Therefore, it prevents the plant from photooxidative damage. These observations led to the proposal that the ER body is involved in defence against environmental stresses other than pathogens/herbivores by accumulating, aggregating, and compartmentally separating the protein PYK10 from other constituents of the cells. However, this is speculation, and further experiments on PYK10 aggregation in the presence of cations should be tested.

The results of this study indicate that ER bodies may be involved in defence against other environmental stresses in addition to substrate hydrolysis. PYK10 hydrolysis of IGs results in the formation of isothiocyanates that contribute to the organic mode of defence. However, based on the accumulation of cations like Fe and Zn, it is also possible that ER bodies may be involved in the inorganic mode of defence. Future research should investigate whether ER bodies are used for both inorganic and organic modes of defence against pathogen and/or herbivore attack.

Previous studies showed that MEB1 and MEB2 support yeast growth in $FeSO_4$ when they lack their native iron transporter. The function of the membrane proteins could be to allocate cations to

facilitate the function of the NAI2 and PYK10 proteins; thus, they may be indirectly associated with ER body function. Further experiments are required to understand the role of MEB1 and MEB2 in the function of NAI2 and PYK10 because the function of MEB1 and MEB2 could differ from protein complex formation. Alternatively, the cation transport function of MEB1 and MEB2 could be associated with the enzymatic function of PYK10. The conversion of glucosinolate into sulforaphane and glucose was reported to benefit from increased Zn concentration (Liang et al., 2006). This could indicate that MEB1 and MEB2 allocate Zn or divalent cations from the cytosol to ER bodies, which plays a role in PYK10 myrosinase activity.

I found that the general ionome of the MEB1- and MEB2-deficient mutants significantly differed from that of the wild-type plants, which revealed a difference in the accumulation of ions within plant tissue. Specifically, I found that the overall accumulation of Fe, P, and Zn significantly reduced in the in the absence of the MEB1 and MEB2 proteins; this indicated that the overall accumulation of these cations in the ER or ER bodies is mediated by the MEB proteins. Therefore, there is an impact of ER body membrane proteins on the ionome. This is also consistent with the accumulation of toxic metals such as arsenic and strontium, which suggests a possible role in metal detoxification or increasing the inorganic mode of defence strategy. However, the role of ER bodies in metal detoxification remains speculation.

Interestingly, Fe accumulation was lower when the seedlings MEB2 mutants were subjected to meJA stress treatment. Perhaps, after stress induction, the MEB1 and MEB2 proteins coordinate Fe efflux and influx, either for the ER body constituents or by coordinating ER body movement. This could suggest that ER body and glucosinolate activation may be mediated by iron through the MEB1 and MEB2 proteins. However, there was a slight difference in Fe abundance between *nai1* mutant and wild-type plants. I found this difference to be consistent in mutant plants when treated with jasmonic acid. I also found that ER body movement and abundance of MEB2 deficit mutants was reduced compared to wild-type. The VIT1 membrane proteins located in vacuoles and the IRT1 proteins located in the plasma membrane are both responsible for Fe exchange (Connolly et al., 2002; Dubeaux et al., 2018; Kato et al., 2019). Similarly, Fe exchange could be facilitated within ER body and cytosol by MEB1 and MEB2. In our data we found a reduction in Fe accumulation in ER body mutants indicating the possible role of MEB1 and MEB2 in distribution Fe within the ER bodies. Further analysis is required to investigate the ER body phenotype in IRT1- or VIT1-deficient mutants.

IRT1-deficient plants were reported to show stunted growth in Fe-deficient medium, which indicates relevance of channelling Fe for cell use (Cointry & Vert, 2019; Connolly et al., 2002; Dubeaux et al., 2018). Similarly, Zn abundance was reduced in the MEB2-deficient mutants. The allocation of Zn may differ because of the lack of influx of Zn in ER bodies. In the absence of Zn in the medium, the mutants without MEB1 showed slight reduction in growth. However, the growth of MEB1 and

MEB2 double knockout mutants differed from that of single knockout mutants. This may suggest dependency on MEB1 and MEB2. The null mutant also showed reduced growth, which indicated that ER bodies may require accumulation of Zn and Fe. Similarly, at the subcellular level, MEB1 and MEB2 may play a role in cation homeostasis. MEB1 and MEB2 are similar to VIT1, which allows the influx of Fe from the cytosol into the vacuoles, decreasing the cytosolic iron. Alternatively, IRT1 increases the cytosolic iron by transporting iron from the media. Therefore, in ER bodies, MEB1 and MEB2 may function similarly to VIT1 and IRT1 by transporting cations across ER body compartments. These metal ions could act as cofactors for the ER body constituents. Because PYK10 has myrosinase activity, PYK10 may have specific metal binding sites that allow it to function.

The myrosinase activity of PYK10 in *A. thaliana* mostly occurs at an acidic pH, which is not the case with the myrosinase extracted from *S. alba* (Burmeister et al., 1997). It is possible that, within the plant cell, a proton gradient is required for PYK10 myrosinase activity, and MEB1 and MEB2 contribute to the function of ER bodies by facilitating the influx and/or efflux of H^+. Because MEB1 and MEB2 are associated with cation exchange, it is possible that these proteins exchange cations across ER body and cytosol to activate PYK10. However, further experiments are needed to determine whether myrosinase activity is increased in the presence of cations.

3. CHAPTER II: The role of ER body localized PYK10 myrosinase and its substrate in shaping root microbiota

3.1. Summary

Plant roots are colonized by a plethora of microbes that are collectively called the root microbiota. Recent studies suggested a potential role for host secondary metabolic pathways in shaping root microbiota (Hu et al., 2018; Huang et al., 2019; Voges et al., 2019). In *Arabidopsis thaliana* roots, indole glucosinolates (IGs), a class of tryptophan-derived sulfur-containing secondary metabolites, play a crucial role in interaction with surrounding microbes (Hiruma, 2019; Hiruma et al., 2016; Lahrmann et al., 2015). IGs in *A. thaliana* roots are hydrolyzed by the PYK10 myrosinase stored in the endoplasmic reticulum (ER) body and converted into bioactive compounds. However, the role of ER bodies in the root microbiota assembly remains unclear. It is known that root-secreted compounds play a role in the root microbiota assembly. A broad range of compounds are exuded by roots, including both primary and secondary metabolites. Despite the clear evidence for PYK10 hydrolyzing IGs, its role in root-secretion of IGs and/or their catabolic products is elusive. In this chapter, I describe investigations of the impact of the ER body pathway on the metabolome of root exudates and on root microbiota assembly. To evaluate the metabolome of the root exudates, I collected root exudates from ER body mutant plants, Trp-pathway and IG knockout mutant plants, and Col-0 wild-type plants grown under axenic conditions. Our results showed that both the Trp and ER body pathways have an impact on the metabolome of the exudates. To investigate the role of the Trp-derived metabolic pathway and the ER bodies on the structure of root microbiota, we cultured the same set of mutants along with the Col-0 wild type in different soil types under greenhouse conditions. We profiled the microbiome by amplicon sequencing of the 16S rRNA V5-V7 region (bacteria) and the ITS1 region (fungi) of the root endosphere and rhizoplane compartments at the stage of flowering. Our results revealed that the mutant plants accommodated different bacterial communities at the rhizoplane and fungal communities in the endosphere. Next, we hypothesized that the difference in the community structure was due to a difference in root secreted compounds. We tested our hypothesis by treating natural soils as well as bacterial synthetic communities with root exudates and root extracts collected from axenically grown *pyk10bglu21* and *cyp79b2b3* mutant plants and Col-0 wild-type plant. Interestingly, we found that ER body-mediated root secretions contribute to the microbiota assembly. We also tested the growth of a taxonomically diverse set of fungal strains isolated from healthy *A. thaliana* plants in these mutant and wild-type plants. We found that most of tested fungal strains inhibited the growth of the *cyp79b2b3* mutant plants, while only a few strains negatively impacted the growth of *pyk10bglu21* mutants compared to the wild type. Overall, we demonstrated that, in *A.*

thaliana, root-secreted compounds downstream of PYK10-mediated hydrolysis of IGs and Trp-derived secondary metabolism have an impact on shaping root microbiota.

3.2. Introduction and hypotheses

In nature, plants are colonized by microbes that constitute a microbial community, collectively called the plant microbiota. Among the plant-associated microbiota, the root microbiota is a community of microbes that colonize roots. These microbes colonize inside the root epidermis (root endosphere) and on the surface of the roots (rhizoplane) (Durán et al., 2018). Plant-associated factors such as root morphology, their development, and plant immunity are believed to play a crucial role in the structure of the microbiota (Bulgarelli et al., 2015; Castrillo et al., 2017; Edwards et al., 2015; Hacquard, 2016; Lebeis et al., 2015). However, the role of root-secreted compounds in modulating the microbiota composition remains unclear.

3.2.1. The function link between root microbiota and root secretions

The plant microbiota is thought to be metabolically adapted to utilize plant-derived organic compounds (Bai et al., 2015; Demoling et al., 2007; Nguyen, 2003). These members of the microbiota can utilize plant-derived chemical compounds such as carbohydrates, organic acids, and amino acids, and plant cell wall components for their metabolism (Eilers et al., 2010). On the other hand, members of the microbiota under diverse environmental conditions produce compounds that may support plant growth and survival. These microbes provide benefits to plant growth and health by influencing nutrient status, modulating plant pathogen interactions, and modifying tolerance to abiotic and biotic stresses(Berendsen et al., 2012; Bulgarelli et al., 2013; Mendes et al., 2011; Vorholt, 2012). For example, diverse members of the plant microbiota promote host growth indirectly by protecting them from biotic stress (Berendsen et al., 2012; Berg & Smalla, 2009; Lugtenberg & Kamilova, 2009; Mendes et al., 2013; Turner et al., 2013), also by nutrient fortification, by facilitating nutrient bioavailability, or by enhancing nutrient acquisition capacity in the soil.

Earlier studies have suggested that the composition of soil microbiota is related to the flowering time of multiple *Arabidopsis* species (Panke-Buisse et al., 2015; Wagner, 2014). Different genotypes of the plant show distinct microbiota communities in the roots (Bulgarelli et al., 2012, 2015; Edwards et al., 2015; Lundberg et al., 2012; Peiffer et al., 2013; Schlaeppi et al., 2014). Therefore, plant-microbiota interactions are bidirectional process where the host genotype has an effect on the microbiota structure and a change in microbiota composition affects the plant health (Haney & Ausubel, 2015; Müller et al., 2016). It has been suggested that root-secreted compounds can specifically alter the abundance of certain microbes, which could promote their colonization in the rhizosphere and ensure nutrient fortification (Mondy et al., 2014; Müller et al., 2016).

3.2.2. Factors that modulate the root-associated microbiota

Abiotic factors are the major drivers of the root-associated microbiota assembly. The soil texture, nutrient composition and geochemical factors define the type of nutrition and matrix of the root microbiota, and a compositional change in these factors triggers a community shift in soil microbiota as well as rhizosphere microbiota (Delgado-Baquerizo, 2018; Fierer & Jackson, 2006; Karimi, 2018). In addition to these edaphic factors (soil-related), plants secrete various compounds and alter the microbial niche in and around the roots. This may create a gradient of root-secreted compounds from the roots towards the soil (Badri & Vivanco, 2009; Okutani et al., 2020). This raises the possibility that root-secreted compounds play a role in the root microbiota assembly (Badri & Vivanco, 2009; Okutani et al., 2020; Vives-Peris et al., 2020). In other words, the composition of the root-secreted compounds are partly responsible for the difference between the soil and root microbiota. It was shown that the microbiota composition also varies across the root compartments from the rhizosphere to the endosphere (Coleman-Derr et al., 2016; Durán et al., 2018). The alpha diversity (within-sample diversity) of the microbial community decreases from rhizosphere to endosphere, indicating a filtering process across different compartments within the root. The differences in the root microbiota across compartments could be triggered by plant metabolism, as the abundance of a metabolite differs across root compartments. These root-secreted compounds have a potential link with the members of the root microbiota, including the symbionts and pathogens.

3.2.3. Role of glucosinolates in the structure of the root microbiota

Plants of the order Brassicales have established a unique defence strategy to fight against foliar and root pathogens. These plants use Tryptophan (Trp) to synthesize a wide variety of secondary metabolites, including indole glucosinolate (IG), camalexin, indole carboxylic acid (ICA) and indole acetic acid (IAA) (Klein & Sattely, 2017; Sanchez-Vallet et al., 2010). Previous studies showed that, in the absence of IG, plants are susceptible to a necrotrophic fungal pathogen *Plectosphaerella cucumerina* (Frerigmann et al., 2016). Trp derivatives are suggested to have a potential role in plant-microbe interactions (Bednarek et al., 2009; Clay et al., 2009), as well as for proper management of interactions with beneficial microbes (Hiruma et al., 2016; Lahrmann et al., 2015). Importantly, IGs and other Trp-derived metabolites are highly abundant in roots (Brown et al., 2003) and secreted into the rhizosphere as a part of root exudation (Bressan et al., 2009; Hiruma, 2019; D. Xu et al., 2017). In addition to glucosinolates, other root-secreted secondary metabolites such as coumarin and camalexin have an impact on root microbiota, but glucosinolates need an activation system. Glucosinolate bioactivation requires myrosinase (see 1.Introduction), and roots of *A. thaliana* Col-0

express a high level of TGG4 and TGG5 myrosinases. It has been shown that PYK10 also has a myrosinase activity that hydrolyses glucosides, including IGs (Bednarek et al., 2009; Clay et al., 2009; Nakano et al., 2017). The hydrolysed products of glucosinolates include secondary metabolites like nitriles, epithionitriles, and isothiocyanates that interact with herbivores and pathogens, acting as a chemical repellent (Wittstock & Halkier, 2002).

3.2.4. Arabidopsis produces root-secreted compounds that shape the microbiota of the rhizosphere

Several studies have suggested the importance of root-secreted metabolites in modulating the composition of the plant microbiota (Harbort et al., 2020; Hu et al., 2018; Huang et al., 2019; Korenblum et al., 2020; Stringlis, 2018; Voges et al., 2019). A diverse range of compounds are secreted by roots that are present within the root epidermis and the root surface (Badri & Vivanco, 2009; Oburger et al., 2014; Strehmel et al., 2014; Tawaraya et al., 2014). The process by which these compounds are secreted to the root surface and to the rhizosphere is called root exudation. Root exudation is crucial for the interaction between plants and soil biota (Badri et al., 2013; Czarnota et al., 2003; Inceoğlu et al., 2010; Micallef et al., 2009). However, the impact of root exudation due to glucosinolate pathway and hydrolysis of its products by myrosinase stored in ER body remains unclear. Root exudates are mainly composed of primary metabolites (sugars, amino acids, and organic acids) and diffuse from the surface of the roots to the rhizosphere (Badri & Vivanco, 2009). Root exudates also contain a pool of secondary metabolites (Badri & Vivanco, 2009; Strehmel et al., 2014). Importantly, the exudate includes compounds that are downstream of hydrolysis of secondary metabolites. It is not clear whether the enzyme is transported to the location of the substrate or *vice versa*, or both enzyme and substrate are released as exudates and react in the rhizoplane compartment. Plant metabolic pathways play a crucial role in the root exudation process, and several studies have suggested that the root-associated microbiota are modulated by the composition of the root-secreted compounds. It is not clear whether the root ER bodies have an impact on root-secreted compounds. If they do, it remains unclear whether the microbiota composition is altered specifically by the hydrolysis of the secondary metabolites.

3.2.5. PYK10 myrosinase in ER bodies and IGs in plant microbe interactions

Among the reported myrosinases in plants, PYK10 myrosinase is one of the most abundant in roots (Nakano et al., 2017). Both PYK10 and IG are abundant in the roots of *A. thaliana*. Therefore, it is plausible to assume that the activation of IGs by PYK10 myrosinase synthesizes compounds that are secreted by roots. These root-secreted compounds may be crucial for the structure of the root microbiota. Past studies focusing on another root-abundant myrosinase, PENETRATION 2 (PEN2),

showed that a broad spectrum of PEN2-dependent metabolism of Trp-derived IG in *A. thaliana* plays a role in plant-microbe interactions (Bednarek, 2012; Bednarek et al., 2009; Clay et al., 2009). In contrast, the role of the ER body-localized PYK10 myrosinase in plant-microbe interactions remains unclear.

3.2.6. Research question and hypothesis

This chapter aims to address whether PYK10 myrosinase localized in ER bodies has a role in the formation of root-associated microbial assemblages. I hypothesize that the compounds that are downstream of PYK10 and Trp-metabolism play an important role in plant-microbe interactions in root.

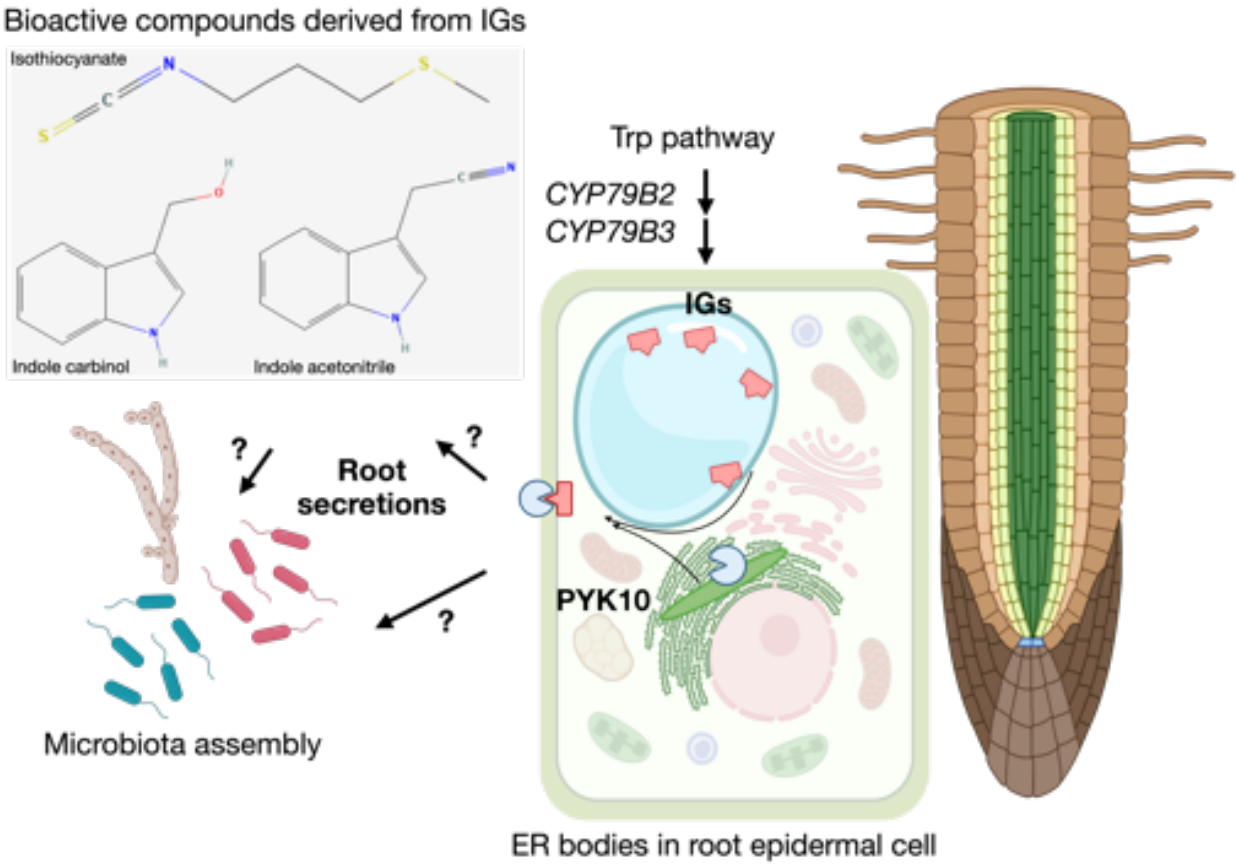

Figure 3.1: Model of research design; What is the role of ER body-localized PYK10 myrosinase and its substrate in Trp-derived secondary metabolites in shaping root microbiota?

To address this, I first used knockout mutants of ER bodies *nai1-1* and *pyk10bglu21,* Trp pathway *cyp79b2b3,* and indole glucosinolate *myb34/51/*122 to profile untargeted metabolites in the root exudates collected from these mutants and to show the diversity of root-secreted compounds that are coordinated by ER bodies and the Trp pathway.

Second, by performing microbiota profiling of the endosphere and rhizoplane compartments of mutant plants and wild-type plants grown under greenhouse conditions, I show the impact of the

PYK10 myrosinase system and Trp-derived secondary metabolites on the structure of bacterial and fungal community in the rhizoplane and endosphere, respectively.

Third, I show the direct impact of the root-secreted compounds produced by the PYK10 myrosinase system and the products of Trp-derived secondary metabolism in shaping the soil microbiota. I also tested the effect of these pathways directly on the bacterial community by reconstituting a synthetic bacterial community.

At last, I investigated the direct role of the ER body and Trp pathway on fungal strains by performing a plant-fungus mono-association assay.

My results revealed that the PYK10 myrosinase system and the terminal products of the Trp pathway have a role in shaping the root microbiota by coordinating the composition of root-secreted compounds.

3.3. Materials and Methods

3.3.1. Plant, microbial, and soil materials with growth conditions

3.3.1.1. Plant genotypes

Wild-type Col-0 seeds of *Arabidopsis thaliana* were obtained from Nottingham Arabidopsis Stock Centre (NASC). The seeds of *pyk10bglu21*, *nai1-1*, *myb34/51/122*, and *cyp79b2b3* mutant plants were obtained from the authors of the previous studies (Frerigmann & Gigolashvili, 2014; Matsushima, Hayashi, et al., 2003; Yamada et al., 2009; Zhao et al., 2002).

3.3.1.2. Microbial strains

The bacterial and fungal strains used in this study have previously been described (Bai et al., 2015; Hiruma et al., 2016; Mesny et al., 2021). Bacterial strains were selected as a representative family of the root microbiota of *A. thaliana* root microbiota (Table 3.1). The fungal strains were selected from various ecological niches like different locations with different soil compositions (Table 3.2).

Table 3.1: Summary of bacterial strains used in the synthetic community (SynCom) experiment (Bai et al., 2015).

Bacterial strain ID	Phylum	Class	Order	Family	Genus
Root4	Actinobacteria	Actinobacteria	Actinomycetales	Microbacteriaceae	*Agromyces*
Root9	Proteobacteria	Gammaproteobacteria	Pseudomonadales	Pseudomonadaceae	*Pseudomonas*
Root11	Firmicutes	Bacilli	Bacillales	Bacillaceae	*Bacillus*
Root22	Actinobacteria	Actinobacteria	Actinomycetales	Promicromonosporaceae	
Root29	Proteobacteria	Betaproteobacteria	Burkholderiales	Comamonadaceae	
Root31	Proteobacteria	Alphaproteobacteria	Rhizobiales	Rhizobiaceae	*Sinorhizobium*
Root50	Proteobacteria	Alphaproteobacteria	Sphingomonadales	Sphingomonadaceae	*Sphingomonas*
Root52	Firmicutes	Bacilli	Bacillales	Paenibacillaceae	*Paenibacillus*
Root53	Actinobacteria	Actinobacteria	Actinomycetales	Microbacteriaceae	*Microbacterium*

Root55	Actinobacteria	Actinobacteria	Actinomycetales	Streptomycetaceae	*Streptomyces*
Root60	Actinobacteria	Actinobacteria	Actinomycetales	Microbacteriaceae	
Root61	Actinobacteria	Actinobacteria	Actinomycetales	Microbacteriaceae	*Microbacterium*
Root63	Actinobacteria	Actinobacteria	Actinomycetales	Streptomycetaceae	*Streptomyces*
Root65	Proteobacteria	Gammaproteobacteria	Xanthomonadales	Xanthomonadaceae	*Pseudoxanthomonas*
Root68	Proteobacteria	Gammaproteobacteria	Pseudomonadales	Pseudomonadaceae	*Pseudomonas*
Root70	Proteobacteria	Betaproteobacteria	Burkholderiales	Comamonadaceae	*Acidovorax*
Root71	Proteobacteria	Gammaproteobacteria	Pseudomonadales	Pseudomonadaceae	*Pseudomonas*
Root73	Proteobacteria	Alphaproteobacteria	Rhizobiales	Rhizobiaceae	*Rhizobium*
Root74	Proteobacteria	Alphaproteobacteria	Rhizobiales	Rhizobiaceae	*Sinorhizobium*
Root76	Proteobacteria	Gammaproteobacteria	Xanthomonadales	Xanthomonadaceae	
Root77	Proteobacteria	Alphaproteobacteria	Caulobacterales	Caulobacteraceae	
Root79	Actinobacteria	Actinobacteria	Actinomycetales	Nocardioidaceae	*Nocardioides*
Root81	Actinobacteria	Actinobacteria	Actinomycetales	Microbacteriaceae	*Agromyces*
Root83	Proteobacteria	Betaproteobacteria	Burkholderiales	Alcaligenaceae	*Achromobacter*
Root85	Actinobacteria	Actinobacteria	Actinomycetales	Intrasporangiaceae	
Root96	Proteobacteria	Gammaproteobacteria	Xanthomonadales	Xanthomonadaceae	
Root100	Proteobacteria	Alphaproteobacteria	Rhizobiales	Phyllobacteriaceae	
Root101	Actinobacteria	Actinobacteria	Actinomycetales	Intrasporangiaceae	*Janibacter*
Root102	Proteobacteria	Alphaproteobacteria	Rhizobiales	Phyllobacteriaceae	*Mesorhizobium*
Root105	Proteobacteria	Alphaproteobacteria	Rhizobiales	Hyphomicrobiaceae	
Root107	Actinobacteria	Actinobacteria	Actinomycetales	Streptomycetaceae	
Root122	Actinobacteria	Actinobacteria	Actinomycetales	Nocardioidaceae	*Nocardioides*
Root127	Proteobacteria	Alphaproteobacteria	Rhizobiales	Rhizobiaceae	*Sinorhizobium*
Root131	Firmicutes	Bacilli	Bacillales	Bacillaceae	*Bacillus*
Root133	Proteobacteria	Betaproteobacteria	Burkholderiales	Oxalobacteraceae	*Massilia*
Root135	Actinobacteria	Actinobacteria	Actinomycetales	Mycobacteriaceae	*Mycobacterium*
Root136	Actinobacteria	Actinobacteria	Actinomycetales	Nocardiaceae	*Nocardia*
Root137	Actinobacteria	Actinobacteria	Actinomycetales	Cellulomonadaceae	*Cellulomonas*
Root140	Actinobacteria	Actinobacteria	Actinomycetales	Nocardioidaceae	*Nocardioides*
Root147	Firmicutes	Bacilli	Bacillales	Bacillaceae	
Root149	Proteobacteria	Alphaproteobacteria	Rhizobiales	Rhizobiaceae	*Rhizobium*
Root151	Actinobacteria	Actinobacteria	Actinomycetales	Nocardioidaceae	Nocardioides
Root154	Proteobacteria	Alphaproteobacteria	Sphingomonadales	Sphingomonadaceae	
Root157	Proteobacteria	Alphaproteobacteria	Rhizobiales	Phyllobacteriaceae	*Mesorhizobium*
Root166	Actinobacteria	Actinobacteria	Actinomycetales	Microbacteriaceae	*Microbacterium*
Root170	Proteobacteria	Betaproteobacteria	Burkholderiales	Alcaligenaceae	*Achromobacter*
Root172	Proteobacteria	Alphaproteobacteria	Rhizobiales	Phyllobacteriaceae	*Mesorhizobium*
Root180	Actinobacteria	Actinobacteria	Actinomycetales	Microbacteriaceae	
Root181	Actinobacteria	Actinobacteria	Actinomycetales	Intrasporangiaceae	
Root186	Bacteroidetes	Flavobacteriia	Flavobacteriales	Flavobacteriaceae	*Flavobacterium*
Root187	Actinobacteria	Actinobacteria	Actinomycetales	Streptomycetaceae	
Root190	Actinobacteria	Actinobacteria	Actinomycetales	Nocardioidaceae	*Nocardioides*
Root209	Proteobacteria	Betaproteobacteria	Burkholderiales	Comamonadaceae	
Root217	Proteobacteria	Betaproteobacteria	Burkholderiales	Comamonadaceae	*Acidovorax*

Root219	Proteobacteria	Betaproteobacteria	Burkholderiales	Comamonadaceae	*Acidovorax*
Root224	Actinobacteria	Actinobacteria	Actinomycetales	Nocardioidaceae	*Nocardioides*
Root227	Actinobacteria	Actinobacteria	Actinomycetales	Microbacteriaceae	
Root236	Actinobacteria	Actinobacteria	Actinomycetales	Nocardioidaceae	*Aeromicrobium*
Root239	Firmicutes	Bacilli	Bacillales	Bacillaceae	*Bacillus*
Root240	Actinobacteria	Actinobacteria	Actinomycetales	Nocardioidaceae	*Nocardioides*
Root241	Proteobacteria	Alphaproteobacteria	Sphingomonadales	Sphingomonadaceae	*Sphingomonas*
Root258	Proteobacteria	Alphaproteobacteria	Rhizobiales	Rhizobiaceae	*Sinorhizobium*
Root264	Actinobacteria	Actinobacteria	Actinomycetales	Streptomycetaceae	*Streptomyces*
Root265	Actinobacteria	Actinobacteria	Actinomycetales	Mycobacteriaceae	*Mycobacterium*
Root267	Proteobacteria	Betaproteobacteria	Burkholderiales	Comamonadaceae	*Acidovorax*
Root274	Proteobacteria	Alphaproteobacteria	Rhizobiales	Rhizobiaceae	
Root275	Proteobacteria	Betaproteobacteria	Burkholderiales	Comamonadaceae	*Acidovorax*
Root278	Proteobacteria	Alphaproteobacteria	Rhizobiales	Rhizobiaceae	*Sinorhizobium*
Root322	Actinobacteria	Actinobacteria	Actinomycetales	Microbacteriaceae	*Microbacterium*
Root329	Proteobacteria	Gammaproteobacteria	Pseudomonadales	Pseudomonadaceae	*Pseudomonas*
Root332	Actinobacteria	Actinobacteria	Actinomycetales	Microbacteriaceae	
Root335	Proteobacteria	Betaproteobacteria	Burkholderiales	Oxalobacteraceae	*Massilia*
Root342	Proteobacteria	Alphaproteobacteria	Caulobacterales	Caulobacteraceae	*Caulobacter*
Root343	Proteobacteria	Alphaproteobacteria	Caulobacterales	Caulobacteraceae	*Caulobacter*
Root344	Actinobacteria	Actinobacteria	Actinomycetales	Nocardioidaceae	*Aeromicrobium*
Root369	Actinobacteria	Actinobacteria	Actinomycetales	Streptomycetaceae	*Streptomyces*
Root381	Proteobacteria	Alphaproteobacteria	Rhizobiales	Bradyrhizobiaceae	*Bosea*
Root401	Proteobacteria	Gammaproteobacteria	Pseudomonadales	Pseudomonadaceae	*Pseudomonas*
Root402	Proteobacteria	Betaproteobacteria	Burkholderiales	Comamonadaceae	*Acidovorax*
Root404	Proteobacteria	Betaproteobacteria	Burkholderiales	Comamonadaceae	
Root405	Proteobacteria	Betaproteobacteria	Burkholderiales	Comamonadaceae	
Root411	Proteobacteria	Betaproteobacteria	Burkholderiales	Comamonadaceae	*Variovorax*
Root418	Proteobacteria	Betaproteobacteria	Burkholderiales	Oxalobacteraceae	*Janthinobacterium*
Root420	Bacteroidetes	Flavobacteriia	Flavobacteriales	Flavobacteriaceae	*Flavobacterium*
Root423	Proteobacteria	Alphaproteobacteria	Rhizobiales	Rhizobiaceae	*Sinorhizobium*
Root434	Proteobacteria	Betaproteobacteria	Burkholderiales	Comamonadaceae	*Variovorax*
Root436	Proteobacteria	Alphaproteobacteria	Rhizobiales	Hyphomicrobiaceae	
Root456	Actinobacteria	Actinobacteria	Actinomycetales	Intrasporangiaceae	
Root480	Proteobacteria	Gammaproteobacteria	Xanthomonadales	Xanthomonadaceae	
Root482	Proteobacteria	Alphaproteobacteria	Rhizobiales	Rhizobiaceae	*Rhizobium*
Root485	Actinobacteria	Actinobacteria	Actinomycetales	Cellulomonadaceae	*Cellulomonas*
Root491	Proteobacteria	Alphaproteobacteria	Rhizobiales	Rhizobiaceae	*Agrobacterium*
Root494	Proteobacteria	Gammaproteobacteria	Xanthomonadales	Xanthomonadaceae	
Root495	Actinobacteria	Actinobacteria	Actinomycetales	Nocardioidaceae	*Aeromicrobium*
Root552	Proteobacteria	Alphaproteobacteria	Rhizobiales	Phyllobacteriaceae	*Mesorhizobium*
Root553	Actinobacteria	Actinobacteria	Actinomycetales	Microbacteriaceae	
Root558	Proteobacteria	Alphaproteobacteria	Rhizobiales	Rhizobiaceae	*Sinorhizobium*
Root559	Proteobacteria	Gammaproteobacteria	Xanthomonadales	Xanthomonadaceae	
Root561	Proteobacteria	Gammaproteobacteria	Xanthomonadales	Xanthomonadaceae	*Rhodanobacter*

Root562	Proteobacteria	Gammaproteobacteria	Pseudomonadales	Pseudomonadaceae	*Pseudomonas*
Root563	Actinobacteria	Actinobacteria	Actinomycetales	Intrasporangiaceae	*Janibacter*
Root564	Proteobacteria	Alphaproteobacteria	Rhizobiales	Rhizobiaceae	*Agrobacterium*
Root565	Proteobacteria	Betaproteobacteria	Burkholderiales	Alcaligenaceae	*Achromobacter*
Root568	Proteobacteria	Betaproteobacteria	Burkholderiales	Comamonadaceae	
Root569	Proteobacteria	Gammaproteobacteria	Pseudomonadales	Pseudomonadaceae	*Pseudomonas*
Root604	Proteobacteria	Gammaproteobacteria	Xanthomonadales	Xanthomonadaceae	
Root608	Proteobacteria	Alphaproteobacteria	Caulobacterales	Caulobacteraceae	*Brevundimonas*
Root614	Actinobacteria	Actinobacteria	Actinomycetales	Nocardioidaceae	
Root627	Proteobacteria	Gammaproteobacteria	Xanthomonadales	Xanthomonadaceae	*Rhodanobacter*
Root630	Proteobacteria	Gammaproteobacteria	Xanthomonadales	Xanthomonadaceae	*Pseudoxanthomonas*
Root635	Proteobacteria	Alphaproteobacteria	Rhizobiales	Hyphomicrobiaceae	
Root651	Proteobacteria	Alphaproteobacteria	Rhizobiales	Rhizobiaceae	*Agrobacterium*
Root655	Proteobacteria	Alphaproteobacteria	Caulobacterales	Caulobacteraceae	*Caulobacter*
Root656	Proteobacteria	Alphaproteobacteria	Caulobacterales	Caulobacteraceae	*Caulobacter*
Root667	Proteobacteria	Gammaproteobacteria	Xanthomonadales	Xanthomonadaceae	
Root670	Proteobacteria	Alphaproteobacteria	Rhizobiales	Bradyrhizobiaceae	*Bosea*
Root672	Proteobacteria	Alphaproteobacteria	Sphingomonadales	Sphingomonadaceae	*Novosphingobium*
Root682	Actinobacteria	Actinobacteria	Actinomycetales	Nocardioidaceae	
Root685	Proteobacteria	Alphaproteobacteria	Rhizobiales	Hyphomicrobiaceae	
Root690	Proteobacteria	Gammaproteobacteria	Xanthomonadales	Xanthomonadaceae	
Root695	Proteobacteria	Alphaproteobacteria	Rhizobiales	Phyllobacteriaceae	*Mesorhizobium*
Root700	Proteobacteria	Alphaproteobacteria	Caulobacterales	Caulobacteraceae	
Root708	Proteobacteria	Alphaproteobacteria	Rhizobiales	Rhizobiaceae	*Rhizobium*
Root710	Proteobacteria	Alphaproteobacteria	Sphingomonadales	Sphingomonadaceae	*Sphingomonas*
Root901	Bacteroidetes	Flavobacteriia	Flavobacteriales	Flavobacteriaceae	*Flavobacterium*
Root916	Proteobacteria	Gammaproteobacteria	Xanthomonadales	Xanthomonadaceae	
Root918	Actinobacteria	Actinobacteria	Actinomycetales	Promicromonosporaceae	
Root954	Proteobacteria	Alphaproteobacteria	Rhizobiales	Rhizobiaceae	*Rhizobium*
Root983	Proteobacteria	Gammaproteobacteria	Xanthomonadales	Xanthomonadaceae	
Root1203	Proteobacteria	Alphaproteobacteria	Rhizobiales	Rhizobiaceae	*Rhizobium*
Root1204	Proteobacteria	Alphaproteobacteria	Rhizobiales	Rhizobiaceae	*Rhizobium*
Root1212	Proteobacteria	Alphaproteobacteria	Rhizobiales	Rhizobiaceae	*Rhizobium*
Root1217	Proteobacteria	Betaproteobacteria	Burkholderiales	Comamonadaceae	
Root1220	Proteobacteria	Alphaproteobacteria	Rhizobiales	Rhizobiaceae	*Rhizobium*
Root1221	Proteobacteria	Betaproteobacteria	Burkholderiales	Comamonadaceae	
Root1240	Proteobacteria	Alphaproteobacteria	Rhizobiales	Rhizobiaceae	*Agrobacterium*
Root1252	Proteobacteria	Alphaproteobacteria	Rhizobiales	Rhizobiaceae	*Sinorhizobium*
Root1257	Actinobacteria	Actinobacteria	Actinomycetales	Nocardioidaceae	*Nocardioides*
Root1277	Proteobacteria	Alphaproteobacteria	Caulobacterales	Caulobacteraceae	
Root1280	Proteobacteria	Gammaproteobacteria	Pseudomonadales	Moraxellaceae	*Acinetobacter*
Root1290	Proteobacteria	Alphaproteobacteria	Caulobacterales	Caulobacteraceae	
Root1293	Actinobacteria	Actinobacteria	Actinomycetales	Microbacteriaceae	
Root1294	Proteobacteria	Alphaproteobacteria	Sphingomonadales	Sphingomonadaceae	*Sphingomonas*
Root1295	Actinobacteria	Actinobacteria	Actinomycetales	Streptomycetaceae	*Streptomyces*

Root1298	Proteobacteria	Alphaproteobacteria	Rhizobiales	Rhizobiaceae	*Rhizobium*
Root1304	Actinobacteria	Actinobacteria	Actinomycetales	Streptomycetaceae	*Streptomyces*
Root1310	Actinobacteria	Actinobacteria	Actinomycetales	Streptomycetaceae	*Streptomyces*
Root1312	Proteobacteria	Alphaproteobacteria	Rhizobiales	Rhizobiaceae	*Sinorhizobium*
Root1319	Actinobacteria	Actinobacteria	Actinomycetales	Streptomycetaceae	*Streptomyces*
Root1334	Proteobacteria	Alphaproteobacteria	Rhizobiales	Rhizobiaceae	*Rhizobium*
Root1455	Proteobacteria	Alphaproteobacteria	Caulobacterales	Caulobacteraceae	*Caulobacter*
Root1462	Proteobacteria	Alphaproteobacteria	Rhizobiales	Bradyrhizobiaceae	
Root1464	Actinobacteria	Actinobacteria	Actinomycetales	Microbacteriaceae	*Agromyces*
Root1471	Proteobacteria	Alphaproteobacteria	Rhizobiales	Phyllobacteriaceae	*Mesorhizobium*
Root1472	Proteobacteria	Alphaproteobacteria	Caulobacterales	Caulobacteraceae	*Caulobacter*
Root1485	Proteobacteria	Betaproteobacteria	Burkholderiales	Oxalobacteraceae	*Massilia*
Root1497	Proteobacteria	Alphaproteobacteria	Sphingomonadales	Sphingomonadaceae	*Sphingopyxis*
Root112D2	Actinobacteria	Actinobacteria	Actinomycetales	Microbacteriaceae	
Root123D2	Proteobacteria	Alphaproteobacteria	Rhizobiales	Bradyrhizobiaceae	*Afipia*
Root1433D1	Actinobacteria	Actinobacteria	Actinomycetales	Microbacteriaceae	*Microbacterium*
Root1480D1	Proteobacteria	Betaproteobacteria	Burkholderiales	Oxalobacteraceae	
Root16D2	Proteobacteria	Betaproteobacteria	Burkholderiales	Comamonadaceae	
Root198D2	Proteobacteria	Betaproteobacteria	Burkholderiales	Oxalobacteraceae	
Root280D1	Actinobacteria	Actinobacteria	Actinomycetales	Microbacteriaceae	*Microbacterium*
Root318D1	Proteobacteria	Betaproteobacteria	Burkholderiales	Comamonadaceae	*Variovorax*
Root336D2	Proteobacteria	Betaproteobacteria	Burkholderiales	Oxalobacteraceae	
Root444D2	Firmicutes	Bacilli	Bacillales	Paenibacillaceae	*Paenibacillus*
Root483D1	Proteobacteria	Alphaproteobacteria	Rhizobiales	Bradyrhizobiaceae	*Bosea*
Root483D2	Proteobacteria	Alphaproteobacteria	Rhizobiales	Rhizobiaceae	*Rhizobium*
Root487D2Y	Proteobacteria	Alphaproteobacteria	Caulobacterales	Caulobacteraceae	*Caulobacter*
Root66D1	Actinobacteria	Actinobacteria	Actinomycetales	Streptomycetaceae	*Streptomyces*
Soil522	Firmicutes	Bacilli	Bacillales	Paenibacillaceae	*Paenibacillus*
Soil531	Firmicutes	Bacilli	Bacillales	Bacillaceae	*Bacillus*
Soil535	Actinobacteria	Actinobacteria	Actinomycetales	Microbacteriaceae	*Agromyces*
Soil728	Actinobacteria	Actinobacteria	Actinomycetales	Intrasporangiaceae	*Janibacter*
Soil736	Actinobacteria	Actinobacteria	Actinomycetales	Micrococcaceae	*Arthrobacter*
Soil745	Firmicutes	Bacilli	Bacillales	Bacillaceae	*Bacillus*
Soil748	Actinobacteria	Actinobacteria	Actinomycetales	Intrasporangiaceae	*Janibacter*
Soil756	Actinobacteria	Actinobacteria	Actinomycetales	Intrasporangiaceae	*Janibacter*
Soil761	Actinobacteria	Actinobacteria	Actinomycetales	Micrococcaceae	*Arthrobacter*
Soil762	Actinobacteria	Actinobacteria	Actinomycetales	Micrococcaceae	*Arthrobacter*
Soil763	Actinobacteria	Actinobacteria	Actinomycetales	Micrococcaceae	*Arthrobacter*
Soil764	Actinobacteria	Actinobacteria	Actinomycetales	Micrococcaceae	*Arthrobacter*
Soil766	Firmicutes	Bacilli	Bacillales	Paenibacillaceae	*Paenibacillus*
Soil772	Proteobacteria	Gammaproteobacteria	Xanthomonadales	Xanthomonadaceae	*Rhodanobacter*
Soil773	Proteobacteria	Gammaproteobacteria	Xanthomonadales	Xanthomonadaceae	*Rhodanobacter*
Soil774	Actinobacteria	Actinobacteria	Actinomycetales	Nocardioidaceae	*Nocardioides*
Soil777	Actinobacteria	Actinobacteria	Actinomycetales	Nocardioidaceae	*Nocardioides*
Soil782	Actinobacteria	Actinobacteria	Actinomycetales	Micrococcaceae	*Arthrobacter*

Soil787	Firmicutes	Bacilli	Bacillales	Paenibacillaceae	*Paenibacillus*
Soil796	Actinobacteria	Actinobacteria	Actinomycetales	Nocardioidaceae	*Nocardioides*
Soil797	Actinobacteria	Actinobacteria	Actinomycetales	Nocardioidaceae	*Nocardioides*
Soil802	Actinobacteria	Actinobacteria	Actinomycetales	Intrasporangiaceae	*Janibacter*
Soil803	Actinobacteria	Actinobacteria	Actinomycetales	Intrasporangiaceae	*Janibacter*
Soil805	Actinobacteria	Actinobacteria	Actinomycetales	Nocardioidaceae	*Nocardioides*
Soil809	Actinobacteria	Actinobacteria	Actinomycetales	Microbacteriaceae	
Soil810	Actinobacteria	Actinobacteria	Actinomycetales	Intrasporangiaceae	
Soil811	Actinobacteria	Actinobacteria	Actinomycetales	Intrasporangiaceae	
Soil724D2	Firmicutes	Bacilli	Bacillales	Paenibacillaceae	*Paenibacillus*
Soil768D1	Firmicutes	Bacilli	Bacillales	Bacillaceae	*Bacillus*

Table 3.2: Summary of fungal strains used in the mono-association experiment with plants (Hacquard et al., 2016; Mesny et al., 2021).

Fungal strain ID	Phylum	Class	Order	Species	Strain	Host	Sampled in	Soil
Morel_U14_1	Mucoromycota	Mortierellomycetes	Mortierellales	*Mortierella elongata*	NEFU14	*Arabis alpina*	Cologne, Germany	Agricultural soil
Fuseq1	Ascomycota	Sordariomycetes	Hypocreales	*Fusarium equiseti*	G328	*Arabis alpina*	Cologne, Germany	Agricultural soil
Verdah1	Ascomycota	Sordariomycetes	Glomerellales	*Verticillium dahliae*	ER1879	*Arabidopsis thaliana*	Cologne, Germany	Agricultural soil
Chame1	Ascomycota	Sordariomycetes	Sordariales	*Chaetomium megalocarpum*	2	*Arabidopsis thaliana*	Cologne, Germany	Agricultural soil
Plecuc1	Ascomycota	Sordariomycetes	Glomerellales	*Plectosphaerella cucumerina*	RP01	*Arabidopsis thaliana*	Cologne, Germany	Agricultural soil
Daces1	Ascomycota	Sordariomycetes	Hypocreales	*Dactylonectria estremocensis*		*Arabidopsis thaliana*	Cologne, Germany	Agricultural soil
Fusre1	Ascomycota	Sordariomycetes	Hypocreales	*Fusarium redolens*	A4	*Arabidopsis thaliana*	Cologne, Germany	Agricultural soil
Ilyeu1	Ascomycota	Sordariomycetes	Hypocreales	*Ilyonectria europaea*	CBS 129078	*Arabidopsis thaliana*	Cologne, Germany	Agricultural soil
Neora1	Ascomycota	Sordariomycetes	Hypocreales	*Neonectria radicicola*		*Arabidopsis thaliana*	Cologne, Germany	Agricultural soil
Zalva1	Ascomycota	Leotiomycetes	Helotiales	*Zalerion varium*	ATCC28788	*Arabidopsis thaliana*	Cologne, Germany	Agricultural soil
Dacma1	Ascomycota	Sordariomycetes	Hypocreales	*Dactylonectria macrodidyma*		*Arabidopsis thaliana*	Cologne, Germany	Agricultural soil
Fusven1	Ascomycota	Sordariomycetes	Hypocreales	*Fusarium venenatum*		*Cardamine hirsuta*	Cologne, Germany	Agricultural soil
Fusoxys1	Ascomycota	Sordariomycetes	Hypocreales	*Fusarium oxysporum*		*Cardamine hirsuta*	Cologne, Germany	Agricultural soil
Mictri1	Ascomycota	Sordariomycetes	Xylariales	*Microdochium trichocladiopsis*	CBS 623.77	*Cardamine hirsuta*	Cologne, Germany	Agricultural soil
Stael1	Ascomycota	Sordariomycetes	Hypocreales	*Stachybotrys elegans*	LAHC-LSPK-M15	*Cardamine hirsuta*	Cologne, Germany	Agricultural soil
Cylol1	Ascomycota	Sordariomycetes	Hypocreales	*Cylindrocarpon olidum*	YIMPH30372	*Cardamine hirsuta*	Cologne, Germany	Agricultural soil
Denna1	Ascomycota	Dothideomycetes	Pleosporales	*Dendryphion nanum*	29	*Cardamine hirsuta*	Cologne, Germany	Agricultural soil
Parch1	Ascomycota	Dothideomycetes	Pleosporales	*Paraphoma chrysanthemicola*	PD 92/468	*Arabidopsis thaliana*	Geyen, Germany	Natural site
Altro1	Ascomycota	Dothideomycetes	Pleosporales	*Alternaria rosae*	DTO 242-I4	*Arabidopsis thaliana*	Pulheim, Germany	Natural site
Copph3	Basidiomycota	Agaricomycetes	Agaricales	*Coprinopsis phaeopunctatus*	AH 18881	*Arabidopsis thaliana*	Pulheim, Germany	Natural site
Phapo1	Ascomycota	Dothideomycetes	Pleosporales	*Phaeosphaeria poagena*	CBS 136771	*Arabidopsis thaliana*	Pulheim, Germany	Natural site
Rhesp1	Ascomycota	Leotiomycetes	Helotiales	*Rhexocercosporidium sp.*		*Arabidopsis thaliana*	Pulheim, Germany	Natural site
Altalt1	Ascomycota	Dothideomycetes	Pleosporales	*Alternaria alternata*	133aPRJ	*Arabidopsis thaliana*	Pulheim, Germany	Natural site
Olipa1	Basidiomycete	Agaricomycetes	Auriculariales	*Oliveonia pauxilla*	KC1149	*Arabidopsis thaliana*	Pulheim, Germany	Natural site
Fustri1	Ascomycota	Sordariomycetes	Hypocreales	*Fusarium tricinctum*		*Arabidopsis thaliana*	Saint-Die, France	Natural site
Fustr1	Ascomycota	Sordariomycetes	Hypocreales	*Fusarium tricinctum*	F194	*Arabidopsis thaliana*	Saint-Die, France	Natural site
Fusco1	Ascomycota	Sordariomycetes	Hypocreales	*Fusarium commune*		*Arabidopsis thaliana*	Saint-Die, France	Natural site
Truan1	Ascomycota	Sordariomycetes	Xylariales	*Truncatella angustata*	HP017	*Arabidopsis thaliana*	Saint-Die, France	Natural site
Chagl1	Ascomycota	Sordariomycetes	Sordariales	*Chaetomium globosum*		*Arabidopsis thaliana*	Saint-Die, France	Natural site
Macpha1	Ascomycota	Dothideomycetes	Botryosphaeriales	*Macrophomina phaseolina*	39R(3)	*Arabidopsis thaliana*	Saint-Die, France	Natural site

Sorhu1	Ascomycota	Sordariomycetes	Sordariales	*Sordaria humana*	xsd08003	*Arabidopsis thaliana*	Saint-Die, France	Natural site
Fusso1	Ascomycota	Sordariomycetes	Hypocreales	*Fusarium solani*	FSIF6	*Arabidopsis thaliana*	Saint-Die, France	Natural site
Fusoxy1	Ascomycota	Sordariomycetes	Hypocreales	*Fusarium oxysporum*	Fox64	*Arabidopsis thaliana*	Saint-Die, France	Natural site
Thacu1	Basidiomycota	Agaricomycetes	Cantharellales	*Thanatephorus cucumeris*	PT424	*Arabidopsis thaliana*	Saint-Die, France	Natural site
Boeex1	Ascomycota	Dothideomycetes	Pleosporales	*Boeremia exigua*	ZJUB106	*Arabidopsis thaliana*	Saint-Die, France	Natural site
Plecucu1	Ascomycota	Sordariomycetes	Glomerellales	*Plectosphaerella cucumerina*		*Arabidopsis thaliana*	Saint-Die, France	Natural site
Lepor2	Ascomycota	Leotiomycetes	Helotiales	*Leptodontidium orchidicola*	ZT98	*Arabidopsis thaliana*	Saint-Die, France	Natural site
Parchr1	Ascomycota	Dothideomycetes	Pleosporales	*Paraphoma chrysanthemicola*		*Arabidopsis thaliana*	Saint-Die, France	Natural site
Phimu1	Ascomycota	Leotiomycetes		*Leotiomycetes sp.*		*Arabidopsis thaliana*	Saint-Die, France	Natural site
Pyrly1	Ascomycota	Dothideomycetes	Pleosporales	*Pyrenochaeta lycopersici*	ISPaVe ER 1252	*Arabidopsis thaliana*	Saint-Die, France	Natural site
Chafu1	Ascomycota	Sordariomycetes	Sordariales	*Chaetomium funicola*	R9	*Arabidopsis thaliana*	Saint-Die, France	Natural site
Colin1	Ascomycota	Sordariomycetes	Glomerellales	*Colletotrichum incanum*	MAFF 238712			
Colto1	Ascomycota	Sordariomycetes	Glomerellales	*Colletotrichum tofieldiae*	strain 0861			

3.3.1.3. Soil batches

The batches CAS11, CAS13, and CAS15 of the Cologne agricultural soil were harvested in February 2015 and February 2017, and in February 2020, respectively, as previously described (Bai et al., 2015). ITA (Italian soil) was harvested from a vineyard in Bologna, Italy, in November 2016 (Harbort et al., 2020). The LRO soil was harvested in Las Rozas, Madrid, Spain in October 2016 (Hiruma et al., 2016).

3.3.1.4. Plant and microbe growth conditions

In the greenhouse experiment, the seeds of Col-0 wild-type, as well as mutant plants were surface sterilized with 70% ethanol, followed by 2% sodium hypochlorite solution from stock bleach solution with 12% active chlorine concentration (4ml bleach in 21ml sterile water + 20μl of Triton-X100 20%) by shaking for 10 mins at 300 rpm (rotator) respectively and finally washing 5 times with sterile water. The seeds were germinated on soil surface under greenhouse condition (16 hours under light at 21°C and 8 hours under dark at 19°C). Plants were grown for 5 weeks after germination.

In axenic conditions, seeds of Col-0 wild-type as well mutant plants were surface-sterilized with 70% (v/v) ethanol and 2% (v/v) bleach (12% (w/v) active chlorine, as above) and germinated on metal meshes placed on a half-strength of Murashige and Skoog (MS) basal salts (Sigma-Aldrich), supplemented with 1% (w/v) sucrose and 1% (w/v) agar. Seeds were stratified for 48 hours at 4ºC under dark conditions and cultured for 4 days under short-day conditions (10 hours under light at 21°C and 14 hours under dark at 19°C). The 4-day-old seedlings on the mesh were transferred aseptically into the glass jars containing sterile glass beads (1 mm) and 26 ml of a half-strength of liquid MS media. Glass jars were placed in a breathable Microbox (Sac O2, Belgium) and cultivated for 5 weeks under short-day condition (10 hours under light at 21°C and 14 hours under dark at 19°C).

For the plant-fungi interaction assay, Col-0 wild-type as well as mutant plants *pyk10bglu21* and *cyp79b2b3* were surface-sterilized with 70% ethanol, followed by 2% (v/v) bleach (12% (w/v) active chlorine, as above) by shaking for 10 min at 300 rpm (rotator) respectively and finally washing 5 times with sterile water and co-inoculated with fungal strains as mentioned in section 3.3.4 below.

3.3.1.5. Harvesting root compartments

After plant cultivation, roots and soils were harvested from pots and fractionated into rhizosphere, rhizoplane, and endosphere, as previously described (Durán et al., 2018). The soil particles physically attached to the root surface were collected as a rhizosphere fraction by shaking vigorously in sterile water followed by centrifugation. Microbes on the root surface were collected as a rhizoplane fraction by washing the roots with detergent using 1× Tris-EDTA-Triton-X100 (TE-T) (0.1% of Triton X-100 was added to 1× TE, prepared from autoclaved 10× TE, the ratio was 1/100) buffer followed by filtration through a 0.22-micrometer membrane. The roots were then surface sterilized with 80% ethanol followed by 2% sodium hypochlorite solution from stock bleach solution with 12% active chlorine concentration (4ml bleach in 21ml sterile water) and an endosphere fraction was obtained as described in Durán et al., 2018. All samples were immediately frozen in liquid nitrogen and stored at -80°C until processing (Figure 3.2).

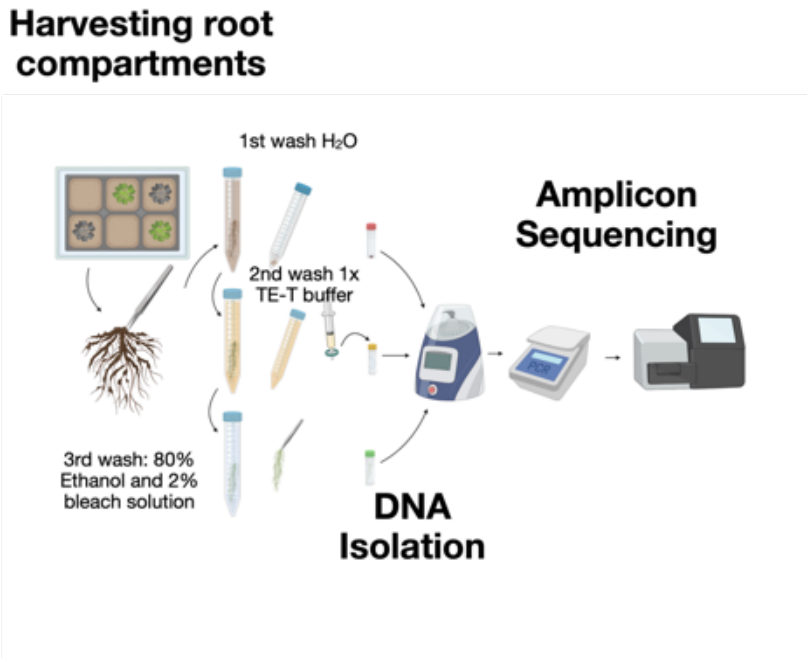

Figure 3.2: Sampling of root compartments: Soil, Rhizosphere (sterile water), Rhizoplane (three times washed with 1× TE-T buffer and filtered by using a membrane) and endosphere (surface sterilized roots using 80% ethanol and 2% bleach solution). The samples were homogenized for DNA isolation. The DNA templates were amplified and used for amplicon sequencing.

3.3.2. Root secreted compounds from plants

3.3.2.1. Collection of root exudates

Root exudates were collected from plants hydroponically grown in axenic glass jars containing glass beads, as previously described (Wippel et al., 2021) (see Figure 3.3). The seeds of Col-0 wild-type, as well as mutant plants *pyk10bglu21* and *cyp79b2b3* were surface sterilized with 70% ethanol,

followed by 2% sodium hypochlorite solution from stock bleach solution with 12% active chlorine concentration (4ml bleach in 21ml sterile water + 20μl of Triton-X100 20%) by shaking for 10 mins at 300 rpm (rotator) respectively and finally washing 5 times with sterile water. The seeds were germinated in metal meshes placed on a half-strength of Murashige and Skoog (MS) basal salts (Sigma-Aldrich), supplemented with 1% sucrose and 1% agar under short-day conditions (10 hours light at 21°C and 14 hours dark at 19°C) for 5 days, after stratification for 48 hours at 4°C under dark conditions. Meshes supporting the growth of 4-day-old seedlings were transferred aseptically into glass jars containing 26 ml of a half-strength liquid MS medium. The glass jars were placed in a breathable Microbox (Sac O2, Belgium) and cultivated for 5 weeks on a short day. Hydroponic media was collected using an aseptic stainless needle in 50 ml tubes and concentrated to 1/10 volume using a freeze-dryer. As a blank, liquid MS was incubated in microboxes without the plant.

Figure 3.3: Hydroponic culture system to extract root exudates from axenic plants. The seeds were sowed on metal mesh. The seedlings of 5 DAG (days after germination) were transferred along with the mesh into the glass jars containing liquid media (1/2 strength MS) under aseptic conditions. After 5 weeks, the media were collected with a syringe and concentrated to 1/10th of the volume using freeze dryer.

3.3.2.2. Collection of root extracts

To collect root extracts, we cultured Col-0 wild-type plants as well as mutant plants of *pyk10bglu21* and *cyp79b2b3* in half-strength MS medium with 1% agar (Bacto Agar) without vitamins and sucrose for 21 days (as mentioned in section 3.3.2.1). The roots were weighed, harvested in tubes containing 1-mm zirconium beads, and frozen in liquid nitrogen and stored at -80°C until further processing. Immediately before treatment, roots were homogenized using Precellys 24 at 6300 rpm and flash freeze in liquid nitrogen. Phospho-buffered saline was added, and the sample was homogenized for another 30 seconds to obtain a concentration of 10 mg/ml of root extracts. After homogenization, the tubes were centrifuged at 20,000 rpm for 5 mins (Eppendorf desktop centrifuge) and the supernatant was immediately used for the soil treatment (Section 3.3.3.1).

3.3.2.3. Metabolite profiles

The liquid chromatography and mass spectrometry (LC-MS) system consisted of ultra-pressure liquid chromatography (UPLC) with a photodiode array detector PDAeλ (Acquity System; Waters) hyphenated to a high resolution QExactive hybrid MS/MS quadrupole Orbitrap mass spectrometer (Thermo Scientific). The chromatographic profiles of the metabolites and the quantitative measurements were obtained using water acidified with 0.1% formic acid (solvent A) and acetonitrile (solvent B) with a mobile phase flow of 0.35 ml min−1 on an ACQUITY UPLC HSS T3 C18 column (2.1 × 50 mm, 1.8 µm particle size; Waters) at 22°C. The sample of volume 5 µl was injected into the inlet port after cleaning and rinsing the system. The QExactive MS operated in Xcalibur version 3.0.63 with the following settings: heated electrospray ionization ion source voltage 3 kV; sheath gas flow 30 L min^{-1}; auxiliary gas flow 13 L min^{-1}; ion source capillary temperature 250°C; auxiliary gas heater temperature 380°C. The MS / MS mode (data dependent acquisition) was recorded in negative and positive ionization, with resolution 70000 and AGC (ion population) target $3e^6$, scan range 80 to 1000 mass-to-charge ratio (m/z).

3.3.2.4. Data Analysis

The LC-MS data were processed for peaks detection, deisotoping, alignment, and gap filling by MZmine 2.51 (Pluskal et al., 2010) separately for positive and negative ionization mode, then data from both modes were combined. The prepared data table was post-processed for missing value imputation, log_2 transformation, and data filtering by MetaboAnalyst (Pang et al., 2021). The data were then visualized by CCA using *vegan* (Dixon, 2003) package in R environment, differential analysis of the normalized peak intensities was conducted using generalised linear model GLM by using the *limma* package in R environment.

3.3.3. *In-vitro* microbiota reconstitution

3.3.3.1. Soil treatment with root-secreted compounds

Approximately 500 mg of CAS soil was transferred to 2 ml screw caps and treated with 50 *µ*l of root exudates or root extracts. The tubes were covered with breathable tape and incubated at 28°C in dark conditions. Root exudates or freshly prepared root extracts were added every 3 days to replenish the weight lost due to evaporation of the moisture content. Root-derived compounds were added to maintain the moisture level constant. The soil-containing tubes were freeze-dried and stored at -80°C until further processing.

3.3.3.2. SynCom experiment

Bacterial cultures were recovered from glycerol stocks on plates containing 50% trypsin soy broth (TSB) supplemented with 1.5% agar and cultured in 96 deep well plates, each well containing 1 ml of 50% TSB, at 25°C for 4 days. Sixty μL of cultures were transferred to 600 μL of 50% sterile TSB media in another set of 96-well plates and both 4-day old and freshly prepared plates were further cultured under the same conditions. Cultures from different plates were pooled for each strain and OD_{600} was approximately adjusted to 0.5. Strains were then pooled into a new tube to have the final OD_{600} bacteria concentration as 1. The bacterial inoculum was centrifuged at 3000 rpm (Eppendorf centrifuge with the rotor that can accommodate 15ml falcon tubes) for 10 min to remove the TSB, followed by washing twice in 10mM $MgCl_2$. The obtained pellet was dissolved in $MgCl_2$ and OD_{600} was adjusted to 1. The starting inoculum was incubated at 25 ºC overnight in $MgCl_2$ without any carbon source as a starvation process to let the bacteria fully rely on the root exudate as the sole nutrient source. During the day of treatment, the concentration of the starting inoculum was adjusted to OD_{600} 0.5. The inoculum was diluted to OD_{600} 0.05 and 0.005 by adding root exudates, obtaining a final volume of 50 μl. The bacterial cells were harvested after 24 and 72 hours. A strain of *Escherichia coli* (DH5α) was used as a spike-in for calculating the quantitative abundance. The cells were adjusted to OD_{600} 0.01 and 0.001 and used as spike-in at the time of harvest. We assume that after 72 hours post-inoculation (hpi) of SynCom treatment (50μl of inocula and 50μl of root exudates in each well) will result an OD_{600} of ~2. The starting concentration of the *E.coli* cells was OD_{600} 0.05 in LB media, therefore the amount of spike-in should be estimated such that 30% of the sequencing reads belong to spike-in and they are estimated in the sequencing coverage. Approximately, 1.2 μl of *E.coli* OD_{600} 0.05 is to be added into 100 μl of the culture. The harvested cultures were immediately processed for DNA isolation.

3.3.3.3. DNA isolation

Ten μl buffer1 (NaOH 25 mM- 1g/l and EDTA (Na) 0.2mM - 74,448 mg/l at pH 12) was added to each 96-well plate using filtered pipet tips. Six μl of bacterial culture and 1μl of spike-in (normal tips) were added to each well. The plate was quickly vortexed and centrifuged at top speed for 1 min (Eppendorf tabletop centrifuge with rotor that can accommodate 1.5 ml or 2 ml tubed) and incubated at 95°C for 30 min. Ten μl buffer2 (Tris-HCl 40mM – 0,484g/l -adjust pH 7.46 adjusted by HCl) was added to each well. After mixing with equal volumes of buffers 1 and 2, the final pH was 8.56, which is similar to PCR buffer (pH 8.8). The samples were stored at -20°C.

3.3.4. Binary interaction between plants and fungi

3.3.4.1. Preparation of fungi

Fungi were inoculated as previously described in Frerigmann et al., (2021) and Mesny et al., (2021). A fresh batch of fungi was cultured before the co-inoculation experiment. Fungal mycelia (~50 mg) were collected from a fresh culture in potato glucose agar (PGA) plates and homogenized in 10 mM $MgCl_2$. The homogenate was then used to inoculate surface-sterilized seeds.

3.3.4.2. Co-inoculation of fungi and plants

The plants and fungi were co-cultured in half-strength MS medium supplemented with 1% agar and without vitamins and sucrose for 21 days under short-day conditions (10 h of light 21°C and 14 h of dark 19°C). As a mock treatment, we did not co-inoculate seeds with fungal mycelium instead we treated the same batch of seeds with 10mM $MgCl_2$.

3.3.4.3. Quantification of plant phenotype

The shoot fresh weight was measured after 21 days of cultivation and the plant phenotype photos were captured after 21 days of co-inoculation.

3.3.5. Microbiome analysis

3.3.5.1. Molecular analysis

Total DNA from the samples harvested from greenhouse experiments was extracted using the FastDNA SPIN Kit for Soil (MP Biomedicals, Solon, USA), as previously described (Durán et al., 2018). Bacterial cells in liquid cultures were lysed in sodium hydroxide and then Tris-HCl was added, and the lysate was directly used as a PCR template, as previously described (Bai et al., 2015). DNA templates obtained from the root compartments and soil were diluted to 3.5 ng/ml or less and used in a two-step PCR amplification protocol: First, the V5–V7 region of the 16S bacterial rRNA gene and the fungal ITS1 gene were amplified in triplicate reactions for each sample with primers 799F and 1192R for bacteria and ITS1F and ITS2 for fungi. The amplification was performed in a 25-μl reaction volume containing 2 IU of DFS-Taq DNA polymerase (Bioron), incomplete buffer, 2 mM $MgCl_2$, 0.3% bovine serum albumin, 0.2 mM each dNTPs (Life Technologies) and 0.3 mM forward and reverse primers. The same PCR parameters were used for each primer pair (94°C for 2 min, 94°C for 30 s, 55°C for 30 s, 72°C for 30 s and 72°C for 10 min for 25 cycles). Single-stranded DNA and proteins were digested by adding 1 μl of Antarctic phosphatase, 1 μl of Exonuclease I and 2.44 μl Antarctic Phosphatase buffer (New England Biolabs) to 20 ml of the pooled replicate reactions. The PCR-1 product was digested at 37°C for 30 min, followed by enzyme deactivation at 85°C for 15 min. The digested PCR products were centrifuged for 10 min at 4,000 rpm (Eppendorf centrifuge with rotor that

can accommodate 96-well plate), and 3 ml of supernatant were used for the second step in triplicate reactions to add reverse and forward barcodes and sequencing adapters for the Illumina MiSeq platform. The barcoded index primers were used in PCR reactions as above with the number of cycles reduced to ten. This dual barcoding was performed only with SynCom samples and soil treatment samples. In the third PCR, a different set of reverse primers was used to amplify the pooled PCR-2 products. The PCR-2 products were checked by running agarose gel electrophoresis and then pooled at an approximately similar concentration and amplified using barcoded forward primers and reverse primers p7_PAD1 (Wippel et al., 2021). The quality control (QC) of the PCR products was carried out by loading 5 μl of each reaction products on a 1% agarose gel. In the QC step we checked whether the obtained band on the electrophoresis corresponded to the marker specific for the 16S region and ITS1 region. In the case of 16S, the remaining reaction volume was loaded onto a 1.5% agarose gel and run at 80 V for 2 h; bands with the correct size of ~500 base pairs were cut and purified using the QIAquick Gel Extraction Kit (Qiagen). The concentration of purified DNA was determined and 30 ng of DNA from each of the barcoded amplicons was pooled in one library per experiment, then purified and reconcentrated twice with AMPure XP beads (Beckman Coulter). Paired-end Illumina sequencing was performed using the MiSeq sequencer (MiSeq Reagent Kit V3, 600-cycle) and custom sequencing primers.

3.3.5.2. Bioinformatic analysis

Preprocessing, demultiplexing and analysis of amplicon sequence variants (ASV) were performed using the DADA2 pipeline (Callahan et al., 2016). The taxonomy of the ASVs was assigned by referring to the SILVA database version 138 (Quast et al., 2013) for bacteria and UNITE database (Nilsson, 2019) for fungi. The bacterial SynCom data were analysed with the Rbec pipeline (P. Zhang et al., 2021).

3.3.5.3. Statistical data analysis

All statistical analyses were performed in R programming language (https://www.r-project.org/). Unconstrained and constrained principal coordinates analysis (PCoA and CPCoa) was performed based on the Bray-Curtis dissimilarities for the greenhouse experiments and soil treatment experiments and the Euclidean distances for the SynCom experiments, using the *cmdscale* and *capscale* functions in the *stats* and *vegan* packages. Multiple comparison tests were conducted using Tukey-HSD with adjusted *p-value* ≤ 0.05. The statistical difference between the wild type (Col-0) and mutant genotype was examined by Pairwise PERMANOVA using the *adonis2* function in the vegan package. Differential abundance of ASVs, aggregated ASVs, and absolute abundance of strains (SynCom) were conducted using the *edgeR* package by fitting the relative abundance or absolute

abundance to a generalised linear model with negative binomial distribution, controlling for sequencing batch, technical replicates, and the experimental batch as random factors.

3.4. Results

3.4.1. PYK10 and Trp-pathway have an impact on the composition of compounds exuded through roots

To directly test whether PYK10 and BGLU21 are involved in the secretion of secondary metabolites from roots, we analysed root exudates from wild-type *A. thaliana* Col-0, ER body mutant plants *nai1-1* and *pyk10bglu21*, indole glucosinolate mutant *myb34/51/122* and Trp pathway impaired mutant *cyp79b2b3* by collecting hydroponic cultures (Wippel et al., 2021). Seedlings were pregerminated in a metal mesh, transferred to the hydroponic culture system using liquid MS media after 4 days of preculture, and axenically cultivated for 5 weeks under short-day conditions (10 hours light at 21°C and 14 hours dark at 19°C until flowering). Root exudates were then collected and concentrated to 1/10 volume and subjected to untargeted high performance liquid chromatography followed by 2-dimensional mass spectrometry (HPLC-MS/MS) analysis (see the method in Figure 3.3, section 3.3.2.1). By assessing the metabolite profile of the peaks detected from the chromatogram, I performed a canonical correlation analysis. In this analysis I reduced the number of peaks in two dimensions and found a significant impact of genotype on the metabolome which could explain 20.09% of the variance in the data (Figure 3.4). Interestingly, I found that the composition of the metabolome in mutant root exudates differed from that of Col-0 and also differed from the media (5× MS, considered as blank-without exudates) (Figure 3.4). This revealed that ER body pathway, the Trp pathway, and the indole glucosinolate pathway have an impact on the root exudate metabolome.

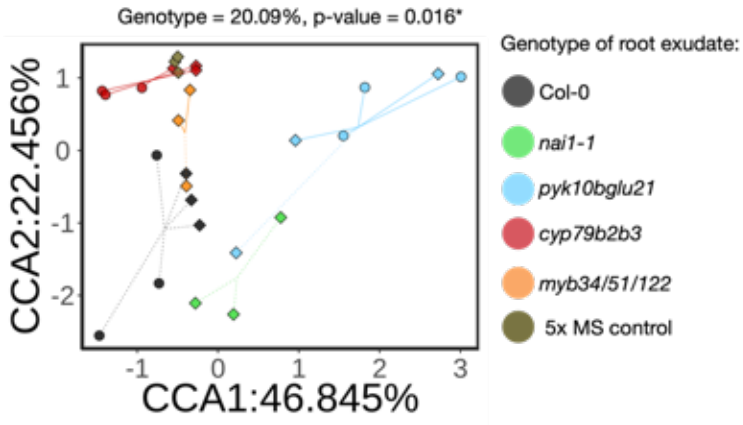

Figure 3.4: The metabolome of root exudates; constrained canonical analysis using genotype as a constraint factor. The dotted and solid lines indicate further separation of the data points in the third component. Genotypes are indicated in colours.

I identified 85 metabolites that are commonly depleted in all mutants compared to the wild-type exudates, which indicates that the ER body pathway and Trp-pathways influence the secretion of an overlapping set of compounds (Figure 3.5, n = 3, FDR ≤0.05, GLM analysis). Among the root exuded

metabolites, we detected peaks in Col-0 exudates that were not present in the blank (5× MS media), indicating that these compounds were indeed secreted from the roots. Among the metabolites that are detected in the Col-0 root exudates but not in the blank, we find a group of signals that were depleted in mutant exudates compared to Col-0 exudates (Figure 3.6).

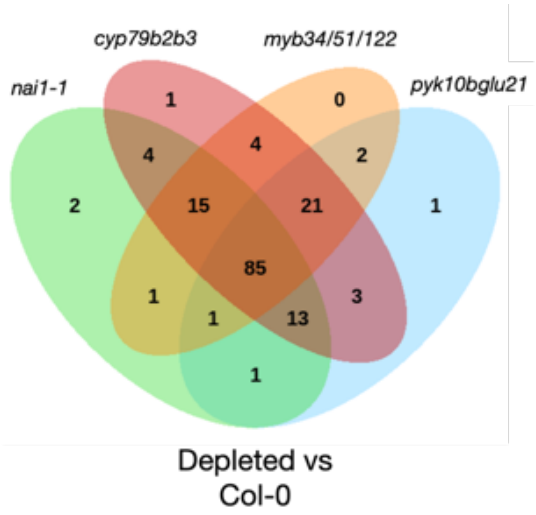

Figure 3.5: The PYK10 and Trp pathway are involved in the secretion of secondary metabolites in roots; Venn-diagram of depleted metabolites compared to Col-0 obtained by conducting GLM analysis.

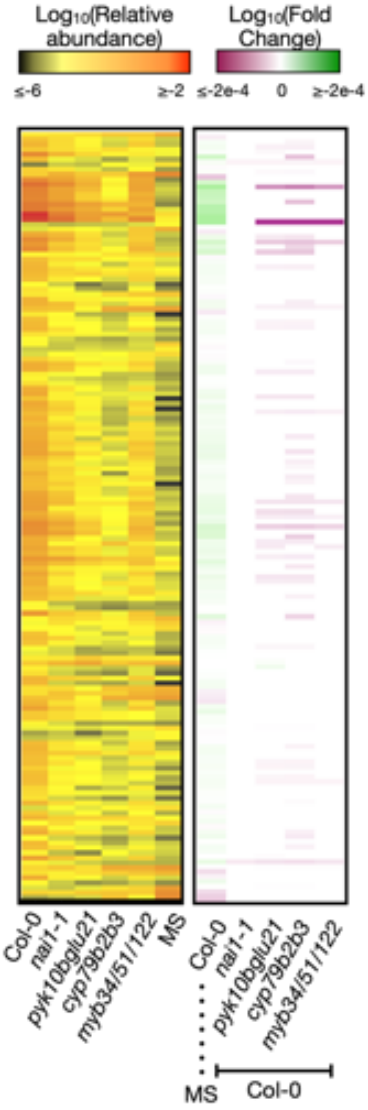

Figure 3.6: Heatmap showing (left) the relative abundance of a subset of metabolites (y-axis) for the plant genotype (x-axis) in $\log_{10}$ scale (black to red) and (right) $\log_2$ fold change (magenta to green) of mutant genotypes compared to Col-0 and Col-0 compared to MS (compounds that are potentially secreted in the media in the presence of the plant) at FDR ≤0.05. The compounds were clustered using the WARD.D2 algorithm.

Among the compounds that were depleted in *pyk10bglu21* root-exuded secondary metabolites, the mass-to-charge ratios (m/Z) and retention time (RT) of 16 peaks were similar to those of metabolites that were previously identified in the root-exuded secondary metabolite database (Strehmel et al., 2014) (Figure 3.5). This suggests that the PYK10 is involved in the secretion of a group of compounds that are exuded by roots.

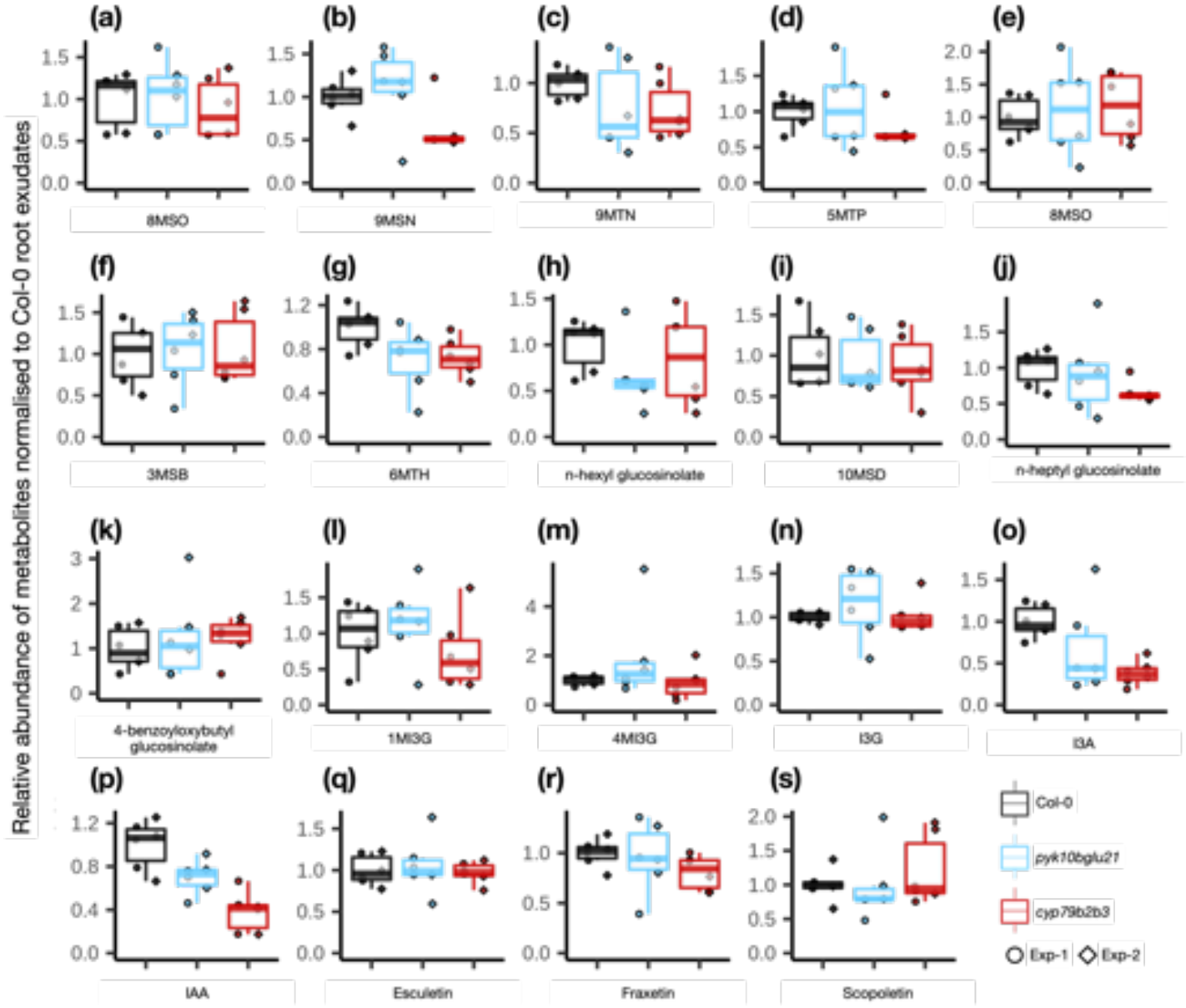

Figure 3.7: Composition of targeted secondary metabolites within mutant root exudates (n = 6). The box plots represent the group of aliphatic glucosinolates (a-j), benzyl glucosinolates (k), indole glucosinolates (l-n), indolic compounds (o and p), and coumarins (q-s) that show differences in the peak intensity (y-axis) in $\log_2$ scale across the genotypes (colours) across the biological replicates (shapes). The abbreviations of the chemical compounds are in list of abbreviations (see section 8).

Furthermore, by annotating the compounds based on the mass-to-charge ratio and retention time with respect to a custom database (using standard compounds), we found that compounds derived from Trp such as IAA (indole acetic acid), I3A (indole-3-acetonitrile), and 6MTH (6-methylthio-*n*-hexyl glucosinolate) are commonly depleted in *cyp79b2b3* mutant exudates. The same set of compounds were depleted to a lesser extent in *pyk10bglu21* mutant exudates (Figure 3.7p, o, and g, respectively). The abundances gluosinolates like 9MSN (9-methylsulfinylnonyl glucosinolate) and I3G (indole-3-glucosinolate) increased in *pyk10bglu21* mutants, suggesting that PYK10 contributes to their degradation (Figure 3.7b and n, respectively). This indicates that the PYK10 contributes to the

production and/or secretion of compounds that are exuded by roots sharing a similarity with the compounds downstream of Trp pathway.

3.4.2. ER bodies and Trp-pathway coordinate the root microbiota assembly

To investigate the impact of ER bodies and Trp-derived secondary metabolites on the assembly of the root microbiota, I cultured the same set of mutants (*pyk10bglu21*, *nai1-1*, *myb34/51/122*, and *cyp79b2b3*) along with wild-type Col-0 plants on three different natural soils in a greenhouse and profiled the bacterial and fungal communities associated with their roots by an amplicon sequencing approach. I sequenced the V5-V7 region of 16S ribosomal RNA gene for bacterial community profiling and internal transcribed spacer region 1 (ITS1) for fungal community profiling. We included nutrient-rich clay soil from Cologne, Germany (Cologne Agricultural Soil; CAS; batches CAS11 and CAS13) (Bulgarelli et al., 2012), calcareous clay soil from a vineyard in Bologna, Italy (ITA, limited available iron content) (Harbort et al., 2020), and phosphorus-limiting sandy soil from Madrid, Spain (LRO - Las Rozas, limited in phosphorous content) (Hiruma et al., 2016). A previous study showed that a mutant impaired in coumarin biosynthesis possessed an altered composition of root microbiota in comparison to Col-0 wild-type, and this effect was more prominent in the iron-deficient ITA soil (Harbort et al., 2020). It was also shown that root-secreted coumarin is associated with recruitment of beneficial microbes that are capable of supporting iron acquisition in roots. *Colletotrichum tofieldiae*, a fungal endophyte isolated from *A. thaliana* plants growing in Las Rozas, where our LRO soil was collected, exerts plant-growth promoting activity only under phosphorus-limited conditions, and it was reported that this beneficial trait was not observed in *cyp79b2b3*, showing a negative effect on the growth (Hiruma et al., 2016). These findings indicate that the behaviour of plant-microbe interactions depends on nutrient conditions, and the Trp pathway plays a role in this process. Therefore, by comparing these different soil types, I aimed to address whether there is a consistent effect of root compartment in shaping root microbiota in different soil types. The sequenced reads were classified into amplicon sequence variants (ASVs) and used to quantify the relative abundance of each ASV and to perform multivariate analysis. A principal coordinates analysis (PCoA) based on Bray-Curtis dissimilarity indices revealed that the root compartment and soil type has a major impact on the microbiota composition (Figure 3.8). The differences in the structure of bacterial community are captured in the PCoA 2 by the soil geochemical factors (Figure 3.8a). Consistent with previous reports, I observed that the bacterial community structure in the roots from different soil types converges in the endosphere fraction (Durán et al., 2018) (Figure 3.8a). This indicates that *A. thaliana* roots accommodate a similar structure of bacterial communities irrespective of the soil geochemical characteristics.

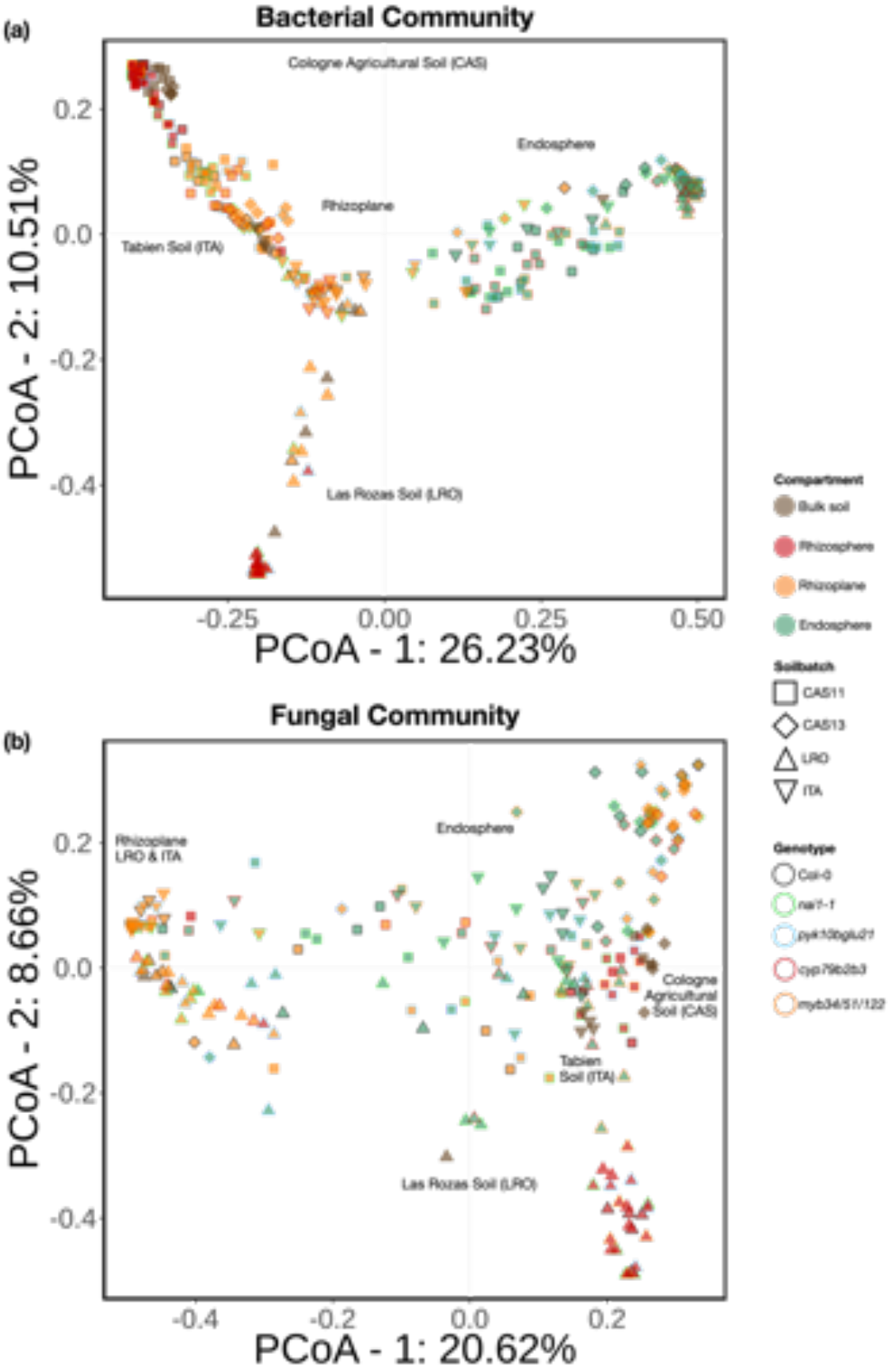

Figure 3.8: The composition of the root-associated community; the composition of the overall (a) bacterial community and (b) fungal community in different root compartments and soil (indicated in colour fill). The point border colour indicates the different genotypes and the shapes indicate different soil batches.

On the other hand, the structures of the fungal communities did not converge in the endosphere (Figure 3.8b). The community structures of the rhizoplane and rhizosphere compartments differed in different soil types, which is similar to the bacterial community structures. On the other hand, the across sample diversity or the β-diversity within the endosphere and rhizoplane compartments of the mutant and wildtype plants were mainly due to the different soil batches. The beta diversity within these compartments indicates that soil-geochemical factors are crucial for the plant-fungal interactions. These results suggest that the structure of the fungal community differs in the endosphere as well as in rhizoplane and rhizosphere compartments depending on the soil type.

To investigate the effect of genotype within CAS soil, I conducted a constrained PCoA in which the effect of genotypes was considered as the constraining factor and the effect of different soil batches was considered as a conditioning factor to account for the randomness in the data (Figure 3.9). The genotype explains 5.398% and 3.625% of variation in the structure of the bacterial community of the rhizoplane and endosphere respectively (Figure 3.9a). The community structure was significantly different from that of Col-0 bacterial community structure. This indicates that the PYK10 pathway and Trp-derived secondary metabolites have an impact on the rhizoplane community structure. However, the variations in the fungal community structure due to genotype are 10.34% and 11.01% at rhizoplane and endosphere compartments, respectively. Interestingly, we found that PYK10 and Trp-derived secondary metabolites have a significant impact on the endosphere, as shown by a community shift in the *pyk10bglu21* and *cyp79b2b3* mutants compared to Col-0 wild type within the endosphere compartment (Figure 3.9b). These results indicate that the Trp pathway has a crucial role in plant-microbiota interactions and that ER body-localized PYK10 and BGLU21 have a role in the root microbiota assembly. Given the fact that ER bodies and Trp-derived secondary metabolites are abundant in roots, it is possible that the downstream compounds produced or secreted in a manner dependent on PYK10 play a role in the structure of the bacterial community in the rhizoplane compartment, and these compounds are also crucial for resistance against fungi.

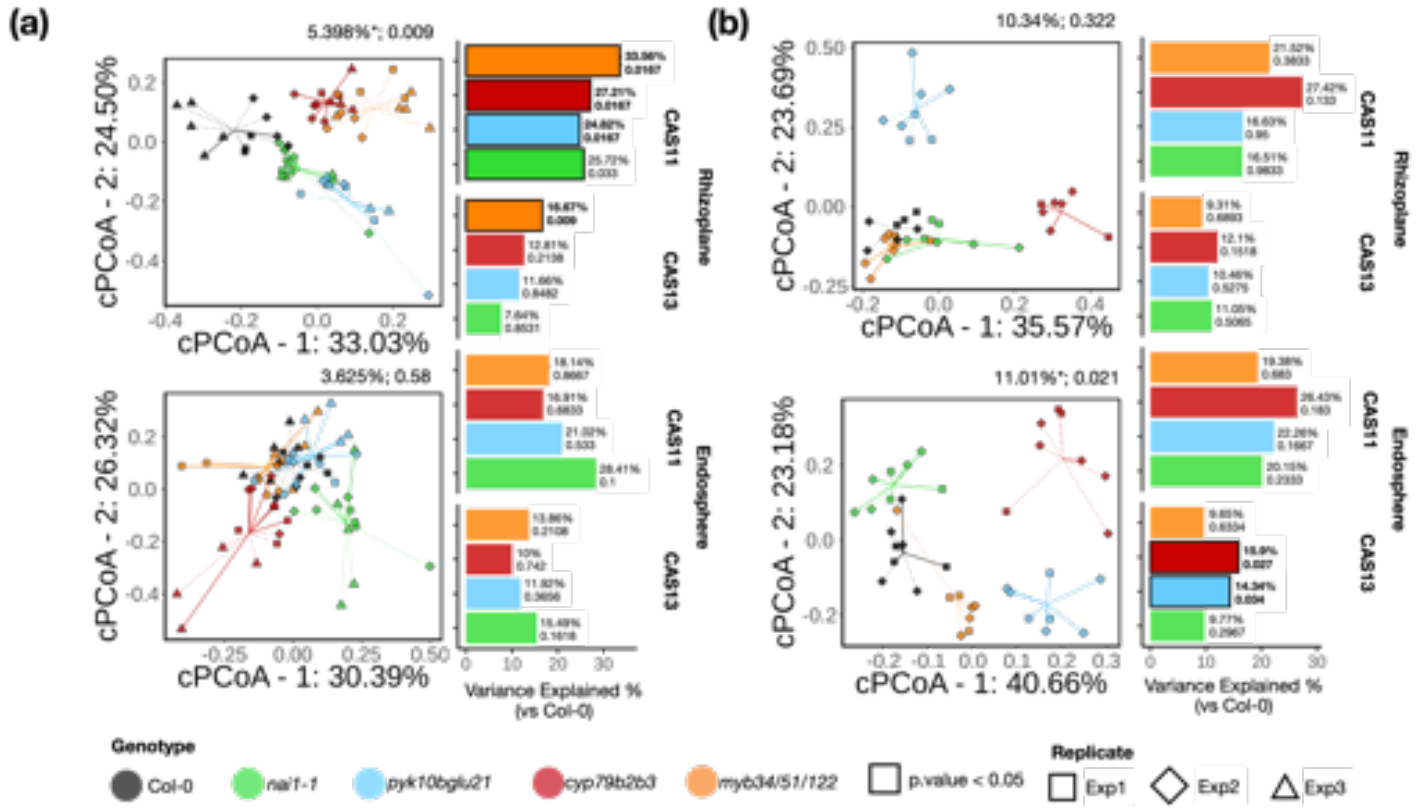

Figure 3.9: The change in the microbial community due to the lack of PYK10 myrosinase and its substrate in the host root microbiota; the microbiome community structure is represented in the cPCoA scatter plots and the variation explained by the mutant genotype compared to Col-0 is represented in the barplots. The bacterial community is represented in panel (a) with rhizoplane (above) and endosphere (below), and the fungal community is represented in panel (b) with rhizoplane and endosphere placed above and below respectively. The colours represent the genotypes and the shape represent biological replicates. Barplots that are statistically significant are marked (pseudo p.value ≤ 0.05). The constrained variance explained (%) and the pseudo p.value is mentioned in the text beside the barplots.

Overall, my analysis illustrates that the assembly of the microbial community is primarily dependent on the geochemical factors of the soil and the difference between the rhizoplane and endosphere fractions. The soil geochemical parameters show that the nutrient, chemical and texture composition is different across the soil types used in the greenhouse experiments (Table 3.3). Besides, within the rhizoplane and endosphere compartments, the ER body and Trp pathway metabolites play a role in the assembly of the microbial community. These findings demonstrated that PYK10-mediated metabolism and Trp-derived metabolites play a role in root microbiota community assembly. The Trp pathway is responsible for the biosynthesis of indolic compounds, including IGs, the potential substrate of PYK10 (Nakano et al., 2017). This finding, combined with our previous findings that the metabolite profile secreted by these mutant roots differs from that of Col-0 wild-type plants, raises the possibility that the community change was mediated by the root-secreted compounds. Alternatively, the community shift was triggered due to the presence of other eukaryotes in the soil, as the behaviour of the inter-specific interaction between the microbes could be modulated by the presence or absence of the plant. Further analysis in my research will reveal whether the

observed community shift in the mutant compartment is due to the difference in the terminal products of the pathway secreted by the roots.

Table 3.3: Summary of the soil geochemical factors used in the greenhouse experiment.

Factor	CAS11 (Cologne Agricultural Soil)	LRO (Las Rozas)	ITA (Tebano)
Humus % (g/g)	1.5	1.5	1.5
Clay % (g/g)	16	1	26
Sand % (g/g)	11	1	11
pH	7.6	6.7	7.6
Available Nitrate (mg/kg)	10.9	3	9.2
Available Phosphorus (mg/kg)	0.7	3.3	1.2
Available Potassium (mg/kg)	6.5	15.2	45.3
Available Calcium (mg/kg)	75.6	25.7	178.6
Available Magnesium (mg/kg)	9	4.5	18.4
Total Phosphorus (mg/kg)	17	19,5	12
Total Potassium (mg/kg)	90.5	93.1	280.1
Total Calcium (mg/kg)	2178	2000	69360
Total Magnesium (mg/kg)	160.9	278.9	720.9
Boron (mg/kg)	0.1	-0.1	0.5
Manganese (mg/kg)	79	8	269
Copper (mg/kg)	2.7	1.2	30.6
Iron (mg/kg)	148	55	378

3.4.3. Root secreted compounds modulated by the PYK10 myrosinase and Trp pathways have an impact on the microbiota community structure

To directly investigate the impact of root secreted metabolites downstream of PYK10 and Trp-pathway on root microbiota community structure, I treated natural soils (CAS15) with root exudates collected from *pyk10bglu21* and *cyp79b2b3* mutant plants along with Col-0 wild type plants (see Section 3.2.1) and analysed the structure of the bacterial and fungal community. To discriminate the effects of root-secreted and root-accumulating metabolites, I also treated the soil with root crude extracts from these genotypes. The community structure was analysed by determining the number of ASVs obtained from 16S V5-V7 region and ITS1 region amplicon sequencing. Constrained PCoA was performed and found a significant effect of the genotype on the bacterial and fungal community structure when the soil was treated with root exudates and root extracts of the mutant plants and wild-type plants (Figure 3.10). Firstly, root exudates and root extracts triggered community assembly that was different from the soil treatment with respective treatment with 5x MS and phosphate saline buffer (PBS) as mock. In addition, treatments of soils with mutant root exudates resulted in a significantly different microbiota community compared to soils treated with Col-0 exudates (Figure 3.10a and b).

This clearly indicates that the compounds exuded by roots in a manner dependent on PYK10 and on the Trp pathway influence the process of the microbial community assembly. This could be due to an active secretion of the secondary metabolites downstream of Trp pathway, such as camalexin, I3C, or IGs, or the hydrolysed products produced by the ER body pathway. However, while soil treatments with the extracts of *cyp79b2b3* roots triggered both bacterial and fungal community changes that were significantly different from Col-0 root extract treatment, the difference between soils treated with *pyk10bglu21* and Col-0 root extracts was relatively small. Preparation of root extracts involves complete homogenization of root tissues, which allows myrosinases to react with glucosinolates, which are normally physically separated in intact roots under physiological conditions. The difference in the effect of root secretion on soil-microbiota composition was estimated between mutants and Col-0 extract and exudate treatments respectively. The effects of *pyk10bglu21* root extracts on soil microbiota was not prominent and less compared to the effect of *pyk10bglu21* root exudates on the microbiota. This is in contrasts to the difference between *cyp79b2b3* and Col-0 root extracts, as both root extracts and root exudates from *cyp79b2b3* triggered the community shift in soil microbiota compared to treatment with Col-0 root secretions. These observations indicate that the PYK10- and BGLU21-dependent hydrolysis of secondary metabolites is actively regulated in intact roots to control the profiles of root-secreted compounds. Combined with the greenhouse experiments, these findings suggest that ER body-regulated secretion of root metabolites play a role in shaping the root microbiota assembly.

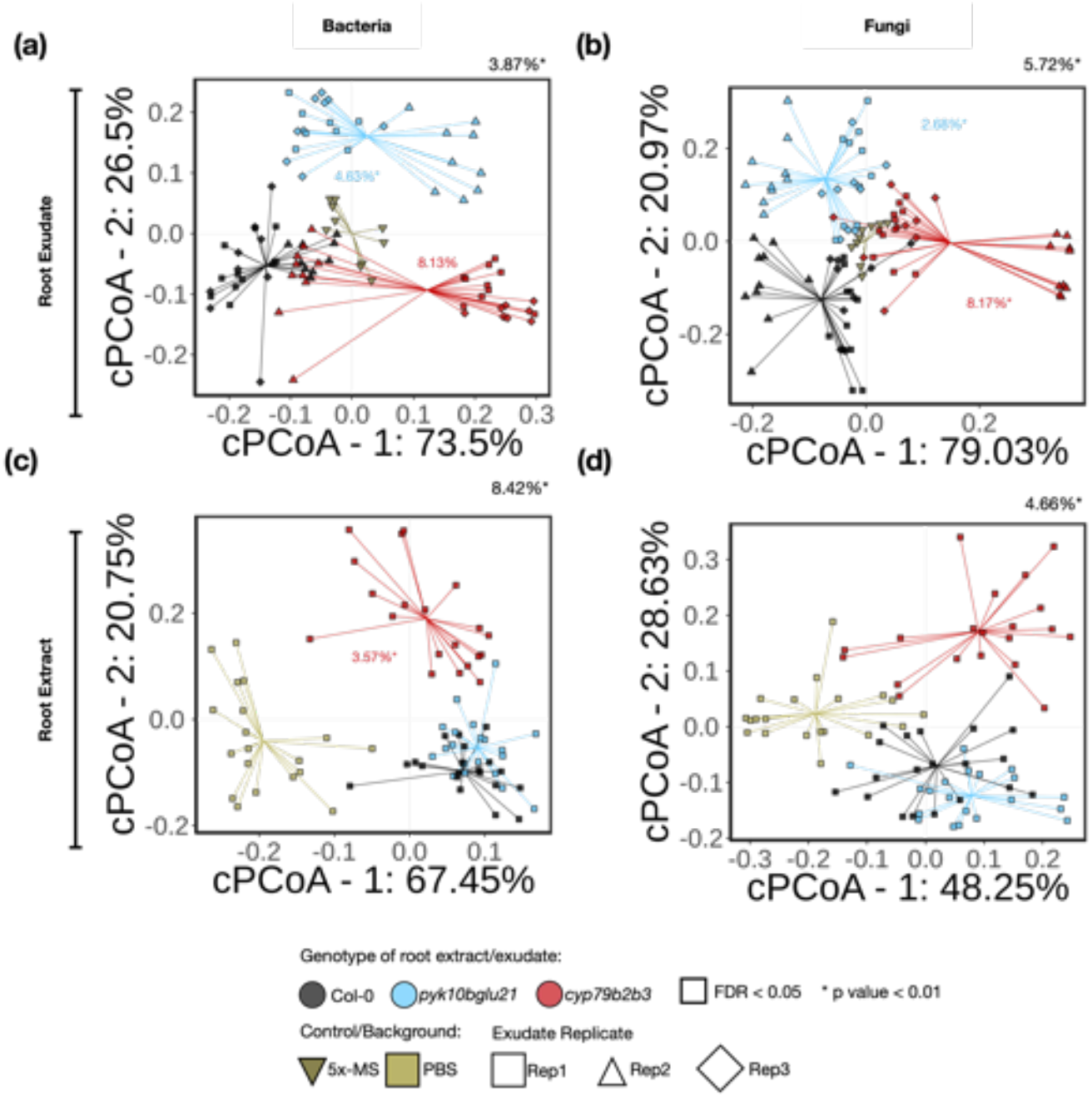

Figure 3.10: Root-secreted compounds coordinated by PYK10 trigger a community shift in soil-microbiota; (a) bacterial community and (b) fungal community structure in soil treated with root exudates, shapes indicate the batch of root exudates collected from mutant and wild-type plants. The bottom panel shows (c) bacterial community and (b) fungal community structure in soil treated with root extracts. The colours indicate the genotypes from which root exudates (a-b) and root extracts (c-d) were prepared and the respective mock treatment. The overall impact of the genotype is indicated on the top right corner of each panel. Only the statistically significant difference between the impact of root exudate of mutants compared to wild-type on the soil microbiota structure is marked within each panel.

3.4.4. The PYK10 myrosinase system and Trp-derived secondary metabolites modulate the structure of bacterial community via root-secreted compounds

To address whether or not the observed impact of Trp-derived metabolites on bacterial community assembly requires the presence of fungi, I cultivated a bacterial synthetic community (SynCom) composed of bacterial strains isolated from healthy roots of *A. thaliana* grown in the CAS soil (Bai et al., 2015), (see Section 2.4.12). We cultivated 200 strains, including 171 strains isolated from roots

and 29 strains isolated from unplanted soil to allow competition between strains adapted and not adapted to root environments. Strains in this complete SynCom sometimes share identical 16S rRNA sequences, which disallowed us to discriminate based on an amplicon sequencing approach. On the other hand, this allowed us to cover strain-level functional variations within a given taxon. Before extraction, we added a fixed amount of *Escherichia coli* cells, whose 16S rRNA sequence is distinguishable from all isolates in the SynCom, to estimate the overall amounts of microbial cells. This allowed us to track the growth of individual strains, so-called quantitative abundance (QA), in addition to the quantification of their relative abundance (RA).

Consistent with the soil treatment analysis, the SynCom experiment revealed that a bacterial community shift is triggered by treating the SynCom with mutant root exudates compared to Col-0 root exudates. I revealed that the composition of the bacterial community in the Col-0 root exudates was significantly different from the composition in the mutant root exudates, and pairwise PERMANOVA showed that the difference in the overall community structure of SynCom treated with *cyp79b2b3* root exudate compared to Col-0 root exudates was higher than the difference in the community structure of SynCom treated with *pyk10bglu21* root exudates compared to wild-type Col-0. Importantly, the community shift in SynCom treated with mutant root exudates of *cyp79b2b3* and *pyk10bglu21* was different compared to Col-0 (Figure 3.11). We prepared starting inocula at two different titers (OD_{600} of 0.05 or 0.005) and analysed the community structure at two different time points (24 and 72 hours post inoculation; hpi). I found that the community shift was retained at the later time point and the difference between genotypes was slightly higher when a lower titer of bacteria was used as a starting inoculum (Figure 3.11). This suggests that the community shift following root exudate treatment is a dynamic process that is dependent on the culture density, and that the community assembly in response to plant-derived compounds is rapid and stable. The greater impact of the mutant root exudates on the SynCom with lower titer provides further evidence of the importance of interspecific interactions between the different species of bacteria in the presence of root exudates (Figure 3.11a and b). On the other hand, when the higher titer of the SynCom was used, competition for the nutrients may induce an earlier growth phase (Figure 3.11c and d). It is likely that at the lower titer, the interspecific competition of the bacterial strains for the compounds in the root exudates is lower. Overall, these results demonstrate that the exudates from the PYK10 pathway and Trp pathway are capable of directly manipulating the composition of the bacterial community in the absence of plants and other eukaryotic microbes.

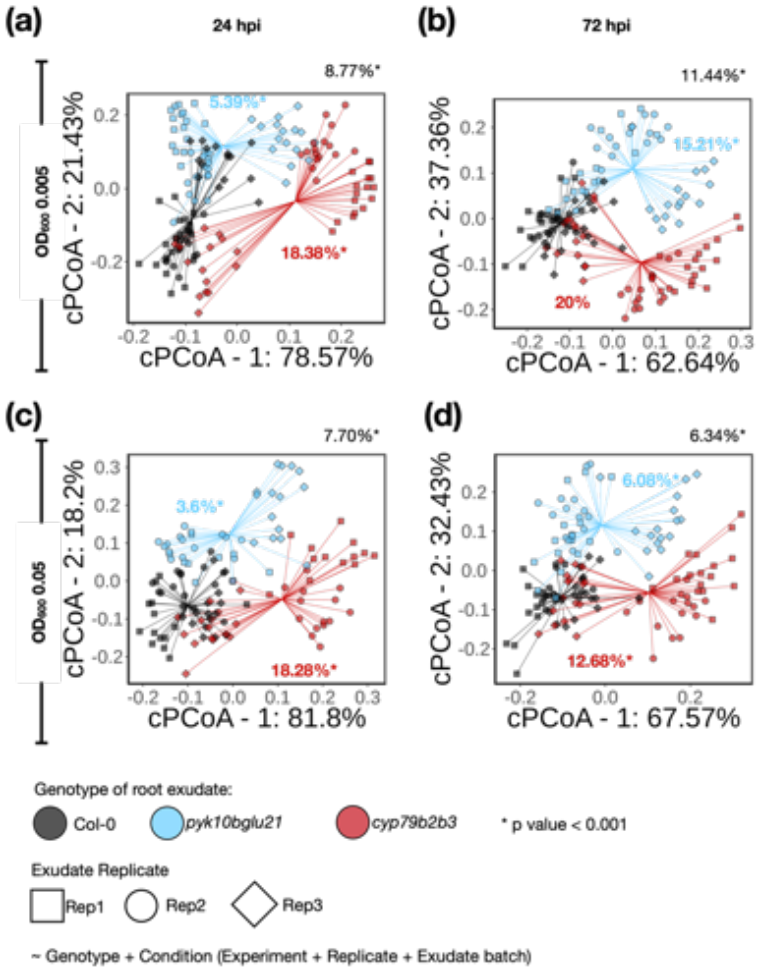

Figure 3.11: The shift in the synthetic bacterial community with 200 bacterial strains is triggered by root-secreted compounds modulated by the PYK10 myrosinase and Trp pathways; (a) The overall change in the bacterial community in OD_{600} 0.005 at 24 hours and (b) retained at 72 hours. Similarly, (c) Change in the overall bacterial community in dense culture OD_{600} 0.05 at 24 hours and (d) retained at 72 hours. The overall impact of the genotype is indicated on the top right corner of each panel. The difference between the impact of root exudate of mutants compared to wild-type on the SynCom is marked within each panel. The formula used in the CPCoA analysis is indicated below. The genotype is taken as fixed factor others are used as random factors.

Interestingly, I found a group of strains that were commonly depleted or enriched in SynCom treated with mutant root exudates compared to Col-0 (Figure 3.12). These results suggest that the bacterial community composition is partially affected by the terminal products of the Trp and PYK10 pathways, raising the possibility that the root-secreted compounds downstream of the Trp pathway and the hydrolysis of secondary metabolite IGs by PYK10 and BGLU21 play a role in the bacterial community assembly. This is similar with the experiments from the soil treatment in the absence of intact plants and in the greenhouse experiment in the presence of plants where we found significant bacterial community shifts in the rhizoplane compartment. Even though the microbiota consortia in soil and roots are different, we found that mutation in PYK10 triggers the community shift. This indicates that the effect of PYK10 with intact roots is similar to the effect of root secretions on the microbiota community. The SynCom was designed with strains isolated from soil as well as roots. It is possible that the impact of PYK10 is specific to the strains adapted in endosphere. Among the strains isolated from the roots, the strains from the classes Betaproteobacteria, Gammaproteobacteria, and Flavobacteria showed higher QA (≥ 5), indicating that they actively grow in the root exudates. Within the SynCom, strains in the Pseudomonadaceae were commonly depleted in the mutant exudates. We also found that Alcaligenaceae and some strains of Comammonadaceae were enriched in the *cyp79b2b3* mutant exudates, and that strains in the Micrococcaceae showed stochastic differences when grown in mutant root exudates (Figure 3.12). Previous studies indicated that these species have a beneficial role in plant-microbe interactions (Bai et al., 2015). Overall, there results indicate that root-derived

compounds whose secretion to the rhizosphere is dependent on the PYK10 and/or the Trp pathway shape the bacterial community by promoting or inhibiting colonization in the rhizosphere.

Figure 3.12: Heat-map from left to right represents, the class, origin of the strains, the quantitative abundance of the strains in SynCom including inoculum at two-time points (24 hpi and 72 hpi) of two titers (OD_{600} = 0.005 and 0.05), and differential abundance of QA for the strains in the SynCom when treated with root exudates of the mutants compared to Col-0 root exudates (in log_2 scale).

3.4.5. The PYK10 myrosinase system in roots is crucial for plant-fungus interactions

Lastly, I tested whether the ER body pathway and Trp-derived metabolism have a direct impact on plant-fungus interactions in the absence of bacteria. Toward this end, I inoculated wild-type Col-0, as well as *pyk10bglu21* and *cyp79b2b3* mutants with fungal strains isolated from roots of healthy *A. thaliana* and related species grown in natural soils (Table 3.2), including CAS soil (Mesny et al., 2021). In our mono-association assay, each host plant was individually inoculated with fungal strain in an agar-based gnotobiotic setup, and their impact on the host shoot and root growth was evaluated after 3 weeks of co-cultivation. Among 43 isolates that were tested, I identified 23 strains that showed a severer impact on *cyp79b2b3* mutants than on Col-0 (Figure 3.13). Most of the fungal strains belonging to the classes Leotiomycetes and Dothideomycetes restricted the growth of *cyp79b2b3* mutant plants, while those belonging to the class Sodiromycetes had variable impacts on its growth. Among these 23 strains, 7 strains also caused a phenotype similar to that of the *pyk10bglu21* mutants, resulting in a severer growth inhibition than was observed in Col-0 under the same conditions. Interestingly, the impact of Dothideomycetes on the growth of the *pyk10bglu21* mutant was generally similar to that of the *cyp79b2b3* mutants. This suggests that PYK10-mediated hydrolysis of Trp-derived secondary metabolites, such as IGs, plays a common role in this class of fungi. In contrast, despite the severe impact of Leotiomycetes strains on the growth of the *cyp79b2b3* mutant, the *pyk10bglu21* mutants were able to grow as well as Col-0 in the presence of these strains (Figure 3.14). This indicates that the Trp-derived secondary metabolites and indolic compounds, whose production, accumulation, and/or secretion is not dependent on PYK10 and BGLU21, are crucial for resisting the invasion of fungi belonging to Leotiomycetes. Lastly, strains *Stael1, Fuseq1, and Boeex1* suppressed only the growth of *pyk10bglu21* mutant plants with a decrease in shoot fresh weight (SFW) compared to the wild type. This could indicate that endophytic accommodation of these fungi in *A. thaliana* roots is partly regulated by ER bodies but not by Trp-derived metabolism, pointing towards the role of PYK10 in hydrolysis of other glucosides.

Considering the previous result from the greenhouse and soil treatment experiments, we show here that both the ER body and Trp-pathways affect the fungal community in the root endosphere. The root-secreted compounds triggered the fungal community shift in soil, which may be potentially critical for plants to ensure their growth.

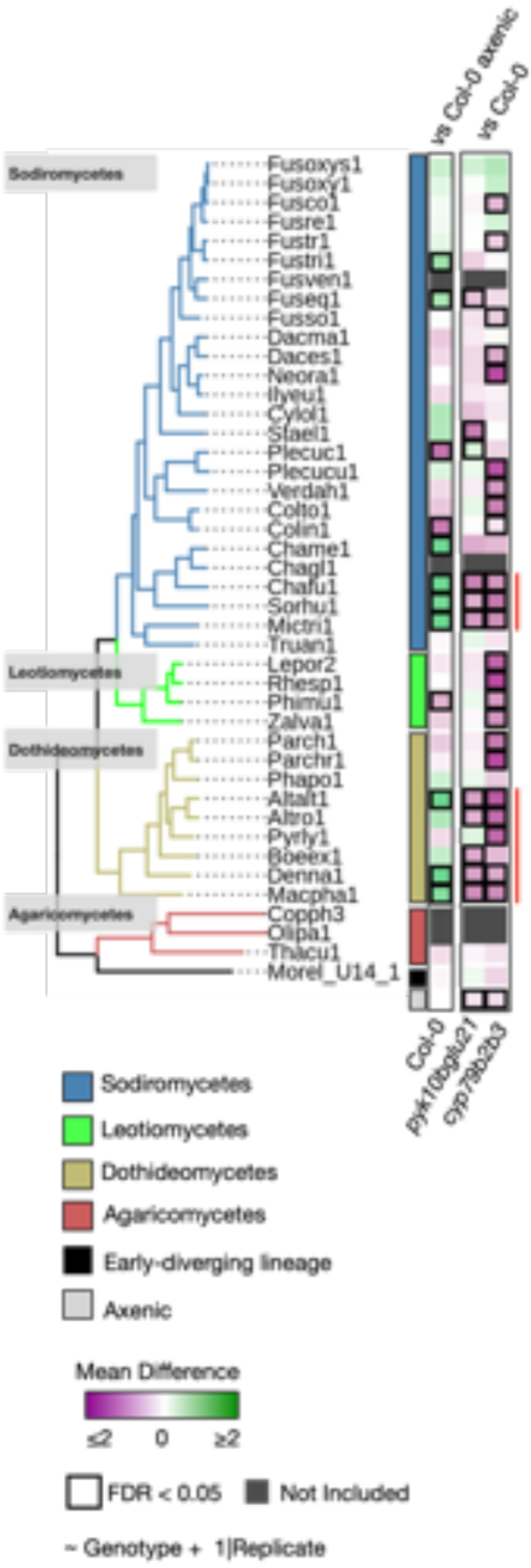

Figure 3.13: The heat map shows the difference in fresh shoot weight (Log_2 fold change) and the taxonomic signature of fungal colonization that is affected by the PYK10 myrosinase and Trp pathway. The strains marked in red shows similar impact within the growth of mutant genotype compared Col-0 under the same treatment (FDR ≤ 0.05).

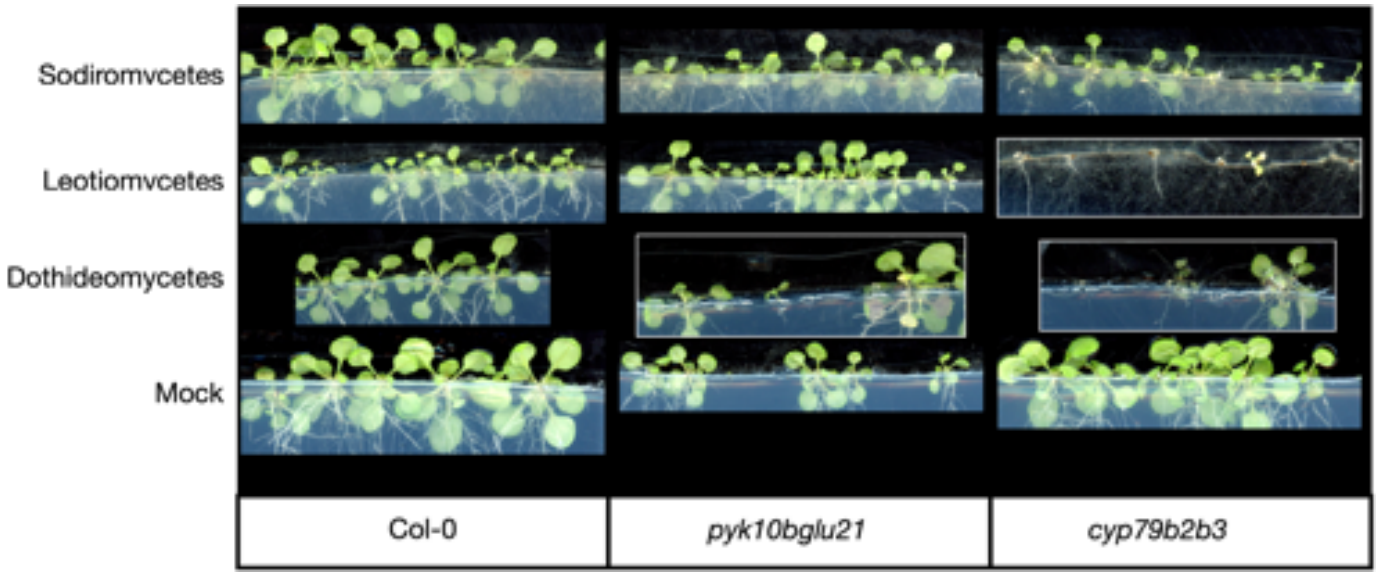

Figure 3.14: The phenotype of the binary plant-fungus interaction within mutant plants and Col-0 shows that fungal colonization is modulated by the PYK10 myrosinase and Trp pathway. Marked white shows fungal overgrowth.

Overall, these results demonstrate a common role for PYK10-mediated metabolism and Trp-derived metabolites in accommodating root-associated fungal strains. They also show the specific role of the metabolites whose production, secretion, and/or activation are independent of PYK10. It suggests that PYK10-mediated metabolism plays a role in manipulating fungal behaviour. Combined with our results in the greenhouse experiments, the soil treatment experiments, and the bacterial SynCom experiments, our findings illustrate the importance of ER bodies in plant-microbiota interactions that are modulated either directly or indirectly by root-exuded compounds.

3.5. Discussion

3.5.1. The type of soil and the root compartment are the main drivers of root microbiota assembly

In my results, I have shown that root-associated microbial assemblages are primarily dependent on soil-geochemical parameters and the root compartments, followed by the plant metabolic pathways. The soil geochemical factors drive a different microbiota composition and the root endosphere compartment of the bacterial community showed similar microbiota composition, which is consistent with previous studies (Durán et al., 2018; Thiergart et al., 2020). On the contrary, such convergence in the endosphere was not observed in the microbiota composition of fungi. In different soil geochemical conditions the microbes interact with themselves maintaining soil microbiota homeostasis (Delgado-Baquerizo, 2018; Fierer & Jackson, 2006; Karimi, 2018). The fungal community structure differ across the compartments because the community composition in the soil is mainly dependent on the soil geochemical conditions. In addition to soil-geochemical factors, the microbiota composition across the root compartment is different. However, the bacterial composition of the endosphere remains similar even when there is a difference in the soil type. In the rhizosphere, the soil particles are attached to the roots, therefore, both soil and root microbes may dominate the microbiota composition. In my results, I show that there is a difference between soil and rhizosphere communities. On the other hand, the rhizoplane compartment is devoid of soil particles due to repetitive washing of the roots and this compartment is devoid of roots. Therefore, the rhizoplane compartment is crucial for the microbiota characterization, as this compartment holds the bridge between the microbes present within the roots and on the surface of the roots. Overall, my results show that the composition of the microbiota is primarily dependent on the root compartment and geochemical parameters of the soil, which is consistent with previous studies.

3.5.2. ER bodies and Trp pathway are crucial for root associated microbiota

I demonstrated the potential impact of root-secreted compounds that are downstream of the Trp-pathway and ER body pathway on the assembly of the root-associated microbiota. I showed that PYK10 plays a role in shaping the microbiota assembly, pointing to the importance of the ER bodies in root microbiota. This indicates that the hydrolytic activity of ER body localized PYK10 myrosinase and its substrates have a role in shaping the root microbiota. The secondary metabolites whose secretion, activation, and/or accumulation are downstream of the Trp-pathway constitute a plethora of root-secreted compounds in the rhizoplane compartment. For example, camalexin and glucosides like IGs and coumarin and are known to have roles in plant-microbe interactions (Bednarek et al., 2009; Frerigmann et al., 2016; Koprivova et al., 2019). Our data showed that the community shift was triggered in the *cyp79b2b3* mutants, pointing to the relevance of Trp derivatives in root microbiota

community structure. The structure of the microbial community of the *pyk10bglu21* mutant was also different from the community structures of Col-0 and the *cyp79b2b3* mutant, which shows that PYK10 myrosinase not only hydrolyses IGs but possibly other glucosides, such as coumarins. Indeed, PYK10 was shown to have specific activity towards indole glucosinolates. However, the *in vitro* activation of PYK10 towards non-Trp-derived glucosides such as 4MUG and scopolin (Nakano et al., 2017) indicates that PYK10 also targets other glucosides, such as coumaryl glucosides or aliphatic glucosinolates. Further studies are needed to see to what degree the effect of PYK10 on root microbiota is dependent on soil nutrient and geochemical conditions.

Alternatively, the microbial community differences among the mutants and the Col-0 wild type could be due to differences in the chemical compositions of the rhizoplane compartment as a nutritional source for microbes, rather than as a signalling molecule. Root-secreted compounds include organic acids that could trigger changes in the microbial community (Chaparro et al., 2013). The soil geochemical factors are known to be crucial for the soil microbiota homeostasis (Koprivova et al., 2019), and plants likely play an important role in adding root secretion into the rhizosphere and soil microbiota (Hu et al., 2018). Microbes in the rhizosphere/rhizoplane may compete for these plant-derived carbon sources, and the downstream compounds of the ER body and Trp pathways exuded by roots may contribute to the net carbon source. Nonetheless, our overall findings demonstrate that plants coordinate the dynamics of the root-associated microbiota across compartments, probably by using these metabolites and hydrolysed products (Hiruma, 2019).

It has been proposed that microbe-microbe interactions play a crucial role in microbial community assembly (Getzke et al., 2019; Hassani et al., 2018). Hence, it is also possible that the alteration in fungal community structures in mutants in the endosphere is due to the absence/presence of certain bacterial members. I showed that the PYK10 pathway has a direct impact on the bacterial community both in the presence and absence of fungi. This points to a scenario in which bacteria are the main target of this pathway; the bacterial composition, in turn, have a secondary impact on the fungal community structure. Alternatively, the lack of Trp-derived metabolites and the ER body myrosinase system might promote fungal invasion or colonization in the endosphere, which would alter the bacterial community. This is in line with a previous report showing that Trp-derived metabolism play a key role in restricting fungal load in root compartments (Wolinska et al., 2021). However, the impact of soil microbiota on wild-type and mutant plants from the greenhouse experiments showed that bacteria-fungi interactions may be considered while studying root microbiota assembly. As, in the mono-association assays with only plant and fungi independent of other prokaryotes and eukaryotes, we found plants growth were negatively affected when co-inoculated with fungi. The results from the greenhouse experiments and soil treatment experiments showed that the invading behaviour of fungi is reduced in the presence of bacterial community. The

results of soil experiments and mono-association assays indicate the importance of the PYK10 and Trp pathways in microbe-microbe interactions. The downstream compounds of both PYK10 and Trp pathways may have anti-microbial properties that resist the pathogens thereby having an impact on the microbial behaviour. It is also possible that, these downstream compounds may enrich rhizobacteria population to resist against pathogens. Further, ternary interaction assays with bacteria, fungi, and mutant and wild type plants, are needed to confirm that ER bodies influence microbe-microbe interactions.

3.5.3. Root ER bodies modulate root secreted compounds

ER bodies are predominantly developed in roots, and PYK10 is the major component of ER bodies (Matsushima, Hayashi, et al., 2003). Therefore, it is possible that the indole glucosinolates are hydrolysed by PYK10 to produce bioactive compounds like indole-3-carbinol and isothiocyanates and secrete them to the rhizosphere to influence the assembly of root-associated microbial communities. My findings that fungi of the class Doethidiomycetes had a negative impact on the growth of both *pyk10bglu21* and *cyp79b2b3* mutants compared to Col-0 suggest a scenario in which the ER body pathway triggers the hydrolysis of Trp-derived indole glucosinolates, which may trigger changes in the community. However, the effects of *pyk10bglu21* and *cyp79b2b3* mutations on root-microbiota interactions differ from each other, indicating that substrates other than IGs, such as aliphatic glucosinolates and coumaryl glucosides, also play a role in root microbiota assembly (Harbort et al., 2020; Voges et al., 2019). The hydrolysed products of glucosinolates such as nitriles, thiocyanates and isothiocyanates, might contribute to the total nitrogen or sulfur availability for microbes or have an antibiotic activity at the soil-root interface. Alternatively, the exuded glucose or other monosaccharides as a part of hydrolysis could alter the composition of sugars near the soil-root interface, which would also have an impact on the microbial recruitment. Notably, hydrolysis of glucosides produce glucose as a by-product, and an alteration of sugar content in the root exudates may lead to a compositional change in the microbiota assembly. The primary metabolite profiling of the exudates from *pyk10bglu21* and *cyp79b2b3* mutants in comparison to Col-0 wild type is needed to assess whether either mutation creates a deficit in sugars within the root exudates.

3.5.4. Potential root-exuded compounds downstream of the ER body and Trp pathways modulate the microbiota community

Myrosinases catalyze the hydrolysis of glucosinolates to produce glucose and residual aglycone, which is further converted into so-called terminal products, such as isothiocyanates (ITC), nitriles, and epithionitriles (Winde & Wittstock, 2011; Wittstock & Halkier, 2002). These terminal products are proposed to be bioactive compounds that influence the behaviour of pathogenic microbes (Fan et al.,

2011; Zhu et al., 2020) and herbivores (Bai et al., 2015; Burow et al., 2006; Ferber et al., 2020). An alteration in the glucosinolate profiles exuded to the rhizosphere has been shown to have an impact on the root-associated bacterial and fungal microbiota (Bressan et al., 2009). A previous report suggested that isothiocyanates can inhibit the expression of the Type III secretion system in *Pseudomonas syringae pv. tomato DC3000*, thus suppressing its virulence (W. Wang et al., 2020). Similarly, isothiocyanates were found to manipulate mitochondrial activity in fungal phytopathogens (Calmes et al., 2015). I show that the relative abundances of metabolites derived from Trp metabolism are different in mutants and the relative abundances of indole glucosinolate (I3G) are slightly higher in PYK10 mutant exudates compared to Col-0 exudates (Figure 3.7n). ER bodies have an impact on the metabolome of root exudates, indicating the secretion of a wide range of compounds is dependent on PYK10 and BGLU21. In contrast, the Trp pathway has an impact on a limited range of the root-exudated compounds. This may be explained by the fact that the Trp pathway specifically regulates the production of indolic compounds. The first compounds produced from Trp by CYP79B2 and CYP79B3 is indole-acetaldoxime (IAOx), which is responsible for the biosynthesis of IGs and other Trp-secondary metabolites. IAOx is also responsible for the biosynthesis of a downstream indolic compound, indole acetic acid (IAA) (Rajagopal & Larsen, 1972; Sugawara et al., 2009). IAA is one of the most abundant forms of Trp derived secondary metabolites and is crucial for plant growth. The metabolic profile of the root-secreted compounds in the absence of CYP79B2 and CYP79B3 shows reduced indolic compounds and the community shift triggered by the root-secreted compounds strongly suggest that IAOx-derived metabolites have an impact on the microbiota assembly. The transcription factors MYB34, MYB51 and MYB122 specifically regulate the synthesis of indole glucosinolates but not other Trp-derived metabolites (Frerigmann & Gigolashvili, 2014), and my finding that *myb34/51/122* mutant roots secrete a relatively similar set of metabolites as those secreted by *cyp79b2b3* mutants suggests that the majority of Trp-derived root exudates is derived from IGs, which are shown to be actively secreted into the rhizosphere by GLUCOSINOLATE TRANSPORTER (GTR) transporters (D. Xu et al., 2017). The impact of ER bodies on the diversity of root-secreted metabolites is also evident from our HPLC-MS/MS analysis, which can explain the role of ER bodies in shaping the microbiota community. However, the effect of other myrosinases like TGG4 and TGG5 on the microbiota assembly remains to be tested. My results show that community shift is triggered by the *pyk10bglu21* root exudates, and this effect was less when the soil was treated with its root extract, suggesting that other myrosinases that complement the lack of PYK10 and BGLU21 are present in the homogenates. Unlike PYK10, TGG4 and TGG5 are localised in the vacuoles of cells located in the interior of the root tip. It was reported that upon cellular damage TGG4 and TGG5 mix with the glucosinolates to produce the bioactive compounds that act as repellent.

Whether these myrosinases also play a role in glucosinolate-mediated regulation of root microbiota under physiological conditions remains to be addressed.

Overall, these findings suggest that the impact of Trp-derived metabolites on the assembly of the microbial community that we observed in the absence of plant roots may be explained by the terminal products of IG hydrolysis by PYK10. Interestingly, on the other hand, we did not detect substantial amounts of indole glucosinolates in root exudates, even when they were collected from wild-type Col-0 plants. This may be explained by a low level of secretion of these metabolites or a rapid conversion to intermediate/terminal products after exudation to the rhizosphere, as indole glucosinolates and their derivatives are unstable and difficult to detect by LC-MS/MS. Because BGLUs that accumulate in the ER body have myrosinase activity towards IGs (Nakano et al., 2017; Nakazaki et al., 2019), it is plausible that unknown/undetected terminal products of IG hydrolysis play a role in the assembly of the root microbiota and that root ER bodies are important for the exudation of the responsible metabolites.

Alternatively, it is also possible that PYK10 influences the secretion of other Trp-derived metabolites that play key roles in manipulating the composition of the microbial community. A wide variety of Trp-derived secondary metabolites, such as IGs, indole acetic acid (IAA), indole aceto-nitrile (IAN) and indole carboxylic acid (ICA), are exuded into the rhizosphere (Hiruma, 2019; Hull et al., 2000). These metabolites were indeed detected in our exudate samples (Figure 3.7). Interestingly, the relative abundance of IAA in the exudates collected from the roots of mutant *pyk10bglu21* and *cyp79b2b3* was lower than in the exudates from Col-0 roots (Figure 3.7), possibly pointing to the role of auxin in the observed community shift in the mutant roots. Recent studies have reported that auxin itself has an impact on microbial behaviour (Kunkel & Harper, 2018; Kunkel & Johnson, 2021; Tzipilevich et al., 2021), and root-associated commensal bacteria are capable of modulating root accumulation of auxin (Eichmann et al., 2021; Finkel et al., 2020; Zhalnina et al., 2018). IAA can be produced from IAN, one of the IG degradation products, by the activity of NITRILASE enzymes (Normanly et al., 1997), and a recent simulation modelling study suggested that plants can alter the dynamics of the IAA signalling after IG hydrolysis in a manner dependent on the IG-hydrolysing myrosinases Is the word “responsibl” really necessary? (Vik et al., 2018). It remains to be shown whether the reduced amount of IAA in the *pyk10bglu21* exudates was due to a lower level of IG degradation or a secondary effect caused by loss of ER bodies. On the basis of these data, we cannot exclude the possibility that the modulation of the microbial community by root exudates is partly accounted for by auxin. Furthermore, Trp is another source of phytoalexins, such as camalexin, ICA, brassinin, and 4-hydroxyindole-3-carbonyl nitrile (4OH-ICN), some of which have been reported to play a role in root microbial accommodation (Koprivova et al., 2019; Rajniak et al., 2015; Wolinska et al., 2021). Consistently, we found that IAA and I3A levels are reduced in mutants (Figure 3.7o and p).

Therefore, it remains possible that the ER body system is important for the secretion of these Trp-derived metabolites and, in turn, influences the assembly of the root microbiota.

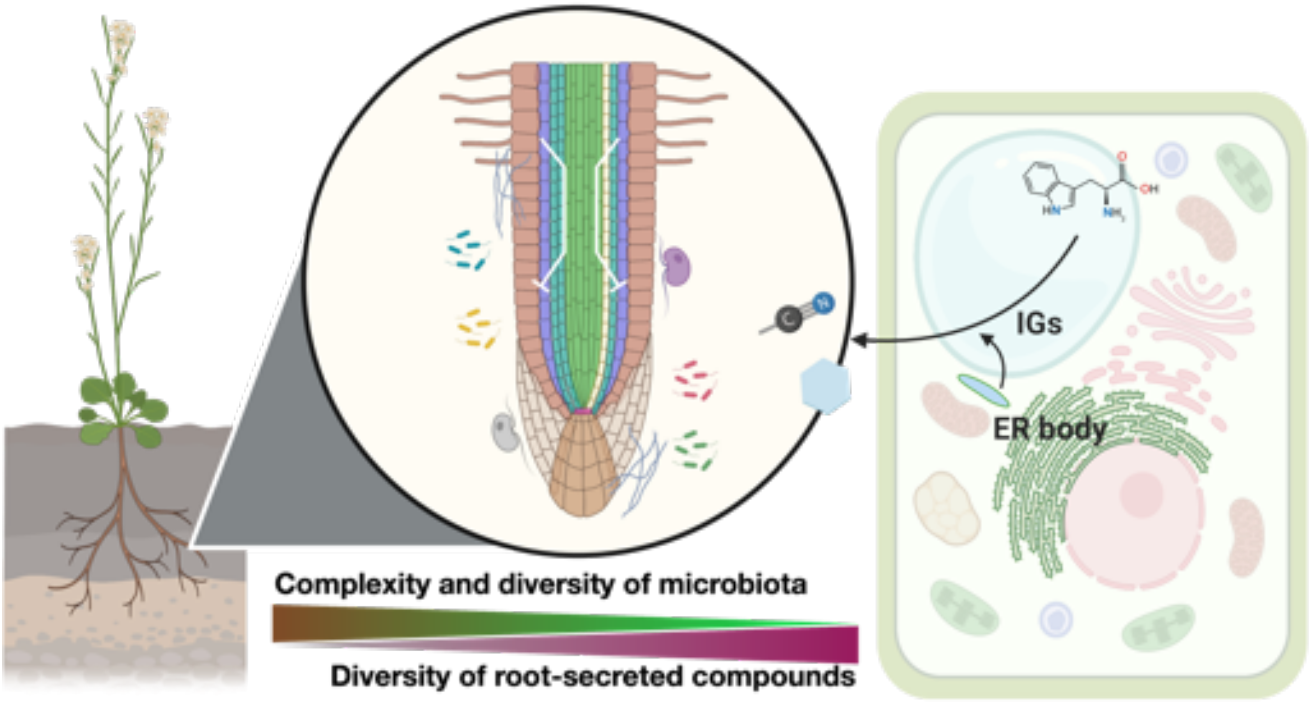

Figure 3.15: Proposed model of ER body myrosinase system in shaping the root microbiota assembly by modulating the root secreted compounds.

The rhizoplane compartment corresponds to the extracellular microbial biofilm on the surface of the root epidermal cell and the root endosphere corresponds to the endophytic microbes (Hassani et al., 2018), and it is possible that the composition of the chemical compounds in the root secretions and accumulation modulates the dynamics of the microbes (Münch et al., 2007; Pandit et al., 2020; Pietrangelo et al., 2018). Root surface or rhizoplane consists of complex carbohydrate structures that are the products of root-microbiota interactions. These biofilms are composed of exopolysaccharides that are structurally stable, and that act as a matrix to accommodate microbial cells and their products. The chemical compounds secreted by the plants may be accommodated in the matrix where they might promote microbial colonization (Yang et al., 2021). However, these possibilities remain to be tested, as little is known about the role of biofilms in plant-microbe interactions. The chemical composition of the root-secreted exudates is likely one of the factors that shape the root microbiota (Harbort et al., 2020; Koprivova et al., 2019; Wippel et al., 2021) (Figure 3.12).

Overall, we propose that the ER body pathway shapes the structure of the root microbiota community by changing the composition of the root secreted compounds. The impacts of the ER body and Trp pathways were greatest in the bacterial community in the rhizoplane compartment and in the fungal community in the endosphere compartment. The chemical composition of the root-secreted compounds downstream of the ER body and Trp-pathway plays a role in the bacterial and fungal microbiota structure (Figure 3.15). In this chapter, I have shown that the composition of root-secreted

compounds is crucial for the root microbiota assembly. However, the molecular mechanisms by which ER bodies modulate the microbes in the rhizoplane and endosphere are unknown, mainly because intact ER bodies in epidermal cells are fragile and easily damaged. Because an exopolysaccharide matrix is present in the rhizoplane compartment, ER bodies or PYK10 might be trapped in the matrix along with its substrate like IGs. Further, this possibility of entrapment can be investigated by measuring the extracellular molecules like transcriptional and translational elements exchanged between the host and associated microbes at the interface of the root epidermis where these biofilms are produced. It is possible that the biofilm itself may define a root-specific microbial niche for a given plant species and its unique root-secreted elements.

4. OVERALL DISCUSSION AND CONCLUSIONS

4.1. ER body membrane proteins are associated with ER body morphology, movement, and allocation of cations at the sub-cellular level

Overall in my thesis, I showed by image analysis that ER body movement and morphology is modulated by the MEB1 and MEB2 proteins. The molecular factors that interact with the MEB1 and MEB2 proteins could be intrinsic to ER bodies. NAI2 protein that act as a scaffold to ER bodies could be potentially interacting with MEB2 and MEB1 proteins thereby the maintaining the shape of the spindle shaped ER body structure. The aggregated structures frequently observed in the MEB2 deficit mutant show that the interaction of MEB proteins could be with the intrinsic proteins and/or cytosolic proteins. However, further molecular experiments are required to study the potential function of MEB1 and MEB2 proteins and their link with the ER body movement and morphology.

I showed that ER bodies have an impact on the seedling ionome. The MEB1 and MEB2 transporters localised in ER bodies are involved in cation exchange between cytosol and the compartment itself. I showed that the overall ion accumulation in ER body mutants is different from that of wild-type. The elements like Zn and Fe are distributed differently in mutants lacking MEB1 and MEB2. As ER bodies are linked with the defence, it may be a plausible scenario that MEB1 and MEB2 are involved in the major function of ER body mediated defence activation directly by accumulating elements in ER bodies and/or indirectly providing metals required for the molecular function of ER body constituents. Increasing metal toxicity could elevate a defence strategy against herbivory or pathogens by sequestering metal ions from cytosol (Hörger et al., 2013). Alternatively, sequestered metal ions could be accumulated in the ER bodies from the cytosol in order to elevate the function of the ER body. However, due to the limitation in detecting these events at such resolutions, the precise role of MEB1 and MEB2 proteins in plant defence by metal ion accumulation remains to be addressed in further research. Behaviour of potential interactors might change depending on the availability of metal ions in plants. It is possible to test this by measuring the impact of herbivores and pathogens on wild type and mutant plants under nutrient deficit condition. It is of interest whether and how ER bodies mediate defence activation in plants, from the perspective of metal ion accumulation. However, it remains a question whether plants accumulate metal ions in their sub-cellular compartments like ER bodies. This points to a strategy where plants defend either directly by hyper accumulation of metals in vacuoles or indirectly by activating the metallozymes. Our results indicated to the impact of ER bodies on ion accumulation in seedlings. It is possible that the accumulation of trace elements is an additive or synergistic effect to that of the organic mode of defence (Martos et al., 2016). In both cases MEB1 and MEB2 may play role as there is an impact in the cation accumulation in the mutants.

4.2. ER bodies are responsible for root secreted compounds that play a role in root associated microbiota community structure

Here, I have verified a long-standing hypothesis that ER bodies have an impact on root microbiota (Yamada et al., 2011) by showing an altered structure of root-associated microbiota in the mutants impaired in the ER body system. The impact triggered by the defects in ER bodies was similar to what was triggered by the lack of Trp-derived secondary metabolism, further supporting the link between ER bodies and Trp-derived compounds, such as IGs (Nakano et al., 2017; Nakazaki et al., 2019; Yamada et al., 2020). Interestingly, although PYK10 is intracellularly stored in ER bodies, it influences the root-exuded metabolic profile either by changing metabolism or secretion to the rhizosphere of these metabolites, which in turn contributes to the root-microbiota interactions. This indicates that PYK10 hydrolyses the glucosides stored or secreted by roots and produces compounds that have antibiotic properties. In nature, the physicochemical conditions of root compartment like light, temperature, pressure and pH are different from that of shoot compartment. The specific activity of PYK10 is either sensitive or specific to these physicochemical conditions. Overall, my research provides substantial evidence for the role of root ER bodies in interaction with root-associated microbiota. Further transcriptome analysis on root ER bodies are required to understand the mechanism by which PYK10 contributes to the root-secreted compounds. This should be tested by measuring the impact of the PYK10 on root transcriptome under different physicochemical conditions.

The cry-for-help hypothesis suggests that the host primary and secondary metabolism, as well as hormonal responses, alter the composition of the root exudates upon the environmental and biotic stresses, thereby altering the compositions of the root-associated microbial communities (Rolfe et al., 2019; Sasse et al., 2018). Root microbiota play a crucial role in plant physiology, for example, by conferring abiotic stress tolerance, helping nutrition, and directly or indirectly protecting the hosts from pathogens (Bulgarelli et al., 2013). Thus, it is crucial for plants to maintain the beneficial (meliorbiotic) or at least harmless (eubiotic) status of the root microbiota and prevent them from being detrimental to plant health (dysbiotic) (Paasch & He, 2021). Toward this end, plants exploit an active process to appropriately assemble root-associated microbiota from the pool of microbes in the soil environment (Bulgarelli et al., 2012; Hacquard, 2016; Lundberg et al., 2012). For example, recent studies demonstrated an important role for secondary metabolites accumulated in and/or secreted by roots in modulating the composition of the root microbiota (Harbort et al., 2020; Hu et al., 2018; Huang et al., 2019; Korenblum et al., 2020; Shimasaki et al., 2021; Stringlis, 2018; Voges et al., 2019). In addition to previous studies on the effect of secondary metabolites on root microbiota, my results clearly illustrate that indole glucosinolates and other Trp-derived compounds also play a significant role in root microbiota assembly. I showed that root secreted compounds in rhizosphere are

dependent on ER bodies and PYK10 myrosinases, and these compounds are needed for root microbiota assembly. A broad range of compounds are exuded into the rhizosphere (Bais et al., 2006; Strehmel et al., 2014; Vives-Peris et al., 2020), including secondary metabolites, and it is conceivable that the root microbiota composition is dictated by a combination of different pathways (Shimasaki et al., 2021). Hence, it remains intriguing to address the interaction of these Trp-derived metabolites with other root-exuded metabolites that impact root microbiota, such as coumarins.

5. BIBLIOGRAPHY

Adie, B. A. T., Pérez-Pérez, J., Pérez-Pérez, M. M., Godoy, M., Sánchez-Serrano, J.-J., Schmelz, E. A., & Solano, R. (2007). ABA Is an Essential Signal for Plant Resistance to Pathogens Affecting JA Biosynthesis and the Activation of Defenses in Arabidopsis. *The Plant Cell*, *19*(5), 1665–1681. https://doi.org/10.1105/tpc.106.048041

Ahn, Y. O., Shimizu, B., Sakata, K., Gantulga, D., Zhou, C., Zhou, Z., Bevan, D. R., & Esen, A. (2010). Scopolin-hydrolyzing beta-glucosidases in roots of Arabidopsis. *Plant & Cell Physiology*, *51*(1), 132–143. https://doi.org/10.1093/pcp/pcp174

Almario, J., Jeena, G., Wunder, J., Langen, G., Zuccaro, A., Coupland, G., & Bucher, M. (2017). Root-associated fungal microbiota of nonmycorrhizal Arabis alpina and its contribution to plant phosphorus nutrition. *PNAS*, *114*(44), E9403–E9412. https://doi.org/10.1073/pnas.1710455114

Andersson, D., Chakrabarty, R., Bejai, S., Zhang, J., Rask, L., & Meijer, J. (2009). Myrosinases from root and leaves of Arabidopsis thaliana have different catalytic properties. *Phytochemistry*, *70*(11), 1345–1354. https://doi.org/10.1016/j.phytochem.2009.07.036

Badri, D. v, Chaparro, J. M., Zhang, R., Shen, Q., & Vivanco, J. M. (2013). Application of natural blends of phytochemicals derived from the root exudates of arabidopsis to the soil reveal that phenolic-related compounds predominantly modulate the soil microbiome. *J Biol Chem*, *288*. https://doi.org/10.1074/jbc.M112.433300

Badri, D. v, & Vivanco, J. M. (2009). Regulation and function of root exudates. *Plant Cell Environ*, *32*. https://doi.org/10.1111/j.1365-3040.2009.01926.x

Bai, Y., Müller, D. B., Srinivas, G., Garrido-Oter, R., Potthoff, E., Rott, M., Dombrowski, N., Münch, P. C., Spaepen, S., Remus-Emsermann, M., Hüttel, B., McHardy, A. C., Vorholt, J. A., & Schulze-Lefert, P. (2015). Functional overlap of the Arabidopsis leaf and root microbiota. *Nature*, *528*(7582), 364–369. https://doi.org/10.1038/nature16192

Bais, H. P., Weir, T. L., Perry, L. G., Gilroy, S., & Vivanco, J. M. (2006). The role of root exudates in rhizosphere interactions with plants and other organisms. *Annu Rev Plant Biol*, *57*. https://doi.org/10.1146/annurev.arplant.57.032905.105159

Barth, C., & Jander, G. (2006). Arabidopsis myrosinases TGG1 and TGG2 have redundant function in glucosinolate breakdown and insect defense. *The Plant Journal*, *46*(4), 549–562. https://doi.org/10.1111/j.1365-313X.2006.02716.x

Basak, A. K., Mirzaei, M., Strzałka, K., & Yamada, K. (2021). Texture feature extraction from microscope images enables a robust estimation of ER body phenotype in Arabidopsis. *Plant Methods*, *17*(1). https://doi.org/10.1186/s13007-021-00810-w

Bayoumi, S. A. L., Rowan, M. G., Blagbrough, I. S., & Beeching, J. R. (2008). Biosynthesis of scopoletin and scopolin in cassava roots during post-harvest physiological deterioration: the E-Z-isomerisation stage. *Phytochemistry*, *69*(17), 2928–2936. https://doi.org/10.1016/J.PHYTOCHEM.2008.09.023

Bednarek, P. (2012). Chemical warfare or modulators of defence responses – the function of secondary metabolites in plant immunity. *Current Opinion in Plant Biology*, *15*(4), 407–414. https://doi.org/10.1016/j.pbi.2012.03.002

Bednarek, P., Piślewska-Bednarek, M., Svatoš, A., Schneider, B., Doubský, J., Mansurova, M., Humphry, M., Consonni, C., Panstruga, R., Sanchez-Vallet, A., Molina, A., & Schulze-Lefert, P. (2009). A Glucosinolate Metabolism Pathway in Living Plant Cells Mediates Broad-Spectrum Antifungal Defense. *Science*, *323*(5910), 101–106. https://doi.org/10.1126/science.1163732

Bednarek, P., Schneider, B., Svatoš, A., Oldham, N. J., & Hahlbrock, K. (2005). Structural Complexity, Differential Response to Infection, and Tissue Specificity of Indolic and Phenylpropanoid Secondary Metabolism in Arabidopsis Roots. *Plant Physiology*, *138*(2), 1058–1070. https://doi.org/10.1104/pp.104.057794

Behnke, H.-D., & Eschlbeck, G. (1978). Dilated cisternae inCapparales—an attempt towards the characterization of a specific endoplasmic reticulum. *Protoplasma*, *97*(4), 351–363. https://doi.org/10.1007/BF01276292

Berendsen, R. L., Pieterse, C. M. J., & Bakker, P. A. H. M. (2012). The rhizosphere microbiome and plant health. *Trends in Plant Science*, *17*(8), 478–486. https://doi.org/10.1016/j.tplants.2012.04.001

Berg, G., & Smalla, K. (2009). Plant species and soil type cooperatively shape the structure and function of microbial communities in the rhizosphere. *FEMS Microbiology Ecology*, *68*(1), 1–13. https://doi.org/10.1111/j.1574-6941.2009.00654.x

Bonnett, H. T., & Newcomb, E. H. (1965). Polyribosomes and cisternal accumulations in root cells of radish. *The Journal of Cell Biology*, *27*(2), 423–432. https://doi.org/10.1083/jcb.27.2.423

Braun, M., Hauslage, J., Czogalla, A., & Limbach, C. (2004). Tip-localized actin polymerization and remodeling, reflected by the localization of ADF, profilin and villin, are fundamental for gravity-sensing and polar growth in characean rhizoids. *Planta*, *219*(3), 379–388. https://doi.org/10.1007/S00425-004-1235-4

Bressan, M., Roncato, M.-A., Bellvert, F., Comte, G., Haichar, F. Z., Achouak, W., & Berge, O. (2009). Exogenous glucosinolate produced by Arabidopsis thaliana has an impact on microbes in the rhizosphere and plant roots. *The ISME Journal*, *3*(11), 1243–1257. https://doi.org/10.1038/ismej.2009.68

Brown, P. D., Tokuhisa, J. G., Reichelt, M., & Gershenzon, J. (2003). Variation of glucosinolate accumulation among different organs and developmental stages of Arabidopsis thaliana. *Phytochemistry*, *62*(3), 471–481. https://doi.org/10.1016/S0031-9422(02)00549-6

Bulgarelli, D., Garrido-Oter, R., Münch, P. C., Weiman, A., Dröge, J., Pan, Y., McHardy, A. C., & Schulze-Lefert, P. (2015). Structure and Function of the Bacterial Root Microbiota in Wild and Domesticated Barley. *Cell Host & Microbe*, *17*(3), 392–403. https://doi.org/10.1016/j.chom.2015.01.011

Bulgarelli, D., Rott, M., Schlaeppi, K., van Themaat, E., Ahmadinejad, N., Assenza, F., Rauf, P., Huettel, B., Reinhardt, R., Schmelzer, E., Peplies, J., Gloeckner, F. O., Amann, R., Eickhorst, T., & Schulze-Lefert, P. (2012). Revealing structure and assembly cues for Arabidopsis root-inhabiting bacterial microbiota. *Nature*, *488*(7409), 91–95. https://doi.org/10.1038/nature11336

Bulgarelli, D., Schlaeppi, K., Spaepen, S., van Themaat, E., & Schulze-Lefert, P. (2013). Structure and functions of the bacterial microbiota of plants. *Annual Review of Plant Biology*, *64*, 807–838. https://doi.org/10.1146/annurev-arplant-050312-120106

Burmeister, W. P., Cottaz, S., Driguez, H., Iori, R., Palmieri, S., & Henrissat, B. (1997). The crystal structures of Sinapis alba myrosinase and a covalent glycosyl-enzyme intermediate provide insights into the substrate recognition and active-site machinery of an S-glycosidase. *Structure (London, England : 1993)*, *5*(5), 663–676. https://doi.org/10.1016/S0969-2126(97)00221-9

Burow, M., Markert, J., Gershenzon, J., & Wittstock, U. (2006). Comparative biochemical characterization of nitrile-forming proteins from plants and insects that alter myrosinase-catalysed hydrolysis of glucosinolates. *The FEBS Journal*, *273*(11), 2432–2446. https://doi.org/10.1111/j.1742-4658.2006.05252.x

Callahan, B. J., McMurdie, P. J., Rosen, M. J., Han, A. W., Johnson, A. J. A., & Holmes, S. P. (2016). DADA2: High resolution sample inference from Illumina amplicon data. *Nature Methods*, *13*(7), 581–583. https://doi.org/10.1038/nmeth.3869

Calmes, B., N'Guyen, G., Dumur, J., Brisach, C. A., Campion, C., Iacomi, B., Pigné, S., Dias, E., Macherel, D., Guillemette, T., & Simoneau, P. (2015). Glucosinolate-derived isothiocyanates impact mitochondrial function in fungal cells and elicit an oxidative stress response necessary for growth recovery. *Frontiers in Plant Science*, *6*, 414. https://doi.org/10.3389/fpls.2015.00414

Carrió-Seguí, A., Garcia-Molina, A., Sanz, A., & Peñarrubia, L. (2015). Defective copper transport in the copt5 mutant affects cadmium tolerance. *Plant & Cell Physiology*, *56*(3), 442–454. https://doi.org/10.1093/PCP/PCU180

Carrió-Seguí, À., Romero, P., Curie, C., Mari, S., & Peñarrubia, L. (2019). Copper transporter COPT5 participates in the crosstalk between vacuolar copper and iron pools mobilisation. *Scientific Reports*, *9*(1). https://doi.org/10.1038/S41598-018-38005-4

Castrillo, G., Teixeira, P. J. P. L., Paredes, S. H., Law, T. F., de Lorenzo, L., Feltcher, M. E., Finkel, O. M., Breakfield, N. W., Mieczkowski, P., Jones, C. D., Paz-Ares, J., & Dangl, J. L. (2017). Root microbiota drive direct integration of phosphate stress and immunity. *Nature*, *543*(7646), 513–518. https://doi.org/10.1038/nature21417

Chaparro, J. M., Badri, D. v, Bakker, M. G., Sugiyama, A., Manter, D. K., & Vivanco, J. M. (2013). Root exudation of phytochemicals in arabidopsis follows specific patterns that are developmentally programmed and correlate with soil microbial functions. *PLoS One*, *8*. https://doi.org/10.1371/journal.pone.0055731

Chisholm, S. T., Parra, M. A., Anderberg, R. J., & Carrington, J. C. (2001). Arabidopsis RTM1 and RTM2 genes function in phloem to restrict long-distance movement of tobacco etch virus. *Plant Physiol*, *127*(4), 1667–1675.

Clay, N. K., Adio, A. M., Denoux, C., Jander, G., & Ausubel, F. M. (2009). Glucosinolate metabolites required for an Arabidopsis innate immune response. *Science (New York, N.Y.)*, *323*(5910), 95–101. https://doi.org/10.1126/science.1164627

Cointry, V., & Vert, G. (2019). The bifunctional transporter-receptor IRT1 at the heart of metal sensing and signalling. *New Phytologist*, *223*(3), 1173–1178. https://doi.org/10.1111/nph.15826

Coleman-Derr, D., Desgarennes, D., Fonseca-Garcia, C., Gross, S., Clingenpeel, S., Woyke, T., North, G., Visel, A., Partida-Martinez, L. P., & Tringe, S. G. (2016). Plant compartment and biogeography affect microbiome composition in cultivated and native Agave species. *The New Phytologist*, *209*(2), 798–811. https://doi.org/10.1111/nph.13697

Conn, S. J., Conn, V., Tyerman, S. D., Kaiser, B. N., Leigh, R. A., & Gilliham, M. (2011). Magnesium transporters, MGT2/MRS2-1 and MGT3/MRS2-5, are important for magnesium partitioning within Arabidopsis thaliana mesophyll vacuoles. *The New Phytologist*, *190*(3), 583–594. https://doi.org/10.1111/J.1469-8137.2010.03619.X

Connolly, E. L., Fett, J. P., & Guerinot, M. lou. (2002). Expression of the IRT1 metal transporter is controlled by metals at the levels of transcript and protein accumulation. *The Plant Cell*, *14*(6), 1347–1357. https://doi.org/10.1105/TPC.001263

Cresti, M., Pacini, E., & Simoncioli, C. (1974). Uncommon paracrystalline structures formed in the endoplasmic reticulum of the integumentary cells of Diplotaxis erucoides ovules. *Journal of Ultrastructure Research*, *49*(2), 218–223. https://doi.org/10.1016/S0022-5320(74)80033-X

Czarnota, M. A., Rimando, A. M., & Weston, L. A. (2003). Evaluation of root exudates of seven sorghum accessions. *J Chem Ecol*, *29*. https://doi.org/10.1023/A:1025634402071

Deeks, M. J., Fendrych, M., Smertenko, A., Bell, K. S., Oparka, K., Cvrcková, F., Zársky, V., & Hussey, P. J. (2010). The plant formin AtFH4 interacts with both actin and microtubules, and contains a newly identified microtubule-binding domain. *J Cell Sci*, *123*(Pt 8), 1209–1215. https://doi.org/10.1242/jcs.065557

Delgado-Baquerizo, M. (2018). Ecological drivers of soil microbial diversity and soil biological networks in the Southern Hemisphere. *Ecology*, *99*.

Demoling, F., Figueroa, D., & Bååth, E. (2007). Comparison of factors limiting bacterial growth in different soils. *Soil Biology and Biochemistry*, *39*(10), 2485–2495. https://doi.org/10.1016/J.SOILBIO.2007.05.002

Dixon, P. (2003). VEGAN, a package of R functions for community ecology. *J Veg Sci*, *14*. https://doi.org/10.1111/j.1654-1103.2003.tb02228.x

Dräger, D. B., Desbrosses-Fonrouge, A.-G., Krach, C., Chardonnens, A. N., Meyer, R. C., Saumitou-Laprade, P., & Krämer, U. (2004). Two genes encoding Arabidopsis halleri MTP1 metal transport proteins co-segregate with zinc tolerance and account for high MTP1 transcript levels. *Plant J*, *39*(3), 425–439. https://doi.org/10.1111/j.1365-313X.2004.02143.x

Dubeaux, G., Neveu, J., Zelazny, E., & Vert, G. (2018). Metal Sensing by the IRT1 Transporter-Receptor Orchestrates Its Own Degradation and Plant Metal Nutrition. *Molecular Cell*, *69*(6), 953-964.e5. https://doi.org/10.1016/j.molcel.2018.02.009

Durán, P., Thiergart, T., Garrido-Oter, R., Agler, M., Kemen, E., Schulze-Lefert, P., & Hacquard, S. (2018). Microbial Interkingdom Interactions in Roots Promote Arabidopsis Survival. *Cell*, *175*(4), 973–983.e14. https://doi.org/10.1016/j.cell.2018.10.020

Edwards, J., Johnson, C., Santos-Medellín, C., Lurie, E., Podishetty, N. K., Bhatnagar, S., Eisen, J. A., & Sundaresan, V. (2015). Structure, variation, and assembly of the root-associated microbiomes of rice. *Proceedings of the National Academy of Sciences*, *112*(8), E911–E920. https://doi.org/10.1073/pnas.1414592112

Eichmann, R., Richards, L., & Schäfer, P. (2021). Hormones as go-betweens in plant microbiome assembly. *The Plant Journal: For Cell and Molecular Biology*, *105*(2), 518–541. https://doi.org/10.1111/tpj.15135

Eide, D., Broderius, M., Fett, J., & Guerinot, M. lou. (1996). A novel iron-regulated metal transporter from plants identified by functional expression in yeast. *Proceedings of the National Academy of Sciences of the United States of America*, *93*(11), 5624–5628. https://doi.org/10.1073/PNAS.93.11.5624

Eilers, K. G., Lauber, C. L., Knight, R., & Fierer, N. (2010). Shifts in bacterial community structure associated with inputs of low molecular weight carbon compounds to soil. *Soil Biology and Biochemistry*, *42*(6), 896–903. https://doi.org/10.1016/J.SOILBIO.2010.02.003

Elliott, C. E., Harjono, & Howlett, B. J. (2008). Mutation of a Gene in the Fungus Leptosphaeria maculans Allows Increased Frequency of Penetration of Stomatal Apertures of Arabidopsis thaliana. *Molecular Plant*, *1*(3), 471–481. https://doi.org/10.1093/mp/ssn014

Endress, A. G., & Sjolund, R. D. (1976). Ultrastructural Cytology of Callus Cultures of Streptanthus Tortuosus as Affected by Temperature. *American Journal of Botany*, *63*(9), 1213–1224. https://doi.org/10.1002/j.1537-2197.1976.tb13206.x

Fan, J., Crooks, C., Creissen, G., Hill, L., Fairhurst, S., Doerner, P., & Lamb, C. (2011). Pseudomonas sax genes overcome aliphatic isothiocyanate-mediated non-host resistance in Arabidopsis. *Science (New York, N.Y.)*, *331*(6021), 1185–1188. https://doi.org/10.1126/science.1199707

Ferber, E., Gerhards, J., Sauer, M., Krischke, M., Dittrich, M. T., Müller, T., Berger, S., Fekete, A., & Mueller, M. J. (2020). Chemical Priming by Isothiocyanates Protects Against Intoxication by Products of the Mustard Oil Bomb. *Frontiers in Plant Science*, *11*, 887. https://doi.org/10.3389/fpls.2020.00887

Fierer, N., & Jackson, R. B. (2006). The diversity and biogeography of soil bacterial communities. *Proc. Natl Acad. Sci. USA*, *103*.

Finkel, O. M., Salas-González, I., Castrillo, G., Conway, J. M., Law, T. F., Teixeira, P. J. P. L., Wilson, E. D., Fitzpatrick, C. R., Jones, C. D., & Dangl, J. L. (2020). A single bacterial genus maintains root growth in a complex microbiome. *Nature*, *587*(7832), 103–108. https://doi.org/10.1038/s41586-020-2778-7

Frerigmann, H., & Gigolashvili, T. (2014). MYB34, MYB51, and MYB122 distinctly regulate indolic glucosinolate biosynthesis in Arabidopsis thaliana. *Molecular Plant*, *7*(5), 814–828. https://doi.org/10.1093/mp/ssu004

Frerigmann, H., Piotrowski, M., Lemke, R., Bednarek, P., & Schulze-Lefert, P. (2021). A Network of Phosphate Starvation and Immune-Related Signaling and Metabolic Pathways Controls the Interaction between Arabidopsis thaliana and the Beneficial Fungus Colletotrichum tofieldiae. *Molecular Plant-Microbe Interactions: MPMI*, *34*(5), 560–570. https://doi.org/10.1094/MPMI-08-20-0233-R

Frerigmann, H., Piślewska-Bednarek, M., Sánchez-Vallet, A., Molina, A., Glawischnig, E., Gigolashvili, T., & Bednarek, P. (2016). Regulation of Pathogen-Triggered Tryptophan Metabolism in Arabidopsis thaliana by MYB Transcription Factors and Indole Glucosinolate Conversion Products. *Molecular Plant*, *9*(5), 682–695. https://doi.org/10.1016/j.molp.2016.01.006

Gailhofer, M., Thaler, I., & Rücker, W. (1979). Dilatiertes ER in Kalluszellen und in Zellen vonin vitro kultivierten PflÄnzchen vonArmoracia rusticana. *Protoplasma*, *98*(3), 263–274. https://doi.org/10.1007/BF01281443

Getzke, F., Thiergart, T., & Hacquard, S. (2019). Contribution of bacterial-fungal balance to plant and animal health. *Current Opinion in Microbiology*, *49*, 66–72. https://doi.org/10.1016/j.mib.2019.10.009

Gollhofer, J., Schläwicke, C., Jungnick, N., Schmidt, W., & Buckhout, T. J. (2011). Members of a small family of nodulin-like genes are regulated under iron deficiency in roots of Arabidopsis thaliana. *Plant Physiology and Biochemistry : PPB*, *49*(5), 557–564. https://doi.org/10.1016/J.PLAPHY.2011.02.011

Gollhofer, J., Timofeev, R., Lan, P., Schmidt, W., & Buckhout, T. J. (2014). Vacuolar-Iron-Transporter1-Like proteins mediate iron homeostasis in Arabidopsis. *PloS One*, *9*(10). https://doi.org/10.1371/JOURNAL.PONE.0110468

Grotz, N., Fox, T., Connolly, E., Park, W., Guerinot, M. lou, & Eide, D. (1998). Identification of a family of zinc transporter genes from Arabidopsis that respond to zinc deficiency. *Proceedings of the National Academy of Sciences of the United States of America*, *95*(12), 7220–7224. https://doi.org/10.1073/PNAS.95.12.7220

Gunning, B. E. S. (1998). The identity of mystery organelles in Arabidopsis plants expressing GFP. *Trends in Plant Science*, *3*(11), 417. https://doi.org/10.1016/S1360-1385(98)01336-3

Hacquard, S. (2016). Disentangling the factors shaping microbiota composition across the plant holobiont. *The New Phytologist*, *209*(2), 454–457. https://doi.org/10.1111/nph.13760

Hacquard, S., Kracher, B., Hiruma, K., Münch, P. C., Garrido-Oter, R., Thon, M. R., Weimann, A., Damm, U., Dallery, J. F., Hainaut, M., Henrissat, B., Lespinet, O., Sacristán, S., ver Loren Van Themaat, E., Kemen, E., McHardy, A. C., Schulze-Lefert, P., & O'Connell, R. J. (2016). Survival trade-offs in plant roots during colonization by closely related beneficial and pathogenic fungi. *Nature Communications 2016 7:1*, *7*(1), 1–13. https://doi.org/10.1038/ncomms11362

Hakenjos, J. P., Bejai, S., Ranftl, Q., Behringer, C., Vlot, A. C., Absmanner, B., Hammes, U., Heinzlmeir, S., Kuster, B., & Schwechheimer, C. (2013). ML3 Is a NEDD8- and Ubiquitin-Modified Protein. *Plant Physiology*, *163*(1), 135–149. https://doi.org/10.1104/pp.113.221341

Halkier, B. A., & Gershenzon, J. (2006). BIOLOGY AND BIOCHEMISTRY OF GLUCOSINOLATES. *Annual Review of Plant Biology*, *57*(1), 303–333. https://doi.org/10.1146/annurev.arplant.57.032905.105228

Haney, C. H., & Ausubel, F. M. (2015). MICROBIOME. Plant microbiome blueprints. *Science (New York, N.Y.)*, *349*(6250), 788–789. https://doi.org/10.1126/science.aad0092

Haralick, R. M., Dinstein, I., & Shanmugam, K. (1973). Textural Features for Image Classification. *IEEE Transactions on Systems, Man and Cybernetics*, *SMC-3*(6), 610–621. https://doi.org/10.1109/TSMC.1973.4309314

Hara-Nishimura, I., & Matsushima, R. (2003). A wound-inducible organelle derived from endoplasmic reticulum: a plant strategy against environmental stresses? *Current Opinion in Plant Biology*, *6*(6), 583–588. https://doi.org/10.1016/J.PBI.2003.09.015

Harbort, C. J., Hashimoto, M., Inoue, H., Niu, Y., Guan, R., Rombolà, A. D., Kopriva, S., Voges, M. J. E. E. E., Sattely, E. S., Garrido-Oter, R., & Schulze-Lefert, P. (2020). Root-Secreted Coumarins and the Microbiota Interact to Improve Iron Nutrition in Arabidopsis. *Cell Host & Microbe*, *28*(6), 825-837.e6. https://doi.org/10.1016/J.CHOM.2020.09.006

Hassani, M. A., Durán, P., & Hacquard, S. (2018). Microbial interactions within the plant holobiont. *Microbiome*, *6*.

Hastie, T., Tibshirani, R., & Buja, A. (1994). Flexible discriminant analysis by optimal scoring. *J Am Stat Assoc*, *89*. https://doi.org/10.1080/01621459.1994.10476866

Hawes, C., Saint-Jore, C., Martin, B., & Zheng, H.-Q. (2001). ER confirmed as the location of mystery organelles in Arabidopsis plants expressing GFP! *Trends in Plant Science*, *6*(6), 245–246. https://doi.org/10.1016/S1360-1385(01)01980-X

Hayashi, Y., Yamada, K., Shimada, T., Matsushima, R., Nishizawa, NaokoK., Nishimura, M., & Hara-Nishimura, I. (2001). A Proteinase-Storing Body that Prepares for Cell Death or Stresses in the Epidermal Cells of Arabidopsis. *Plant and Cell Physiology*, *42*(9), 894–899. https://doi.org/10.1093/pcp/pce144

Herman, null, & Larkins, null. (1999). Protein storage bodies and vacuoles. *The Plant Cell*, *11*(4), 601–614. https://doi.org/10.1105/tpc.11.4.601

Hiruma, K. (2019). Roles of Plant-Derived Secondary Metabolites during Interactions with Pathogenic and Beneficial Microbes under Conditions of Environmental Stress. *Microorganisms*, *7*(9), 362. https://doi.org/10.3390/microorganisms7090362

Hiruma, K., Gerlach, N., Sacristán, S., Nakano, R. T., Hacquard, S., Kracher, B., Neumann, U., Ramírez, D., Bucher, M., O'Connell, R. J., & Schulze-Lefert, P. (2016). Root Endophyte Colletotrichum tofieldiae Confers Plant Fitness Benefits that Are Phosphate Status Dependent. *Cell*, *165*(2), 464–474. https://doi.org/10.1016/j.cell.2016.02.028

Hiruma, K., Onozawa-Komori, M., Takahashi, F., Asakura, M., Bednarek, P., Okuno, T., Schulze-Lefert, P., & Takano, Y. (2010). Entry Mode–Dependent Function of an Indole Glucosinolate Pathway in Arabidopsis for Nonhost Resistance against Anthracnose Pathogens. *The Plant Cell*, *22*(7), 2429–2443. https://doi.org/10.1105/tpc.110.074344

Hoefert, L. L. (1975). Tubules in Dilated Cisternae of Endoplasmic Reticulum of Thlaspi Arvense (cruciferae). *American Journal of Botany*, *62*(7), 756–760. https://doi.org/10.1002/j.1537-2197.1975.tb14110.x

Hopkins, R. J., van Dam, N. M., & van Loon, J. J. A. (2009). Role of Glucosinolates in Insect-Plant Relationships and Multitrophic Interactions. *Annual Review of Entomology*, *54*(1), 57–83. https://doi.org/10.1146/annurev.ento.54.110807.090623

Hörger, A. C., Fones, H. N., & Preston, G. M. (2013). The current status of the elemental defense hypothesis in relation to pathogens. *Frontiers in Plant Science*, *4*, 395. https://doi.org/10.3389/fpls.2013.00395

Hu, L., Robert, C. A. M., Cadot, S., Zhang, X., Ye, M., Li, B., Manzo, D., Chervet, N., Steinger, T., van der Heijden, M. G. A., Schlaeppi, K., & Erb, M. (2018). Root exudate metabolites drive plant-soil feedbacks on growth and defense by shaping the rhizosphere microbiota. *Nature Communications*, *9*(1), 2738. https://doi.org/10.1038/s41467-018-05122-7

Huang, A. C., Jiang, T., Liu, Y.-X., Bai, Y.-C., Reed, J., Qu, B., Goossens, A., Nützmann, H.-W., Bai, Y., & Osbourn, A. (2019). A specialized metabolic network selectively modulates Arabidopsis root microbiota. *Science*, *364*(6440). https://doi.org/10.1126/science.aau6389

Hull, A. K., Vij, R., & Celenza, J. L. (2000). Arabidopsis cytochrome P450s that catalyze the first step of tryptophan-dependent indole-3-acetic acid biosynthesis. *Proceedings of the National Academy of Sciences*, *97*(5), 2379–2384. https://doi.org/10.1073/pnas.040569997

Inceoğlu, Ö., Salles, J. F., Overbeek, L., & Elsas, J. D. (2010). Effects of plant genotype and growth stage on the betaproteobacterial communities associated with different potato cultivars in two fields. *Appl Environ Microbiol*, *76*. https://doi.org/10.1128/AEM.00040-10

Iuchi, S., Koyama, H., Iuchi, A., Kobayashi, Y., Kitabayashi, S., Kobayashi, Y., Ikka, T., Hirayama, T., Shinozaki, K., & Kobayashi, M. (2007). Zinc finger protein STOP1 is critical for proton tolerance in Arabidopsis and coregulates a key gene in aluminum tolerance. *Proc Natl Acad Sci USA*, *104*. https://doi.org/10.1073/pnas.0700117104

Iversen, T. H. (1970). The morphology, occurrence, and distribution of dilated cisternae of the endoplasmic reticulum in tissues of plants of the Cruciferae. *Protoplasma*, *71*. https://doi.org/10.1007/BF01279689

Iversen, T.-H. (1970). Cytochemical localization of myrosinase (β-thioglucosidase) in root tips ofSinapis alba. *Protoplasma*, *71*(4), 451–466. https://doi.org/10.1007/BF01279688

Iversen, T.-H., & Flood, P. R. (1969). Rod-shaped accumulations in cisternae of the endoplasmic reticulum in root cells of Lepidium sativum seedlings. *Planta*, *86*(3), 295–298. https://doi.org/10.1007/BF00386462

Jacobs, S., Zechmann, B., Molitor, A., Trujillo, M., Petutschnig, E., Lipka, V., Kogel, K.-H., & Schäfer, P. (2011). Broad-Spectrum Suppression of Innate Immunity Is Required for Colonization of Arabidopsis Roots by the Fungus Piriformospora indica. *Plant Physiology*, *156*(2), 726–740. https://doi.org/10.1104/pp.111.176446

Jørgensen, L. B. (1981). Myrosin cells and dilated cisternae of the endoplasmic reticulum in the order Capparales. *Nordic Journal of Botany*, *1*(3), 433–445. https://doi.org/10.1111/j.1756-1051.1981.tb00709.x

Jørgensen, L. B., Behnke, H. D., & Mabry, T. J. (1977). Protein-accumulating cells and dilated cisternae of the endoplasmic reticulum in three glucosinolate-containing genera: Armoracia, Capparis, Drypetes. *Planta 1977 137:3*, *137*(3), 215–224. https://doi.org/10.1007/BF00388153

Kai, K., Shimizu, B., Mizutani, M., Watanabe, K., & Sakata, K. (2006). Accumulation of coumarins in Arabidopsis thaliana. *Phytochemistry*, *67*(4), 379–386. https://doi.org/10.1016/j.phytochem.2005.11.006

Karimi, B. (2018). Biogeography of soil bacteria and archaea across France. *Sci. Adv.*, *4*.

Kato, T., Kumazaki, K., Wada, M., Taniguchi, R., Nakane, T., Yamashita, K., Hirata, K., Ishitani, R., Ito, K., & Nishizawa, T. (2019). Crystal structure of plant vacuolar iron transporter VIT1. *Nat Plants*, *5*. https://doi.org/10.1038/s41477-019-0367-2

Kim, S. A., Punshon, T., Lanzirotti, A., Li, A., Alonso, J. M., Ecker, J. R., Kaplan, J., & Guerinot, M. lou. (2006). Localization of iron in Arabidopsis seed requires the vacuolar membrane transporter VIT1. *Science (New York, N.Y.)*, *314*(5803), 1295–1298. https://doi.org/10.1126/SCIENCE.1132563

Kim, W.-. Y., & Kim, Y.-. S. (2000). A region-based shape descriptor using Zernike moments. *Signal Process Image Commun*, *16*. https://doi.org/10.1016/S0923-5965(00)00019-9

Klein, A. P., & Sattely, E. S. (2017). Biosynthesis of cabbage phytoalexins from indole glucosinolate. *Proceedings of the National Academy of Sciences*, *114*(8), 1910–1915. https://doi.org/10.1073/pnas.1615625114

Koprivova, A., Schuck, S., Jacoby, R. P., Klinkhammer, I., Welter, B., Leson, L., Martyn, A., Nauen, J., Grabenhorst, N., Mandelkow, J. F., Zuccaro, A., Zeier, J., & Kopriva, S. (2019). Root-specific camalexin biosynthesis controls the plant growth-promoting effects of multiple bacterial strains. *Proceedings of the National Academy of Sciences of the United States of America*, *116*(31), 15735–15744. https://doi.org/10.1073/pnas.1818604116

Korenblum, E., Dong, Y., Szymanski, J., Panda, S., Jozwiak, A., Massalha, H., Meir, S., Rogachev, I., & Aharoni, A. (2020). Rhizosphere microbiome mediates systemic root metabolite exudation by root-to-root signaling. *Proceedings of the National Academy of Sciences of the United States of America*, *117*(7), 3874–3883. https://doi.org/10.1073/pnas.1912130117

Kunkel, B. N., & Harper, C. P. (2018). The roles of auxin during interactions between bacterial plant pathogens and their hosts. *Journal of Experimental Botany*, *69*(2), 245–254. https://doi.org/10.1093/jxb/erx447

Kunkel, B. N., & Johnson, J. M. B. (2021). Auxin Plays Multiple Roles during Plant-Pathogen Interactions. *Cold Spring Harbor Perspectives in Biology*, *13*(9), a040022. https://doi.org/10.1101/cshperspect.a040022

Lahrmann, U., Strehmel, N., Langen, G., Frerigmann, H., Leson, L., Ding, Y., Scheel, D., Herklotz, S., Hilbert, M., & Zuccaro, A. (2015). Mutualistic root endophytism is not associated with the reduction of saprotrophic traits and requires a noncompromised plant innate immunity. *The New Phytologist*, *207*(3), 841–857. https://doi.org/10.1111/nph.13411

Lebeis, S. L., Paredes, S. H., Lundberg, D. S., Breakfield, N., Gehring, J., McDonald, M., Malfatti, S., del Rio, T., Jones, C. D., Tringe, S. G., & Dangl, J. L. (2015). PLANT MICROBIOME. Salicylic acid modulates colonization of the root microbiome by specific bacterial taxa. *Science*, *349*(6250), 860–864. https://doi.org/10.1126/science.aaa8764

Li, J., Saxena, S., Pain, D., & Dancis, A. (2001). Adrenodoxin reductase homolog (Arh1p) of yeast mitochondria required for iron homeostasis. *The Journal of Biological Chemistry*, *276*(2), 1503–1509. https://doi.org/10.1074/JBC.M007198200

Li, L., Chen, O. S., McVey Ward, D., & Kaplan, J. (2001). CCC1 is a transporter that mediates vacuolar iron storage in yeast. *The Journal of Biological Chemistry*, *276*(31), 29515–29519. https://doi.org/10.1074/jbc.M103944200

Li, L., & Ward, D. M. (2018). Iron toxicity in yeast: transcriptional regulation of the vacuolar iron importer Ccc1. *Current Genetics*, *64*(2), 413–416. https://doi.org/10.1007/S00294-017-0767-7

Li, M., & Sack, F. D. (2014). Myrosin idioblast cell fate and development are regulated by the Arabidopsis transcription factor FAMA, the auxin pathway, and vesicular trafficking. *Plant Cell*, *26*. https://doi.org/10.1105/tpc.114.129726

Liang, H., Yuan, Q., & Xiao, Q. (2006). Effects of metal ions on myrosinase activity and the formation of sulforaphane in broccoli seed. *Journal of Molecular Catalysis B: Enzymatic*, *43*(1–4), 19–22. https://doi.org/10.1016/J.MOLCATB.2006.03.008

Lipka, V., Dittgen, J., Bednarek, P., Bhat, R., Wiermer, M., Stein, M., Landtag, J., Brandt, W., Rosahl, S., Scheel, D., Llorente, F., Molina, A., Parker, J., Somerville, S., & Schulze-Lefert, P. (2005). Pre- and Postinvasion Defenses Both Contribute to Nonhost Resistance in Arabidopsis. *Science*. https://doi.org/10.1126/science.1119409

Lugtenberg, B., & Kamilova, F. (2009). Plant-growth-promoting rhizobacteria. *Annual Review of Microbiology*, *63*, 541–556. https://doi.org/10.1146/annurev.micro.62.081307.162918

Lundberg, D. S., Lebeis, S. L., Paredes, S. H., Yourstone, S., Gehring, J., Malfatti, S., Tremblay, J., Engelbrektson, A., Kunin, V., del Rio, T. G., Edgar, R. C., Eickhorst, T., Ley, R. E., Hugenholtz, P., Tringe, S. G., & Dangl, J. L. (2012). Defining the core Arabidopsis thaliana root microbiome. *Nature*, *488*(7409), 86–90. https://doi.org/10.1038/nature11237

Maeda, K., Houjyou, Y., Komatsu, T., Hori, H., Kodaira, T., & Ishikawa, A. (2009). AGB1 and PMR5 Contribute to PEN2-Mediated Preinvasion Resistance to Magnaporthe oryzae in Arabidopsis thaliana. *Molecular Plant-Microbe Interactions®*, *22*(11), 1331–1340. https://doi.org/10.1094/MPMI-22-11-1331

Maguire, M. E. (2006). Magnesium transporters: properties, regulation and structure. *Frontiers in Bioscience : A Journal and Virtual Library*, *11*(SUPPL. 3), 3149–3163. https://doi.org/10.2741/2039

Marti, L., Stefano, G., Tamura, K., Hawes, C., Renna, L., Held, M. A., & Brandizzi, F. (2010). A missense mutation in the vacuolar protein GOLD36 causes organizational defects in the ER and aberrant protein trafficking in the plant secretory pathway. *The Plant Journal*, *63*(6), 901–913. https://doi.org/10.1111/j.1365-313X.2010.04296.x

Martos, S., Gallego, B., Cabot, C., Llugany, M., Barceló, J., & Poschenrieder, C. (2016). Zinc triggers signaling mechanisms and defense responses promoting resistance to Alternaria brassicicola in Arabidopsis thaliana. *Plant Science : An International Journal of Experimental Plant Biology*, *249*, 13–24. https://doi.org/10.1016/J.PLANTSCI.2016.05.001

Matsushima, R., Fukao, Y., Nishimura, M., & Hara-Nishimura, I. (2004). NAI1 gene encodes a basic-helix-loop-helix-type putative transcription factor that regulates the formation of an endoplasmic reticulum-derived structure, the ER body. *Plant Cell*, *16*. https://doi.org/10.1105/tpc.021154

Matsushima, R., Hayashi, Y., Kondo, M., Shimada, T., Nishimura, M., & Hara-Nishimura, I. (2002). An endoplasmic reticulum-derived structure that is induced under stress conditions in Arabidopsis. *Plant Physiology*, *130*(4), 1807–1814. https://doi.org/10.1104/PP.009464

Matsushima, R., Hayashi, Y., Yamada, K., Shimada, T., Nishimura, M., & Hara-Nishimura, I. (2003). The ER body, a novel endoplasmic reticulum-derived structure in Arabidopsis. *Plant Cell Physiol*, *44*. https://doi.org/10.1093/pcp/pcg089

Matsushima, R., Kondo, M., Nishimura, M., & Hara-Nishimura, I. (2003). A novel ER-derived compartment, the ER body, selectively accumulates a beta-glucosidase with an ER-retention signal in Arabidopsis. *The Plant Journal: For Cell and Molecular Biology*, *33*(3), 493–502. https://doi.org/10.1046/j.1365-313x.2003.01636.x

Mendes, R., Garbeva, P., & Raaijmakers, J. M. (2013). The rhizosphere microbiome: significance of plant beneficial, plant pathogenic, and human pathogenic microorganisms. *FEMS Microbiology Reviews*, *37*(5), 634–663. https://doi.org/10.1111/1574-6976.12028

Mendes, R., Kruijt, M., Bruijn, I. de, Dekkers, E., Voort, M. van der, Schneider, J. H. M., Piceno, Y. M., DeSantis, T. Z., Andersen, G. L., Bakker, P. A. H. M., & Raaijmakers, J. M. (2011). Deciphering the Rhizosphere Microbiome for Disease-Suppressive Bacteria. *Science*, 1203980. https://doi.org/10.1126/science.1203980

Mesny, F., Miyauchi, S., Thiergart, T., Pickel, B., Atanasova, L., Karlsson, M., Hüttel, B., Barry, K. W., Haridas, S., Chen, C., Bauer, D., Andreopoulos, W., Pangilinan, J., LaButti, K., Riley, R., Lipzen, A., Clum, A., Drula, E., Henrissat, B., … Hacquard, S. (2021). Genetic determinants of endophytism in the Arabidopsis root mycobiome. *Nature Communications*, *12*(1), 7227. https://doi.org/10.1038/s41467-021-27479-y

Micallef, S. A., Channer, S., Shiaris, M. P., & Colón-Carmona, A. (2009). Plant age and genotype impact the progression of bacterial community succession in the Arabidopsis rhizosphere. *Plant Signal Behav*, *4*. https://doi.org/10.1093/jxb/erp053

Mondy, S., Lenglet, A., Beury-Cirou, A., Libanga, C., Ratet, P., Faure, D., & Dessaux, Y. (2014). An increasing opine carbon bias in artificial exudation systems and genetically modified plant rhizospheres leads to an increasing reshaping of bacterial populations. *Molecular Ecology*, *23*(19), 4846–4861. https://doi.org/10.1111/mec.12890

Moussaieff, A., Rogachev, I., Brodsky, L., Malitsky, S., Toal, T. W., Belcher, H., Yativ, M., Brady, S. M., Benfey, P. N., & Aharoni, A. (2013). High-resolution metabolic mapping of cell types in plant roots. *Proceedings of the National Academy of Sciences*, *110*(13), E1232–E1241. https://doi.org/10.1073/pnas.1302019110

Müller, D. B., Vogel, C., Bai, Y., & Vorholt, J. A. (2016). The Plant Microbiota: Systems-Level Insights and Perspectives. *Annual Review of Genetics*, *50*, 211–234. https://doi.org/10.1146/annurev-genet-120215-034952

Münch, C., Neu, T., Kuschk, P., & Röske, I. (2007). The root surface as the definitive detail for microbial transformation processes in constructed wetlands – a biofilm characteristic. *Water Science and Technology*, *56*(3), 271–276. https://doi.org/10.2166/WST.2007.527

Nagano, A. J., Fukao, Y., Fujiwara, M., Nishimura, M., & Hara-Nishimura, I. (2008). Antagonistic Jacalin-Related Lectins Regulate the Size of ER Body-Type β-Glucosidase Complexes in Arabidopsis thaliana. *Plant and Cell Physiology*, *49*(6), 969–980. https://doi.org/10.1093/pcp/pcn075

Nagano, A. J., Maekawa, A., Nakano, R. T., Miyahara, M., Higaki, T., Kutsuna, N., Hasezawa, S., & Hara-Nishimura, I. (2009). Quantitative analysis of ER body morphology in an Arabidopsis mutant. *Plant Cell Physiol*, *50*. https://doi.org/10.1093/pcp/pcp157

Nagano, A. J., Matsushima, R., & Hara-Nishimura, I. (2005). Activation of an ER-body-localized β-Glucosidase via a Cytosolic Binding Partner in Damaged Tissues of Arabidopsis thaliana. *Plant and Cell Physiology*, *46*(7), 1140–1148. https://doi.org/10.1093/pcp/pci126

Nakano, R. T., Matsushima, R., Nagano, A. J., Fukao, Y., Fujiwara, M., Kondo, M., Nishimura, M., & Hara-Nishimura, I. (2012). ERMO3/MVP1/GOLD36 is involved in a cell type-specific mechanism for maintaining ER morphology in Arabidopsis thaliana. *PloS One*, *7*(11), e49103. https://doi.org/10.1371/journal.pone.0049103

Nakano, R. T., Piślewska-Bednarek, M., Yamada, K., Edger, P. P., Miyahara, M., Kondo, M., Böttcher, C., Mori, M., Nishimura, M., Schulze-Lefert, P., Hara-Nishimura, I., & Bednarek, P. (2017). PYK10 myrosinase reveals a functional coordination between endoplasmic reticulum bodies and glucosinolates in Arabidopsis thaliana. *The Plant Journal : For Cell and Molecular Biology*, *89*(2), 204–220. https://doi.org/10.1111/TPJ.13377

Nakano, R., Yamada, K., Bednarek, P., Nishimura, M., & Hara-Nishimura, I. (2014). ER bodies in plants of the Brassicales order: biogenesis and association with innate immunity. *Frontiers in Plant Science*, *5*. https://www.frontiersin.org/article/10.3389/fpls.2014.00073

Nakazaki, A., Yamada, K., Kunieda, T., Sugiyama, R., Hirai, Y. M., Tamura, K., Hara-Nishimura, I., & Shimada, T. (2019). Leaf endoplasmic reticulum bodies identified in Arabidopsis rosette leaves are involved in defense against herbivory. *Plant Physiol*, *179*. https://doi.org/10.1104/pp.18.00984

Nguyen, C. (2003). Rhizodeposition of organic C by plants: Mechanisms and controls. *Agronomie*, *23*(5–6), 375–396. https://doi.org/10.1051/AGRO:2003011

Nilsson, R. H. (2019). The UNITE database for molecular identification of fungi: handling dark taxa and parallel taxonomic classifications. *Nucleic Acids Res.*, *47*.

Normanly, J., Grisafi, P., Fink, G. R., & Bartel, B. (1997). Arabidopsis mutants resistant to the auxin effects of indole-3-acetonitrile are defective in the nitrilase encoded by the NIT1 gene. *The Plant Cell*, *9*(10), 1781–1790. https://doi.org/10.1105/tpc.9.10.1781

Oburger, E., Gruber, B., Schindlegger, Y., Schenkeveld, W. D. C., Hann, S., Kraemer, S. M., Wenzel, W. W., & Puschenreiter, M. (2014). Root exudation of phytosiderophores from soil-grown wheat. *New Phytol*, *203*. https://doi.org/10.1111/nph.12868

Oelmüller, R., Peškan-Berghöfer, T., Shahollari, B., Trebicka, A., Sherameti, I., & Varma, A. (2005). MATH domain proteins represent a novel protein family in Arabidopsis thaliana, and at least one member is modified in roots during the course of a plant–microbe interaction. *Physiologia Plantarum*, *124*(2), 152–166. https://doi.org/10.1111/j.1399-3054.2005.00505.x

Ogasawara, K., Yamada, K., Christeller, J. T., Kondo, M., Hatsugai, N., Hara-Nishimura, I., & Nishimura, M. (2009). Constitutive and inducible ER bodies of Arabidopsis thaliana accumulate distinct beta-glucosidases. *Plant & Cell Physiology*, *50*(3), 480–488. https://doi.org/10.1093/pcp/pcp007

Okutani, F., Hamamoto, S., Aoki, Y., Nakayasu, M., Nihei, N., Nishimura, T., Yazaki, K., & Sugiyama, A. (2020). Rhizosphere modelling reveals spatiotemporal distribution of daidzein shaping soybean rhizosphere bacterial community. *Plant, Cell & Environment*, *43*(4), 1036–1046. https://doi.org/10.1111/PCE.13708

Otsu, N. (1979). A threshold selection method from gray-level histograms. *IEEE Trans Syst Man Cybern*, *9*. https://doi.org/10.1109/TSMC.1979.4310076

Paasch, B. C., & He, S. Y. (2021). Toward understanding microbiota homeostasis in the plant kingdom. *PLoS Pathogens*, *17*(4), e1009472. https://doi.org/10.1371/journal.ppat.1009472

Pandit, A., Adholeya, A., Cahill, D., Brau, L., & Kochar, M. (2020). Microbial biofilms in nature: unlocking their potential for agricultural applications. *Journal of Applied Microbiology*, *129*(2), 199–211. https://doi.org/10.1111/JAM.14609

Pang, Z., Chong, J., Zhou, G., de Lima Morais, D. A., Chang, L., Barrette, M., Gauthier, C., Jacques, P.-É., Li, S., & Xia, J. (2021). MetaboAnalyst 5.0: narrowing the gap between raw spectra and functional insights. *Nucleic Acids Research*, *49*(W1), W388–W396. https://doi.org/10.1093/nar/gkab382

Panke-Buisse, K., Poole, A. C., Goodrich, J. K., Ley, R. E., & Kao-Kniffin, J. (2015). Selection on soil microbiomes reveals reproducible impacts on plant function. *ISME J.*, *9*.

Pastor-Cantizano, N., Bernat-Silvestre, C., Marcote, M. J., & Aniento, F. (2018). Loss of Arabidopsis p24 function affects ERD2 trafficking and Golgi structure, and activates the unfolded protein response. *J Cell Sci*, *131*(2), jcs203802. https://doi.org/10.1242/jcs.203802

Pau, G., Fuchs, F., Sklyar, O., Boutros, M., & Huber, W. (2010). EBImage-an R package for image processing with applications to cellular phenotypes. *Bioinformatics*, *26*. https://doi.org/10.1093/bioinformatics/btq046

Peiffer, J. A., Spor, A., Koren, O., Jin, Z., Tringe, S. G., Dangl, J. L., Buckler, E. S., & Ley, R. E. (2013). Diversity and heritability of the maize rhizosphere microbiome under field conditions. *Proceedings of the National Academy of Sciences of the United States of America*, *110*(16), 6548–6553. https://doi.org/10.1073/PNAS.1302837110/SUPPL_FILE/PNAS.201302837SI.PDF

Peterson, J. K., Harrison, H. F., Jackson, D. M., & Snook, M. E. (2003). Biological Activities and Contents of Scopolin and Scopoletin in Sweetpotato Clones. *HortScience*, *38*(6), 1129–1133. https://doi.org/10.21273/HORTSCI.38.6.1129

Pfalz, M., Mikkelsen, M. D., Bednarek, P., Olsen, C. E., Halkier, B. A., & Kroymann, J. (2011). Metabolic Engineering in Nicotiana benthamiana Reveals Key Enzyme Functions in Arabidopsis Indole Glucosinolate Modification. *The Plant Cell*, *23*(2), 716–729. https://doi.org/10.1105/tpc.110.081711

Pietrangelo, L., Bucci, A., Maiuro, L., Bulgarelli, D., & Naclerio, G. (2018). Unraveling the composition of the root-associated bacterial microbiota of Phragmites australis and Typha latifolia. *Frontiers in Microbiology*, *9*(AUG), 1650. https://doi.org/10.3389/FMICB.2018.01650/BIBTEX

Pluskal, T., Castillo, S., Villar-Briones, A., & Oresic, M. (2010). MZmine 2: modular framework for processing, visualizing, and analyzing mass spectrometry-based molecular profile data. *BMC Bioinformatics*, *11*, 395. https://doi.org/10.1186/1471-2105-11-395

Prats, E., Bazzalo, M. E., León, A., & Jorrín, J. v. (2006). Fungitoxic effect of scopolin and related coumarins on Sclerotinia sclerotiorum. A way to overcome sunflower head rot. *Euphytica*, *147*(3), 451–460. https://doi.org/10.1007/s10681-005-9045-8

Quast, C., Pruesse, E., Yilmaz, P., Gerken, J., Schweer, T., Yarza, P., Peplies, J., & Glöckner, F. O. (2013). The SILVA ribosomal RNA gene database project: improved data processing and web-based tools. *Nucleic Acids Research*, *41*(Database issue), D590. https://doi.org/10.1093/NAR/GKS1219

Rajagopal, R., & Larsen, P. (1972). Metabolism of indole-3-acetaldoxime in plants. *Planta*, *103*(1), 45–54. https://doi.org/10.1007/BF00394605

Rajniak, J., Barco, B., Clay, N. K., & Sattely, E. S. (2015). A new cyanogenic metabolite in Arabidopsis required for inducible pathogen defence. *Nature*, *525*(7569), 376–379. https://doi.org/10.1038/nature14907

Rask, L., Andréasson, E., Ekbom, B., Eriksson, S., Pontoppidan, B., & Meijer, J. (2000). Myrosinase: gene family evolution and herbivore defense in Brassicaceae. *Plant Molecular Biology*, *42*(1), 93–114. https://doi.org/10.1023/A:1006380021658

Ratzka, A., Vogel, H., Kliebenstein, D. J., Mitchell-Olds, T., & Kroymann, J. (2002). Disarming the mustard oil bomb. *Proceedings of the National Academy of Sciences*, *99*(17), 11223–11228. https://doi.org/10.1073/pnas.172112899

Reuzeau, C., McNally, J. G., & Pickard, B. G. (1997). The endomembrane sheath: a key structure for understanding the plant cell? *Protoplasma*, *200*(1–2), 1–9. https://doi.org/10.1007/BF01280729

Ridge, R. W., Uozumi, Y., Plazinski, J., Hurley, U. A., & Williamson, R. E. (1999). Developmental transitions and dynamics of the cortical ER of Arabidopsis cells seen with green fluorescent protein. *Plant & Cell Physiology*, *40*(12), 1253–1261. https://doi.org/10.1093/oxfordjournals.pcp.a029513

Robinson, D. G., Brandizzi, F., Hawes, C., & Nakano, A. (2015). Vesicles versus Tubes: Is Endoplasmic Reticulum-Golgi Transport in Plants Fundamentally Different from Other Eukaryotes?1. *Plant Physiology*, *168*(2), 393–406. https://doi.org/10.1104/pp.15.00124

Rolfe, S. A., Griffiths, J., & Ton, J. (2019). Crying out for help with root exudates: adaptive mechanisms by which stressed plants assemble health-promoting soil microbiomes. *Current Opinion in Microbiology*, *49*, 73–82. https://doi.org/10.1016/j.mib.2019.10.003

Roschzttardtz, H., Conéjéro, G., Curie, C., & Mari, S. (2009). Identification of the endodermal vacuole as the iron storage compartment in the Arabidopsis embryo. *Plant Physiol*, *151*(3), 1329–1338. https://doi.org/10.1104/pp.109.144444

Sanchez-Vallet, A., Ramos, B., Bednarek, P., López, G., Piślewska-Bednarek, M., Schulze-Lefert, P., & Molina, A. (2010). Tryptophan-derived secondary metabolites in Arabidopsis thaliana confer non-host resistance to necrotrophic Plectosphaerella cucumerina fungi. *The Plant Journal*, *63*(1), 115–127. https://doi.org/10.1111/j.1365-313X.2010.04224.x

Sasse, J., Martinoia, E., & Northen, T. (2018). Feed Your Friends: Do Plant Exudates Shape the Root Microbiome? *Trends in Plant Science*, *23*(1), 25–41. https://doi.org/10.1016/j.tplants.2017.09.003

Sauer, J., & Fischer, B. (2019). MaxContrastProjection: Perform a maximum contrast projection of 3D images along the z-dimension into 2D. In *R package version 1.10.0.*

Schlaeppi, K., Abou-Mansour, E., Buchala, A., & Mauch, F. (2010). Disease resistance of Arabidopsis to Phytophthora brassicae is established by the sequential action of indole glucosinolates and camalexin. *The Plant Journal*, *62*(5), 840–851. https://doi.org/10.1111/j.1365-313X.2010.04197.x

Schlaeppi, K., Dombrowski, N., Oter, R. G., van Themaat, E., & Schulze-Lefert, P. (2014). Quantitative divergence of the bacterial root microbiota in Arabidopsis thaliana relatives. *Proc. Natl Acad. Sci. USA*, *111*.

Schmid, M., Simpson, D. J., Sarioglu, H., Lottspeich, F., & Gietl, C. (2001). The ricinosomes of senescing plant tissue bud from the endoplasmic reticulum. *Proceedings of the National Academy of Sciences*, *98*(9), 5353–5358. https://doi.org/10.1073/pnas.061038298

Schmid, U., Rösch, P., Krause, M., Harz, M., Popp, J., & Baumann, K. (2009). Gaussian mixture discriminant analysis for the single-cell differentiation of bacteria using micro-Raman spectroscopy. *Chemometr Intell Lab Syst*, *96*. https://doi.org/10.1016/j.chemolab.2009.01.008

Sherameti, I., Venus, Y., Drzewiecki, C., Tripathi, S., Dan, V. M., Nitz, I., Varma, A., Grundler, F. M., & Oelmüller, R. (2008). PYK10, a beta-glucosidase located in the endoplasmatic reticulum, is crucial for the beneficial interaction between Arabidopsis thaliana and the endophytic fungus Piriformospora indica. *The Plant Journal : For Cell and Molecular Biology*, *54*(3), 428–439. https://doi.org/10.1111/J.1365-313X.2008.03424.X

Shimasaki, T., Masuda, S., Garrido-Oter, R., Kawasaki, T., Aoki, Y., Shibata, A., Suda, W., Shirasu, K., Yazaki, K., Nakano, R. T., & Sugiyama, A. (2021). Tobacco Root Endophytic Arthrobacter Harbors Genomic Features Enabling the Catabolism of Host-Specific Plant Specialized Metabolites. *MBio*, *12*(3), e0084621. https://doi.org/10.1128/mBio.00846-21

Shimizu, B., Miyagawa, H., Ueno, T., Sakata, K., Watanabe, K., & Ogawa, K. (2005). Morning Glory Systemically Accumulates Scopoletin and Scopolin after Interaction with Fusarium oxysporum. *Zeitschrift Für Naturforschung C*, *60*(1–2), 83–90. https://doi.org/10.1515/znc-2005-1-216

Sinclair, S. A., & Krämer, U. (2012). The zinc homeostasis network of land plants. *Biochimica et Biophysica Acta - Molecular Cell Research*, *1823*(9), 1553–1567. https://doi.org/10.1016/j.bbamcr.2012.05.016

Sorribes-Dauden, R., Martínez-Pastor, M. T., & Puig, S. (2021). Expression of a Truncated Yeast Ccc1 Vacuolar Transporter Increases the Accumulation of Endogenous Iron. *Genes*, *12*(8). https://doi.org/10.3390/GENES12081120

Stefanik, N., Bizan, J., Wilkens, A., Tarnawska-Glatt, K., Goto-Yamada, S., Strzałka, K., Nishimura, M., Hara-Nishimura, I., & Yamada, K. (2020). NAI2 and TSA1 Drive Differentiation of Constitutive and Inducible ER Body Formation in Brassicaceae. *Plant and Cell Physiology*, *61*(4), 863–863. https://doi.org/10.1093/PCP/PCAA030

Strehmel, N., Böttcher, C., Schmidt, S., & Scheel, D. (2014). Profiling of secondary metabolites in root exudates of Arabidopsis thaliana. *Phytochemistry*, *108*. https://doi.org/10.1016/j.phytochem.2014.10.003

Stringlis, I. A. (2018). MYB72-dependent coumarin exudation shapes root microbiome assembly to promote plant health. *Proc. Natl Acad. Sci. USA*, *115*.

Sugawara, S., Hishiyama, S., Jikumaru, Y., Hanada, A., Nishimura, T., Koshiba, T., Zhao, Y., Kamiya, Y., & Kasahara, H. (2009). Biochemical analyses of indole-3-acetaldoxime-dependent auxin biosynthesis in Arabidopsis. *Proceedings of the National Academy of Sciences of the United States of America*, *106*(13), 5430–5435. https://doi.org/10.1073/PNAS.0811226106

Suwińska, A., Wasąg, P., Zakrzewski, P., Lenartowska, M., & Lenartowski, R. (2017). Calreticulin is required for calcium homeostasis and proper pollen tube tip growth in Petunia. *Planta*, *245*(5), 909–926. https://doi.org/10.1007/S00425-017-2649-0

Takahashi, S., Yanai, H., Nakamaru, Y., Uchida, A., Nakayama, K., & Satoh, H. (2012). Molecular cloning, characterization and analysis of the intracellular localization of a water-soluble Chl-binding protein from Brussels sprouts (Brassica oleracea var. gemmifera). *Plant Cell Physiol*, *53*(5), 879–891. https://doi.org/10.1093/pcp/pcs031

Tawaraya, K., Horie, R., Shinano, T., Wagatsuma, T., Saito, K., & Oikawa, A. (2014). Metabolite profiling of soybean root exudates under phosphorus deficiency. *Soil Sci Plant Nutr*, *60*. https://doi.org/10.1080/00380768.2014.945390

Thiergart, T., Durán, P., Ellis, T., Vannier, N., Garrido-Oter, R., Kemen, E., Roux, F., Alonso-Blanco, C., Ågren, J., Schulze-Lefert, P., & Hacquard, S. (2020). Root microbiota assembly and adaptive differentiation among European Arabidopsis populations. *Nature Ecology & Evolution*, *4*(1), 122–131. https://doi.org/10.1038/s41559-019-1063-3

Thole, J. M., Vermeer, J. E. M., Zhang, Y., Gadella, T. W. J., & Nielsen, E. (2008). Root hair defective4 encodes a phosphatidylinositol-4-phosphate phosphatase required for proper root hair development in Arabidopsis thaliana. *The Plant Cell*, *20*(2), 381–395. https://doi.org/10.1105/TPC.107.054304

Toyooka, K., Okamoto, T., & Minamikawa, T. (2000). Mass Transport of Proform of a Kdel-Tailed Cysteine Proteinase (Sh-EP) to Protein Storage Vacuoles by Endoplasmic Reticulum–Derived Vesicle Is Involved in Protein Mobilization in Germinating Seeds. *Journal of Cell Biology*, *148*(3), 453–464. https://doi.org/10.1083/jcb.148.3.453

Turner, T. R., James, E. K., & Poole, P. S. (2013). The plant microbiome. *Genome Biology*, *14*(6), 209. https://doi.org/10.1186/gb-2013-14-6-209

Tzipilevich, E., Russ, D., Dangl, J. L., & Benfey, P. N. (2021). Plant immune system activation is necessary for efficient root colonization by auxin-secreting beneficial bacteria. *Cell Host & Microbe*, *29*(10), 1507–1520.e4. https://doi.org/10.1016/j.chom.2021.09.005

Ueda, H., Yokota, E., Kutsuna, N., Shimada, T., Tamura, K., Shimmen, T., Hasezawa, S., Dolja, V. v, & Hara-Nishimura, I. (2010). Myosin-dependent endoplasmic reticulum motility and F-actin organization in plant cells. *Proc Natl Acad Sci U S A*, *107*(15), 6894–6899. https://doi.org/10.1073/pnas.0911482107

Vik, D., Mitarai, N., Wulff, N., Halkier, B. A., & Burow, M. (2018). Dynamic Modeling of Indole Glucosinolate Hydrolysis and Its Impact on Auxin Signaling. *Frontiers in Plant Science*, *9*, 550. https://doi.org/10.3389/fpls.2018.00550

Vives-Peris, V., de Ollas, C., Gómez-Cadenas, A., & Pérez-Clemente, R. M. (2020). Root exudates: from plant to rhizosphere and beyond. *Plant Cell Reports*, *39*(1), 3–17. https://doi.org/10.1007/s00299-019-02447-5

Voges, M. J. E. E. E., Bai, Y., Schulze-Lefert, P., & Sattely, E. S. (2019). Plant-derived coumarins shape the composition of an Arabidopsis synthetic root microbiome. *Proceedings of the National Academy of Sciences of the United States of America*, *116*(25), 12558–12565. https://doi.org/10.1073/pnas.1820691116

Vorholt, J. A. (2012). Microbial life in the phyllosphere. *Nature Reviews. Microbiology*, *10*(12), 828–840. https://doi.org/10.1038/nrmicro2910

Wagner, M. R. (2014). Natural soil microbes alter flowering phenology and the intensity of selection on flowering time in a wild Arabidopsis relative. *Ecol. Lett.*, *17*.

Wang, M., Xu, Q., Yu, J., & Yuan, M. (2010). The putative Arabidopsis zinc transporter ZTP29 is involved in the response to salt stress. *Plant Molecular Biology*, *73*(4–5), 467–479. https://doi.org/10.1007/S11103-010-9633-4

Wang, W., Yang, J., Zhang, J., Liu, Y.-X., Tian, C., Qu, B., Gao, C., Xin, P., Cheng, S., Zhang, W., Miao, P., Li, L., Zhang, X., Chu, J., Zuo, J., Li, J., Bai, Y., Lei, X., & Zhou, J.-M. (2020). An Arabidopsis Secondary Metabolite Directly Targets Expression of the Bacterial Type III Secretion System to Inhibit Bacterial Virulence. *Cell Host & Microbe*, *27*(4), 601–613.e7. https://doi.org/10.1016/j.chom.2020.03.004

Winde, I., & Wittstock, U. (2011). Insect herbivore counteradaptations to the plant glucosinolate-myrosinase system. *Phytochemistry*, *72*(13), 1566–1575. https://doi.org/10.1016/j.phytochem.2011.01.016

Wippel, K., Tao, K., Niu, Y., Zgadzaj, R., Kiel, N., Guan, R., Dahms, E., Zhang, P., Jensen, D. B., Logemann, E., Radutoiu, S., Schulze-Lefert, P., & Garrido-Oter, R. (2021). Host preference and invasiveness of commensal bacteria in the Lotus and Arabidopsis root microbiota. *Nature Microbiology*, *6*(9), 1150–1162. https://doi.org/10.1038/s41564-021-00941-9

Wittstock, U., & Halkier, B. A. (2002). Glucosinolate research in the Arabidopsis era. *Trends in Plant Science*, *7*(6), 263–270. https://doi.org/10.1016/s1360-1385(02)02273-2

Wolinska, K. W., Vannier, N., Thiergart, T., Pickel, B., Gremmen, S., Piasecka, A., Piślewska-Bednarek, M., Nakano, R. T., Belkhadir, Y., Bednarek, P., & Hacquard, S. (2021). Tryptophan metabolism and bacterial commensals prevent fungal dysbiosis in Arabidopsis roots. *Proceedings of the National Academy of Sciences of the United States of America*, *118*(49), e2111521118. https://doi.org/10.1073/pnas.2111521118

Xu, D., Hanschen, F. S., Witzel, K., Nintemann, S. J., Nour-Eldin, H. H., Schreiner, M., & Halkier, B. A. (2017). Rhizosecretion of stele-synthesized glucosinolates and their catabolites requires GTR-mediated import in Arabidopsis. *Journal of Experimental Botany*, *68*(12), 3205–3214. https://doi.org/10.1093/jxb/erw355

Xu, Z., Escamilla-Treviño, L. L., Zeng, L., Lalgondar, M., Bevan, D. R., Winkel, B. S. J., Mohamed, A., Cheng, C. L., Shih, M. C., Poulton, J. E., & Esen, A. (2004). Functional genomic analysis of Arabidopsis thaliana glycoside hydrolase family 1. *Plant Molecular Biology*, *55*(3), 343–367. https://doi.org/10.1007/S11103-004-0790-1

Xue, J., Jørgensen, M., Pihlgren, U., & Rask, L. (1995). The myrosinase gene family in Arabidopsis thaliana: gene organization, expression and evolution. *Plant Molecular Biology*, *27*(5), 911–922. https://doi.org/10.1007/BF00037019

Yamada, K., Goto-Yamada, S., Nakazaki, A., Kunieda, T., Kuwata, K., Nagano, A. J., Nishimura, M., & Hara-Nishimura, I. (2020). Endoplasmic reticulum-derived bodies enable a single-cell chemical defense in Brassicaceae plants. *Commun Biol*, *3*. https://doi.org/10.1038/s42003-019-0739-1

Yamada, K., Hara-Nishimura, I., & Nishimura, M. (2011). Unique defense strategy by the endoplasmic reticulum body in plants. *Plant Cell Physiol*, *52*. https://doi.org/10.1093/pcp/pcr156

Yamada, K., Nagano, A. J., Nishina, M., Hara-Nishimura, I., & Nishimura, M. (2008). NAI2 is an endoplasmic reticulum body component that enables ER body formation in Arabidopsis thaliana. *The Plant Cell*, *20*(9), 2529–2540. https://doi.org/10.1105/tpc.108.059345

Yamada, K., Nagano, A. J., Nishina, M., Hara-Nishimura, I., & Nishimura, M. (2013). Identification of two novel endoplasmic reticulum body-specific integral membrane proteins. *Plant Physiol*, *161*. https://doi.org/10.1104/pp.112.207654

Yamada, K., Nagano, A. J., Ogasawara, K., Hara-Nishimura, I., & Nishimura, M. (2009). The ER body, a new organelle in Arabidopsis thaliana, requires NAI2 for its formation and accumulates specific β-glucosidases. *Plant Signaling & Behavior*, *4*(9), 849–852. https://www.ncbi.nlm.nih.gov/pmc/articles/PMC2802796/

Yang, N., Nesme, J., Røder, H. L., Li, X., Zuo, Z., Petersen, M., Burmølle, M., & Sørensen, S. J. (2021). Emergent bacterial community properties induce enhanced drought tolerance in Arabidopsis. *Npj Biofilms and Microbiomes 2021 7:1*, *7*(1), 1–11. https://doi.org/10.1038/s41522-021-00253-0

Zhalnina, K., Louie, K. B., Hao, Z., Mansoori, N., da Rocha, U. N., Shi, S., Cho, H., Karaoz, U., Loqué, D., Bowen, B. P., Firestone, M. K., Northen, T. R., & Brodie, E. L. (2018). Dynamic root exudate chemistry and microbial substrate preferences drive patterns in rhizosphere microbial community assembly. *Nature Microbiology*, *3*(4), 470–480. https://doi.org/10.1038/s41564-018-0129-3

Zhang, J., Pontoppidan, B., Xue, J., Rask, L., & Meijer, J. (2002). The third myrosinase gene TGG3 in Arabidopsis thaliana is a pseudogene specifically expressed in stamen and petal. *Physiologia Plantarum*, *115*(1), 25–34. https://doi.org/10.1034/j.1399-3054.2002.1150103.x

Zhang, P., Spaepen, S., Bai, Y., Hacquard, S., & Garrido-Oter, R. (2021). Rbec: a tool for analysis of amplicon sequencing data from synthetic microbial communities. *ISME Communications*, *1*(1), 1–3. https://doi.org/10.1038/s43705-021-00077-1

Zhang, Y., Xu, Y.-H., Yi, H.-Y., & Gong, J.-M. (2012). Vacuolar membrane transporters OsVIT1 and OsVIT2 modulate iron translocation between flag leaves and seeds in rice. *Plant J*, *72*(3), 400–410. https://doi.org/10.1111/j.1365-313X.2012.05088.x

Zhao, Y., Hull, A. K., Gupta, N. R., Goss, K. A., Alonso, J., Ecker, J. R., Normanly, J., Chory, J., & Celenza, J. L. (2002). Trp-dependent auxin biosynthesis in Arabidopsis: involvement of cytochrome P450s CYP79B2 and CYP79B3. *Genes & Development*, *16*(23), 3100–3112. https://doi.org/10.1101/gad.1035402

Zhou, C., Tokuhisa, J. G., Bevan, D. R., & Esen, A. (2012). Properties of β-thioglucoside hydrolases (TGG1 and TGG2) from leaves of Arabidopsis thaliana. *Plant Science*, *191–192*, 82–92. https://doi.org/10.1016/j.plantsci.2012.02.004

Zhu, X., He, S., Fang, D., Guo, L., Zhou, X., Guo, Y., Gao, L., & Qiao, Y. (2020). High-Throughput Sequencing-Based Identification of Arabidopsis miRNAs Induced by Phytophthora capsici Infection. *Frontiers in Microbiology*, *11*, 1094. https://doi.org/10.3389/fmicb.2020.01094

6. LIST OF FIGURES

7. LIST OF TABLES

8. LIST OF ABBREVIATIONS

Used form	Description
10MSD	10-methylsulfinyldecylglucosinolate
1MI3G	1-methoxyindol-3-ylmethylglucosinolate
3MSB	3-methylsulphinylbutyl glucosinolate
4M-I3G	4-methoxy-indol-3-ylmethyl glucosinolate
4MU	4-methylumbelliferyl
4MUG	4-methylumbelliferyl-glucoside
5MT-P	5-methylthiopentanoate
6MTH	6-Methylthio-n-hexyl glucosinolate
6MTH	(6-methylthiohexyl glucosinolate
8MSO	-methylsulfinyloctlyglucosinolate
9MSN	9-Methylsulfinylnonyl glucosinolate
9MTN	9-methylthiononanoic aci
AG	aliphatic glucosinolates
ASV	Amplicon sequence vriants
BGLU	β-glucosidase
CAS	Cologne agricultural soil
CCA	Constrained cannonical correlation analysis
COP	Coat protein complex
cPCoA	Constrained principal co-ordinate analysis
DAG	days after germination
DNA	Deoxy rib nucleic acid
dNTP	deoxyribonucleotide triphosphate
dpi	Days post inoculation
EDTA	Ethylenedinitrilotetraacetic acid
ER	Endoplasmic reticulum
FDA	Flexible discriminant analysis
FDR	False discovery rate
GFP	Green fluorescent protein
GLCM	Gray-Level Co-Occurrence Matrix
GLM	Generalised linear model
hpi	Hours post inoculation
HSD	Honest significant difference
I3A	(indole-3-acetonitrile
I3G	Indol-3-ylmethyl glucosinolate
IAA	Indole acetic acid
IAN	Indole acetonitrile
IAOx	Indole acetaldoxime
ICA	indole carboxylic acid
ICN	Indole caribinol
ICP-MS	Inductively coupled plasma mass spectrometry
IGs	Indole glucosinolates
ITA	Italian soil
ITS	Internal transcribed spacer

KV	KDEL-tailed protease-accumulating vesicles
LOESS	locally estimated scatterplot smoothing
LRO	Las Rozas
m/Z	Mass-to-charge ratios
MBD	Membrane binding domain
MDA	Mixed discriminate analysis
MDS	Multi-dimensional scaling
meJA	Methyl jasmonic acid
MES	4-Morpholineethanesulfonic acid
MS	Murasige-Skoog
PAC	Precurser accumulation
PB	Protein bodies
PCC	Pearson's correlation coefficient
PCoA	Principal co-ordinate analysis
PCR	Polymerase chain reaction
PERMANOVA	Permutation based multi-variate analysis of varaince
PGA	Potato glucose agar
PI	Propidium Iodide
QA	Quantitative abundance
QC	Quality control
RA	Relative abundance
rRNA	Ribosomal ribo nucleic acid
RT	Retention time
SynCom	synthetic community
TE-T	Tris-EDTA-Triton-X100
TEM	Transmission electron microscopy
TMD	Transmembrane domain
TSB	Trypsin soy broth
TVIPS	Tietz Video and Image Processing Systems
UPLC	Ultra-performance liquid chromatography

9. LIST OF PUBLICATION

A part of CHAPTER I of this thesis is published, cited below.

Basak, A.K., Mirzaei, M., Strzałka, K. *et al.* Texture feature extraction from microscope images enables a robust estimation of ER body phenotype in Arabidopsis. *Plant Methods*17, 109 (2021). https://doi.org/10.1186/s13007-021-00810-w

Beyond the scope of the thesis contents

Basak SM, O'Mahony DT, Lesiak M, Basak AK, Ziółkowska E, Kaim D, Hossain MS, Wierzbowska IA. Animal-vehicle collisions during the COVID-19 lockdown in early 2020 in the Krakow metropolitan region, Poland. Sci Rep. 2022 May 9;12(1):7572. doi: 10.1038/s41598-022-11526-9. PMID: 35534651; PMCID: PMC9082987.

"Chapter 4: Role of microbe in biofuel production", A K Basak, S M Basak, K Strzałka, P K Chatterjee – Book title Biofuel from microbes and Plants, Nitish Kumar, ISBN 9780367207052, Oct 2021, Taylor & Francis, CRC Press

Yamada K, Basak AK, Goto-Yamada S, Tarnawska-Glatt K, Hara-Nishimura I. Vacuolar processing enzymes in the plant life cycle. New Phytol. 2020 Apr;226(1):21-31. doi: 10.1111/nph.16306. Epub 2019 Dec 7. PMID: 31679161.

10. CONTRIBUTIONS

Mohammedreza Mirzaei contributed in acquiring confocal microscope images, and assisted in performing experiments involving plant culture.

Dr. Kaichiro Endo assisted in designing of experiments and troubleshooting experimental challenges.

Dr. Ryohei Thomas Nakano supervised and assisted in the harvesting process of natural soil experiment, mono-association assay for investigating binary interaction between fungi and plants, bioinformatics, and statistical analysis. Jana Hucklenbroich assisted in the fungal mono-association assay with plants.

Dr inz. Olga Woźnicka performed the TEM analysis at the Department of Zoology, Faculty of Biology, Jagiellonian University.

The plant ionomics by ICP-MS analysis was conducted in collaboration with Prof. Dr. Stanislav Kopriva at University of Cologne, Germany.

The fungal culture collections were obtained in co-ordination with Fantin Mesny and Dr. Stephane Hacquard at Max-Planck Institute of Plant Breeding and Research.

Bioinformatic and statistical analysis for root microbiome dataset were conducted in collaboration with Dr. Rui Guan, and Dr. Ruben Garrido-Oter. Penfang Zhang assisted in bioinformatics of reference-based clustering of amplicons for the SynCom experiments.

Prof. dr. hab Pawel Bednarek and Dr. Ania Picesczka performed the wet lab experiment and analytics for the mass spectrometry analysis of the root exudates.

Prof. Paul Schulze-lefert for providing the culture collection of bacteria, and resources to conduct the experiments at Max-Planck Institute of Plant Breeding and Research, Cologne, Germany.

11. STRESZCZENIE (summary in Polish)

Rośliny w przyrodzie są narażone na stres związany z występowaniem w glebie wielu drobnoustrojów, które konkurują o węgiel organiczny produkowany przez rośliny. Niektóre mikroorganizmy są korzystne dla roślin, a inne są patogenne. Rośliny są także narażone na kontakt z roślinożercami. Niektóre zwierzęta roślinożerne i owady wykazują zachowania mutualistyczne, pomagając w zapylaniu lub broniąc rośliny przed innymi roślinożercami. Na skutek ewolucji rośliny wykształciły systemy obronne, aby przeciwdziałać swoim wrogom. Rośliny należące do rzędu kapustnych wykształciły złożony system obronny, aby chronić się przed wrogami swoje części nadziemne i podziemne. Rośliny te wytwarzają klasę metabolitów wtórnych zwanych glukozynolanami, które po aktywacji systemu obrony zapewniają ochronę przed wrogami. Glukozynolany są magazynowane w wakuolach i aktywowane przez β-glukozydazę zlokalizowaną w tzw. komórkach mirozynowych. Ten system aktywacji jest popularnie znany jako system bomby gorczycowej i występuje w roślinach krzyżowych, w tym w roślinie modelowej *Arabidopsis thaliana*. Wśród β-glukozydaz opisanych u *A. thaliana* jest PYK10, która jest gromadzona w wyspecjalizowanych przedziałach pochodzących z sieci retikulum endoplazmatycznego (ER), a mianowicie w ciałach ER. Co istotne, korzenie *A. thaliana* obfitują w glukozynolany indolowe, które są produktami końcowymi metabolizmu pochodnych Trp. PYK10 jest jedną z najbardziej dominujących mirozynaz w korzeniach, o wysokiej specyficznej aktywności w stosunku do glukozynolanów indolowych. Nie zostało do tej pory wyjaśnione, czy zlokalizowane w ciałach ER mirozynazy odgrywają kluczową rolę w kształtowaniu zespołu korzeń-mikrobiota poprzez hydrolizę wtórnych metabolitów pochodzących z Trp. Ciała ER zawierają PYK10 wraz z potencjalnym białkiem rusztowania NAI2, co czyni z nich przedział komórkowy z dużą zawartością białka. Ciała ER są strukturami związanymi z błoną, zawierającymi dwa integralne białka błonowe MEMBRANE OF ER-BODIES (MEB1) i MEB2. Wykazano, że geny MEB1 i MEB2 są homologiczne do transportera VACUOLAR IRON TRANSPORTER (VIT1) występującego u *A. thaliana*, i że białka te są odpowiedzialne za transport żelaza u drożdży. Jednakże funkcja MEB1 i MEB2 u roślin nie jest znana. Na początku przeprowadziłem badania nad rolę MEB1 i MEB2 u *A. thaliana*. Ponieważ MEB1 i MEB2 są transporterami, wysunąłem hipotezę, że MEB1 i MEB2 biorą udział w homeostazie kationów. Następnie zajmowałem się rolą ciał ER i ich substratów w tworzeniu społeczności mikrobioty korzeni. Do tej pory kilka badań sugerowało, że glukozynolany indolowe i produkty ich degradacji odgrywają rolę w kształtowaniu takiej mikrobioty, ale dokładna rola degradacji glukozynolanów indolowych przez PYK10 nie była znana.

W niniejszej pracy wykazałem, po pierwsze, możliwą rolę MEB1 i MEB2 w kształtowaniu morfologii ciał ER, ich ruchu i homeostazie składników odżywczych. Dzięki zaawansowanej mikroskopowej analizie konfokalnej cech tekstury wykazałam, że MEB1 i MEB2 są odpowiedzialne za morfologię i ruch ciał ER. Opierając się na jonomice badanych roślin i pomiarach ich parametrów fizjologicznych w kontrolowanych warunkach odżywczych zasugerowałem, że ciała ER odgrywają rolę w homeostazie kationów. Ogólnie rzecz biorąc, określiłem przypuszczalną rolę MEB1 i MEB2 w ciałach ER *in planta*.

Po drugie, wykazałem rolę PYK 10 i metabolitów wtórnych wytwarzanych z Trp, w kształtowaniu składu metabolitów znajdujących się w eksudatach korzeniowych, poprzez wykonanie nieukierunkowanej metabolomiki. Ponadto, zbadałem rolę ciał ER w tworzeniu zespołu korzeń-mikrobiota. Biorąc pod uwagę wyniki doświadczeń szklarniowych i korzeniowych, a także fakt, że pochodne PYK10 i Trp występują obficie w korzeniach, jest prawdopodobne, że związki będące rezultatem aktywności szlaku PYK10 i Trp, obecne w eksudatach korzeniowych, są odpowiedzialne za kształtowanie mikrobioty korzeni. Przeprowadzając eksperymenty z wykorzystaniem naturalnej gleby i zrekonstruowanej mikrobioty traktowanych eksudatami korzeniowymi pobranymi od roślin z uszkodzonym ciałem ER i szlakiem Trp, określiłem rolę mirozynazy PYK10 zlokalizowanej w ciałach ER i szlaku Trp w modulowaniu składu mikrobioty korzeniowej. Ponadto stwierdziłem, że metabolity wtórne powstające z Trp przy udziale PYK10, znajdujące się w eksudatach korzeniowych, wywołują zmiany w społecznościach bakterii glebowych, a także syntetycznych. Zbadałem również rolę ciał ER w interakcjach roślina-grzyb w układzie monoasocjacyjnym z wykorzystaniem szczepów grzybów, roślin zmutowanych i typu dzikiego. Stwierdziłem, że zarówno aktywność PYK10, jak i szlak Trp wykazują zbieżne zachowanie w stosunku do różnych szczepów grzybów.

Podsumowując, w mojej pracy zbadałam rolę białek błonowych ciał ER: MEB1 i MEB2, *in planta* oraz rolę białka PYK10 ,zlokalizowanego w ciałach ER w kształtowaniu mikrobioty korzeni.

Słowa kluczowe: *Arabidopsis thaliana*, ciała ER, glukozynolan, obrona roślin, błona, morfologia organelli, ruch organelli, homeostaza kationów, fizjologia roślin, mikrobiota korzeni, wydzieliny korzeniowe, metabolity wtórne.

11. ACKNOWLEDGEMENTS

At first, I would like to thank my supervisor Prof. dr. hab Kazimierz Strzałka and co-supervisor Dr. Kenji Yamada for hosting me during my PhD project at the Faculty of Biology, Jagiellonian University in Krakow. Special thanks to my external supervisor Dr. Ryohei Thomas Nakano for hosting me during my PhD project at the Max Planck Institute of Plant Breeding Research in Cologne, Germany. Both Dr. Yamada and Dr. Nakano funded the research and provided the necessary facilities. I would like to show my gratitude to my thesis advisors, Prof. dr hab Joanna Rutowska and Prof. dr. hab Wiesław Babik for their regular feedback and comments in the progress of my PhD project.

Importantly, I would like to appreciate the funding bodies WIN-POWR, NCN and DFG for funding the research for the development of Plant Sciences in the global scientific community.

Thirdly, I would like to give my thanks to the members of the Plant Molecular Biology laboratory at Malopolska Centre of Biotechnology, and the members of department of Plant-microbe interactions at Max Planck Institute of Plant Breeding Research for always supporting and team spirit during my research stay. Most importantly, I would like to thank the Ms Anna Maria Stec for co-ordinating the administrative and legislative matters with tremendous patience.

Finally, I would like to thank my family and friends for supporting me during the journey of my doctoral thesis.